Measurement of OH and HO_2 in the Troposphere

Dwayne E. Heard* and Michael J. Pilling†

Department of Chemistry, University of Leeds, Leeds LS2 9JT, U.K.

Received June 3, 2003

Contents

* To whom correspondence should be addressed. Tel.: ++44 113 343 6471. Fax: ++44 113 343 6565. E-mail: dwayneh@chem.leeds.ac.uk.
† E-mail: mikep@chem.leeds.ac.uk.

1. Introduction

Volatile organic compounds (VOCs), emitted into the atmosphere, react with a range of oxidants, of which the most important are OH, NO_3, and ozone. Under most atmospheric conditions, and during the day, the removal of VOCs is dominated by their reaction with OH. This ability of the atmosphere to "cleanse itself", and to continue doing so into the future, affects many processes. The concentration of methane, and hence its contribution to radiative forcing, is determined by the balance between its rate of emission and the rate of its removal by reaction with OH. The global distribution and seasonal variability of methane depend on the interaction between emission and reaction with OH. Tropospheric oxidation is also responsible for the formation of ground-level ozone and photochemical smog and for the production of secondary organic aerosols. The spatial distribution and concentrations of oxidants, such as OH, depend on a wide range of factors, including emissions of both volatile organic compounds and nitrogen oxides and the interaction of atmospheric transport and chemical kinetics. Oxidation is a complex chemical process, which proceeds through a series of partially oxidized intermediates; the primary emitted compounds and the intermediates have a wide range of atmospheric lifetimes, from minutes to years, depending, in most cases, on their rate constants for reaction with OH and the OH concentration, [OH]. Thus, the concentrations of photochemically active radical precursors, such as acetone in the upper troposphere, depend on their formation by oxidation of VOCs emitted at the surface, their atmospheric lifetimes, and their rate of vertical transport.

Clearly, OH plays a central role in tropospheric chemistry. The in situ measurement of its concentration has long been a goal, but its short lifetime and consequently low concentration provide a serious challenge. Considerable progress has been made, however, over the last 10 years, and there are now several OH instruments which are actively used for

10.1021/cr020522s CCC: $44.00
Published on Web 11/21/2003

Dwayne Heard has been Reader in Physical Chemistry at the University of Leeds since 2002. His research interests are (a) the field measurement of short-lived free radicals in the atmosphere, in particular the hydroxyl radical, using laser-induced fluorescence, and (b) the reaction kinetics and photochemistry of important processes in the atmosphere, studied using laser methods. He has made measurements of free radicals during a number of field campaigns worldwide under a variety of conditions, ranging from ultraclean marine environments to heavily polluted urban centers.

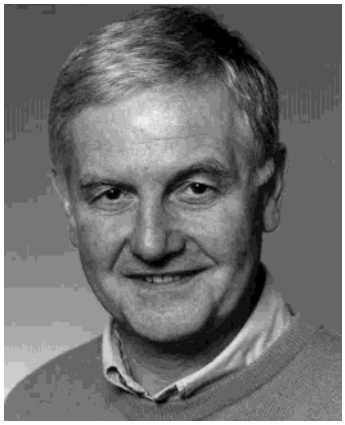

Mike Pilling has been Professor of Physical Chemistry at the University of Leeds since 1989. He is also the Director of the Distributed Institute for Atmospheric Composition, one of the Centres for Atmospheric Science in the UK Natural Environment Research Council. His research interests include the kinetics of radical reactions of importance in atmospheric chemistry and combustion and the construction and application of complex chemical mechanisms. The oxidation of organic compounds in the troposphere provides a major focus of his research.

both ground-based and aircraft-based campaigns, employing principally laser-induced fluorescence, laser absorption, and chemical ionization. Some of these instruments can also be used to measure HO_2, which is closely coupled to OH; [OH]:[HO_2] depends sensitively on the chemical composition of the atmosphere and particularly on the concentrations of VOCs and NO_x.

The atmospheric lifetime of OH is ~1 s or less, and it has been argued that its concentration is determined only by the local concentrations of longer-lived species such as O_3, VOCs, and NO_x, and is not affected directly by atmospheric transport. Thus, field measurements of [OH] can be interpreted through zero-dimensional chemical box models, in which the concentrations of longer-lived species are constrained to simultaneous, co-located measured values. This approach has led to the use of measurements of [OH], coupled with contemporaneous measurements of other species, as a way of evaluating chemical mechanisms for atmospheric oxidation. The interpretation of the box models has also provided a means of investigating the interaction of component reactions in the chemical mechanisms under a range of differing but representative chemical environments.

2. Scope of Review

There is now a considerable body of published work concerning the measurement of OH and HO_2 radicals in the atmosphere. In this review we compare and contrast the methods currently employed to quantitatively detect OH and HO_2 in the atmosphere, and survey the field measurements made during campaigns since 1991. It is not possible to provide a comprehensive coverage of all datasets, and we therefore select representative data from a variety of air mass types that illustrate the factors that control OH and HO_2 concentrations, and enable comparisons with model calculations. We limit the scope of the review to the measurement of *local* concentrations in the boundary layer, and do not discuss OH measurements that have been made by mass-balance approaches, methods involving the controlled co-release of chemically inert tracers and OH removing substances,[1] or the monitoring of long-lived anthropogenically emitted species (e.g., methyl chloroform) whose loss rate is controlled by [OH].[2,3] Down-wind measurement of the concentration ratio of two or more VOCs whose rate coefficients with OH are known, and whose emission strengths at source are also quantified, have been used to infer trajectory-averaged OH concentrations.[4−9] Although these measurements provide an important measurement of average [OH] over regional and global scales, and over extended time periods, they are not able to quantitatively test models of fast photochemistry. We also do not include published material concerned solely with the modeling of OH or HO_2 unless there has been a comparison with field data.

There have been a number of reviews that specifically cover measurement techniques of OH and HO_2 in the atmosphere, but none of these are recent. In 1985, Hewitt and Harrison reviewed the techniques used at the time to detect atmospheric OH, and discussed measured and modeled OH concentrations in field campaigns up to 1981.[10] Crosley hosted two workshops at SRI International in 1985[11] and 1992[12] at which various detection schemes for the measurement of OH and HO_2 were appraised. The report of the 1992 meeting contains an excellent bibliography of local measurements of OH and HO_2 up until 1993.[12] In 1995, Crosley edited a special issue of the *Journal of Atmospheric Sciences*[13] devoted to the measurement of HO_x radicals in the atmosphere. The issue resulted from a symposium held at the American Meteorological Society meeting in 1994.[14] Almost all of the groups involved in field measurements contributed papers, and there was some discussion of model-measurement comparison.[15] In 1993, O'Brien and Hard reviewed in detail methods for the direct measurement of tropospheric OH, using theoretical and experimental results.[16] Also in 1993, Eisele and Bradshaw[17] compared and contrasted methods for

OH measurement,; in 1994, Ehhalt et al. reviewed OH measurements;[18] and in 1995, Crosley[19] reviewed methods for detection of OH [in particular laser-induced fluorescence (LIF) methods], but there was little discussion of field results. There are also a number of review articles that discuss the behavior of OH and HO_2 in the atmosphere through the interpretation of field measurements.[10,20−25] A number of textbooks include a discussion of the measurement techniques for atmospheric HO_x measurements.[26−28] There are also a number of short review articles that provide summaries of the current understanding of OH measurements at the time of publication.[29−32] Although out of the scope of this review, Heard[33] has recently reviewed methods for the detection of HO_x in the stratosphere, together with selected field measurements.

3. What Are the Requirements of a Measurement Technique To Measure OH or HO_2 in the Troposphere?

Prior to field measurements, the OH concentration in the atmosphere could only be estimated from models, and its accuracy was at the mercy of the rather limited kinetic data on key reactions such as $OH + CO \rightarrow H + CO_2$, $HO_2 + NO \rightarrow OH + NO_2$, and $HO_2 + RO_2 \rightarrow ROOH + O_2$. For some of these reactions, the rate coefficient was not accurately known. For example, in 1971, the value for the $HO_2 + NO$ rate coefficient was estimated to be in the range $5 \times 10^{-11}-2 \times 10^{-15}$ cm^3 molecule^{-1} s^{-1} [34] (currently accepted value at 298 K is 8.8×10^{-12} cm^3 molecule^{-1} s^{-1} [35]). The initial order of magnitude estimate for [OH] in the troposphere was calculated in two ways. Weinstock and Niki[36] considered the steady-state rate equations for stable CO and for radioactive CO and calculated a 24-h average OH concentration of 2.3×10^6 molecules cm^{-3} (although their earlier estimate was 7×10^4 molecule cm^{-3} [37]), with a daytime concentration about twice this value. Using a photochemical steady-state model, Levy[34] in 1971 estimated an average daytime [OH] of 1.2×10^6 molecule cm^{-3}, with HO_2 about 100 times more abundant. McConnell et al.,[38] using a similar photochemical model, calculated [OH] as a function of height, with [OH] $\approx 3 \times 10^6$ molecules cm^{-3} up to 6 km, decreasing to 1×10^6 molecules cm^{-3} at the tropopause. The initial estimates were remarkably accurate, despite many rate coefficients being unknown to within a factor of 100. For comparison, measured values are typically a few 10^6 molecule cm^{-3} during the daytime [1×10^6 molecules cm^{-3} is ~0.04 parts per trillion (ppt) at sea level].

The early estimates of [OH] and [HO_2] were crucial in order to assess possible candidate techniques for their measurement in the field. As well as being highly sensitive, any method must also be in situ, as OH is known to react very quickly on surfaces, and will not be transmitted through sample lines. OH concentrations are controlled mainly by the intensity of UV radiation,[22] which can be heavily modulated by the presence of clouds, and also by the concentrations of NO_x ($\equiv NO + NO_2$) and VOCs, which may have very local sources. OH concentrations are therefore expected to vary significantly on short spatial scales, and any measurement technique must ideally sample at a single point, rather than averaging over a large spatial scale, for which the airmass may be inhomogeneous. The OH lifetime is very short (~1 s in clean air but as short as 10 ms in polluted air), and its response to external perturbations is largely determined by the time scale of those perturbations, which can be quite short. Thus, any measurement technique should also have excellent temporal resolution, ideally much less than a minute. Finally, the concentration of OH is many orders of magnitude smaller than the majority of other trace gases, and it is important that the measurement is selective to OH, and is not subject to interference from other species, or from artifact OH that may be generated in the process of making the measurement. For example, an interference that has plagued OH measurements since the very beginning is the laser photolysis of O_3 to generate $O(^1D)$, with subsequent reaction of $O(^1D)$ with atmospheric water vapor to generate OH. Often, it is this last criterion, namely the elimination of interferences, that is the most difficult to achieve.

4. Early Measurements of OH and HO_2

Very soon after the importance of OH in the troposphere was recognized,[34,36−38] it was suggested in 1972[39] that laser-induced fluorescence was particularly suitable for the measurement of OH at atmospheric pressure. A major problem is to separate the weak fluorescence emanating from the low concentrations of OH (10^6 molecule cm^{-3}) from the much more intense laser radiation that is scattered by gaseous constituents of air (Rayleigh scattering), aerosols (Mie scattering), and the walls of the apparatus. With laser excitation at 282 nm in the OH $A^2\Sigma^+ (v' = 1) \leftarrow X^2\Pi_i (v'' = 0)$ band to the vibrationally excited $v' = 1$ level, fluorescence can be collected at longer wavelengths via the (1,1) and (0,0) bands between 308 and 315 nm, hence avoiding scattered light and reducing the background considerably. The OH $A^2\Sigma^+$ $v' = 0$ level is populated by energy transfer resulting from collisions between OH $A^2\Sigma^+$, $v' = 1$, and ambient gases. However, at atmospheric pressure, the rate of nonradiative removal of the electronically excited state by collisional quenching is ca. 1000 times higher than the radiative rate (collision lifetime $\approx$ 1 ns, fluorescence lifetime = 700 ns), and hence very few of the initially excited OH molecules will fluoresce. Despite this, a very favorable detection limit ($< 1 \times 10^6$ molecules cm^{-3}) was calculated,[40] and the first OH measurements were reported in 1974 and shortly thereafter.[40−42] The first results in 1974 gave a maximum [OH] of 1.5×10^8 molecules cm^{-3}, with night-time values of 5×10^6 molecules cm^{-3}.[40]

The initial success was dampened by the realization[43] that at the rather large pulse energies at 282 nm used by the low-repetition-frequency laser systems (e.g., 6 mJ at 0.1 Hz[40]), considerable photolysis

of ambient O_3 was taking place, initiating OH production via

$$O_3 + h\nu\ (282\ nm) \rightarrow O(^1D) + O_2 \quad (1)$$

$$O(^1D) + H_2O \rightarrow OH + OH \quad (2)$$

Ironically, this is the same method by which OH is generated by solar photolysis in the atmosphere, but the much higher O_3 absorption cross-section at 282 nm compared to the value for actinic wavelengths (>290 nm), and the much higher laser photon flux compared with actinic fluxes, meant that laser-generated OH was considerably in excess of ambient OH. Despite the fact that two photons at 282 nm within the *same* 10-ns laser pulse are required to generate an artifact OH signal (one to photolyze O_3, and one to excite OH), modeling[44] and experiment[45,46] clearly showed that artifact signals swamped those from ambient OH, preventing a sensible measurement in the atmosphere. The use of lower laser pulse energies led to problems with signal-to-noise, and after some controversial measurements during the NASA GTE/CITE campaign[47,48] (that were later discredited[49]), OH detection by LIF at atmospheric pressure in the troposphere was abandoned.

Although outside of the scope of this review, it should be noted that OH detection by this method has enjoyed considerable success in the stratosphere, first using balloons[50] (although early experiments used a resonance lamp) and later from the ER-2 aircraft.[33,51,52] Although photolysis of O_3 still occurs, the concentration of H_2O vapor is very low (~5 ppm) compared to that in the troposphere (up to 3% mole fraction), and hence very little OH is generated by reaction 2. Two other factors also help: (i) the lower pressure results in a higher fluorescence quantum yield, and (ii) the OH mole fraction is considerably higher than that in the troposphere.

The ^{14}CO radiocarbon technique, developed at Washington State University and first reported in 1979,[53,54] is a photostationary-state method, in which a small amount of ^{14}CO is added to ambient air, reacting with OH to generate $^{14}CO_2$, which after cryogenic enrichment is measured with excellent sensitivity via its radioactivity using gas-proportional counting.[54,55] The CO_2 concentration, the enrichment factor, the OH + CO rate coefficient, and the reaction time are then used to calculate [OH]. The method is absolute and therefore does not require calibration. It is assumed that the steady-state OH concentration is not significantly perturbed during the ~10-s measurement period required to generate a measurable [$^{14}CO_2$]. The instrument is portable, and an aircraft version was developed, but the technique requires each sample to be analyzed separately, and long counting times (>20 min) for low concentrations of OH.

Measurements of OH and HO_2 in the stratosphere ran in parallel using the LIF technique[50,52,56−59] via the addition of NO to convert HO_2 into OH,

$$HO_2 + NO \rightarrow OH + NO_2 \quad (3)$$

and detecting the additional signal from OH formed in this reaction. However, these early LIF measurements of stratospheric HO_2 were not mirrored in the troposphere.

A method that enjoyed early success (1978)[60] for tropospheric measurements of HO_2 was that of matrix isolation electron spin resonance (MIESR). An air sample is frozen into a polycrystalline D_2O matrix held at 77 K for a period of ~30 min, and the sample is transported back to the laboratory for subsequent analysis by ESR. Although the averaging time is long, these were the first measurements of HO_2. The method is also capable of measuring NO_2, NO_3, $CH_3C(O)O_2$, and the sum of peroxy radicals, RO_2.[61] The latter can also be measured using a peroxy radical chemical amplifier (PERCA), first developed in the early 1980s,[62] and with the first RO_2 measurements made in 1984,[63] but the method is not specific to HO_2, rather measuring the sum of all peroxy radicals. Each HO_2 and RO_2 radical is converted to OH through the addition of NO, generating NO_2 that is measured, with the OH formed being converted back to HO_2 through the addition of CO. The chain reaction produces several hundred NO_2 molecules per initial peroxy radical, although the chain length is not the same for all peroxy radicals. Another method for the field measurement of the sum of peroxy radicals is chemical ionization mass spectrometry (CIMS). Although HO_2 is a component of RO_2, we do not discuss unspeciated RO_2 measurements using PERCA or CIMS in this review. For a review of measurements of the sum of RO_2 radicals and their tropospheric chemistry, the reader is referred to refs 25, 64, and 65.

5. Instruments Currently Employed To Measure Tropospheric OH and HO_2

5.1. Measurement of Tropospheric OH

Table 1 summarizes the detection limit, time response, accuracy, and deployment history for each of the methods used to measure tropospheric OH. The table further divides each method into the research groups that use them, and provides references. Three methods have enjoyed considerable success for the measurement of tropospheric OH. The first two are both spectroscopic methods, namely laser-induced fluorescence spectroscopy at low pressure (FAGE) and long-path differential optical absorption spectroscopy (DOAS). The third is the ion-assisted mass spectroscopy method, whereby OH is converted chemically into $H_2{}^{34}SO_4$, a species that does not occur naturally (and hence has no background), and which is subsequently measured by mass spectrometry. Each of these methods is described in detail below.

Three other methods have been used less widely in the field, and are only considered briefly here. The first, the radiocarbon oxidation method, was discussed above. Ground-based and aircraft instruments for that method have been developed. The second, a conceptually simple method, involves bubbling ambient air through a buffered solution of salicyclic acid (*o*-hydroxybenzoic acid).[66−69] OH adds to the aromatic ring to generate (mainly) 2,5-dihydroxybenzoic acid (DHBA), which after a suitable sampling period (45−

Table 1. Measurement Techniques and Research Groups for Boundary-Layer Detection of Tropospheric OH

method	group	limit of detection/ molecules cm^{-3}[b]	time response[e]	1σ uncertainty[c]	field campaigns where instrument deployed[d]	comments	references
fluorescence assay by gas expansion (FAGE)	Leeds University, UK	1.4×10^5, SNR = 1, 2.5 min	30 s	35%	EASE96, EASE97, AEROBIC, SOAPEX-2, PUMA-1, PUMA-2, PRIME, NAMBLEX	two cells for simultaneous OH and HO_2 measurement	80,86,91,94,136, 184,185,192,221
	Forschungszentrum Jülich, Germany	1.75×10^5, 80 s	40 s	10%	ALBATROSS, POPCORN, BERLIOZ	also deployed on ship, two cells, simultaneous OH, HO_2	87,93,132,133, 148,179,182
or laser-induced fluorescence (LIF) at low pressure	Pennsylvania State University, USA	1.4×10^5, SNR = 2, 30 s[g]	30 s	16%	TOHPE, PROPHET-1, PROPHET-2, SOS-Nashville, TEXAQS, PMTACS-NY (ground); SUCCESS, SONEX, PEM Tropics B, TRACE-P (aircraft)	multipass White cell, also deployed on aircraft, single cell, two optical axes, simultaneous OH, HO_2	75,82,95,98,105, 130,186,222−226
	Portland State University, USA	1×10^6, 6 min	6 min	$\pm 10^6$ molecules cm^{-3}	LAFRE, Pullman	four fluorescence cells, simultaneous OH, HO_2	58,84,90,96,163
	University of Tokyo, Japan (now at Frontier Research System for Global Change, Yokohama)	3.3×10^6, SNR = 2, 1 min (1.9×10^6 without solar scatter)	1 min	23%	ORION, Rishiri Island	single cell, sequential OH and HO_2 data	31,92,227−230
	Nagoya University, Japan	7×10^5, SNR = 2, 1 min			laboratory development only	laboratory instrument only	73
differential optical absorption spectroscopy (DOAS)	Forschungszentrum Jülich, Germany	1.5×10^6, 200 s	15 min	7%	ALBATROSS, POPCORN	folded long path, ~1.8−2.8 km, ship deployment also	110,113,114,180, 231−233
	Johann Goethe University, Frankfurt, Germany[a]	4×10^5, SNR = 1, 1 min	4.5 min	$\pm 10^6$ molecules cm^{-3}	Izana, WAOSE95, Taunus, Schauinsland	folded long path, 1.2−2.2 km	112,116,234−241
	NOAA, Fritz Peak, USA[a,h]	5×10^5, 1 min	10 min	30%	Fritz Peak, TOHPE	path length 20.6 km, single retroreflector	111,175−178,242
	Max Planck Institute fur Chemie, Mainz, Germany[a]	2×10^6, SNR = 2, 15 min			none since 1991	path length 5.6 km	243
chemical ionization mass spectrometry (CIMS)	NCAR, Boulder, USA[i]	$<1 \times 10^5$, SNR = 2, 5 min[g]	30 s	16%	Fritz Peak, TOHPE, ISCAT-1, ISCAT-2, SCATE, MLOPLEX-2 (ground); ACE-1, PEM Tropics A, B, TOPSE, TRACE-P (aircraft)	also deployed on aircraft	17,121−126,158, 159,176,244−248
	DWD, German Weather Service, Hohenpeissenberg, Germany	1.2×10^5, 5 min	30 s	20%	PARFORCE-2, MINOS, HOPE, HAFEX, BAYSOFI		118,249−253
	Georgia Institute of Technology, USA				PROPHET-3		119
^{14}CO oxidation	Washington State University, USA[a]	2×10^5, 2 min	5 min	16%	Pullman	also deployed on aircraft	53−55,181
scrubbing using salicyclic acid	Washington State University, USA[a]	$(3-6) \times 10^5$, 45−90 min	45−90 min	30−50%	TOHPE		66
	York University, Ontario, Canada	9×10^5, 30 min	30 min		PARFORCE-1,[f] SONTAS		67
	Peking University, China	1×10^6			Guangzhou (2000), Peking		68,69
	Max Planck Institute fur Chemie, Mainz, Germany				PARFORCE-1 [f]		
spin trapping	University of Tokyo, Japan	5×10^5, 20 min	20−30 min	<30%	airborne, 6−10 km above Japan	no measurements since 1982	254

[a] Instrument no longer operational. [b] LOD defined using eq 34 where possible, giving the SNR (signal-to-noise ratio) if reported, and signal integration period. The detection limit varies from campaign to campaign, and an attempt has been made to quote the best published detection limit for a given instrument while deployed in the field. Detection limits for operation in the laboratory are not given (unless there are no published field deployments). For FAGE instruments, no attempt has been attempted to standardize the detection limit for a given level of solar scattered radiation. [c] 1σ combined precision and accuracy, unless otherwise stated. [d] See Glossary of Field Campaign Acronyms at end of review and Table 3 for details. Only field campaigns since 1991 are listed. [e] Typical time period for which data are reported in the literature. However, the time response of the instrument may be much better than this, e.g., 1 s. [f] Joint deployment between York University, Ontario, and MPI fur Chemie during PARFORCE-1. [g] Detection limit quoted for ground-based instrument. [h] NOAA, National Oceanic and Atmospheric Administration. [i] NCAR, National Center for Atmospheric Research. A blank entry denotes unknown performance (in the open literature).

90 min) is quantified with good sensitivity using high-pressure liquid chromatography with fluorescence detection. An adaptation of the technique samples air through a salicylic acid-impregnated filter paper, followed by extraction into water and analysis for DHBA.[69] Despite its simplicity, the method has a significant drawback, namely that the measured products are also generated by reactions of species other than OH (e.g., O_3), and very large backgrounds are reported.[67] There are very few accounts of its field deployment in the open literature.[66,70] The quoted detection limit is $(3-6) \times 10^5$ molecules cm^{-3}, but for long averaging periods (90 min). In the same study, a comparison was made with the ion-assisted method. The third method involves selective spin-trapping of OH with later determination in the laboratory using either electron spin resonance or gas chromatography/mass spectrometry.[71] An airborne sampling method involving a sampling sheet impregnated with the OH spin trap was developed, with [OH] found to be $< 5 \times 10^5$ molecules cm^{-3} at 10 km, rising to a maximum of 5×10^6 molecules cm^{-3} at 6-km altitude during a campaign in 1980−1981.[71]

5.1.1. Laser-Induced Fluorescence at Low Pressure—The FAGE Technique

The tropospheric OH measurement community has benefited enormously from the OH LIF measurements in the stratosphere pioneered by the Harvard group.[72] Five groups have developed tropospheric field instruments that utilize detection of OH by laser-induced fluorescence at low pressure (see Table 1 and references therein), and a further group has made good progress in the laboratory.[73] The method, known as fluorescence assay by gas expansion (FAGE), was pioneered by Hard and O'Brien in 1979,[74] and after several modifications, has overcome the O_3 interference that plagued early LIF methods. Operation at low pressure (in the range 0.7−4 Torr) reduces the number density of water vapor by ca. 100−1000, and hence the rate of reaction 2, and during the short laser pulse (∼10 ns) very little OH is generated by the laser. Most of the daylight background from sunlight is excluded by the sampling nozzle, and operation at reduced pressure reduces Rayleigh scattering and hence the laser-scattered background signal. Although a reduction in the ratio $[OH]_{artifact}/[OH]_{ambient}$ is achieved, at first glance it might appear that an associated reduction in the OH number density would lead to negligibly small signal levels. However, any reduction in signal through a decrease in the number density of OH in the laser excitation region is compensated by the concomitant increase in the OH fluorescence quantum yield, as the rate of collisional quenching of the OH $A^2\Sigma^+$ state excited by the laser is reduced. The fluorescence lifetime is now several hundred nanoseconds (cf. ∼1 ns at 760 Torr in air), being much longer than the laser pulse. The detector (photomultipliers or microchannel plates have been used) can now be switched off during the laser pulse by electronic gating,[58,75,76] enabling discrimination against the much more intense signal due to Rayleigh scattering, Mie scattering (fluorescence from aerosols), and fluorescence from the walls of the apparatus that exhibits the same temporal characteristics as the laser pulse. It is also possible to discriminate against fluorescence from other molecules that absorb in the same regions as OH (for example, SO_2 and formaldehyde, which have shorter fluorescence lifetimes) by wavelength-selective excitation and the delayed gating of the detector.

The original FAGE design[58] used excitation of the OH (1,0) band at 282 nm, so that the LIF from OH at a longer wavelength could be almost totally discriminated from scattered light. Although the O_3 interference was reduced, a careful modeling study revealed that interference was still significant[44] at the high laser pulse energies used at a low pulse repetition frequency (prf) of 10−20 Hz. The situation improved dramatically through the use of the OH (0,0) band at 308 nm to excite the fluorescence, a scheme now adopted by all groups using FAGE (see Table 1). The detection sensitivity is better as the OH absorption cross-section at 308 nm is ∼6 times higher than that at 282 nm, and the O_3/H_2O interference is about 30 times smaller at 308 nm compared to that at 282 nm (a combination of the lower O_3 absorption cross-section and lower $O(^1D)$ quantum yield). Effective discrimination against scattered light (through gating) is now of paramount importance, as it is at the same wavelength as the fluorescence, also in the (0,0) band at 308 nm. Although the O_3 interference was reduced to below 10^5 molecules cm^{-3}, the detection limit using 308-nm excitation with 10−20-Hz prf lasers was still only a few 10^6 molecule cm^{-3}, even with quite long averaging periods of ∼10 min.[77] The absorption cross-section of OH at 308 nm is very large ($\sigma_{Q1(2)} = 0.94 \times 10^{-16}$ cm^2),[78] and hence the (0,0) transition is easily saturated, and nothing is gained through the use of higher pulse energies—in fact, the ratio of LIF signal to background becomes worse. A key technological breakthrough came with the use of copper vapor pumped dye lasers,[50,79] which provided UV radiation with lower pulse energies at multi-kHz prf. The low pulse energy reduces optical saturation and scattered light, while the high prf provides a more efficient duty cycle and excites more OH fluorescence per second. All groups using FAGE have adopted the 308-nm excitation route, using a variety of laser types. Recently, an all-solid-state Nd:YAG pumped TiS laser made measurements of OH and HO_2 at Mace Head, Ireland,[80] and Nd:YAG pumped dye laser systems have been flown aboard a variety of aircraft.[81,82] Excellent detection limits (see Table 1) at or below 10^5 molecule cm^{-3} have been achieved. However, the high prf comes at a price. Although very little OH is laser-generated and detected within the same laser pulse, any $O(^1D)$ generated during the laser pulse will continue to react with water vapor, producing OH, after the laser pulse, and it is vitally important that this parcel of gas containing laser-generated OH is removed *before* the next laser pulse arrives. At a prf of 10 kHz, this corresponds to only 100 μs, and given that the laser-excitation region extends between several millimeters and several centimeters, a high linear flow velocity is required to provide a fresh sample of gas, and all FAGE instruments are characterized by bulky (and heavy) vacuum pump systems, usually a Roots blower

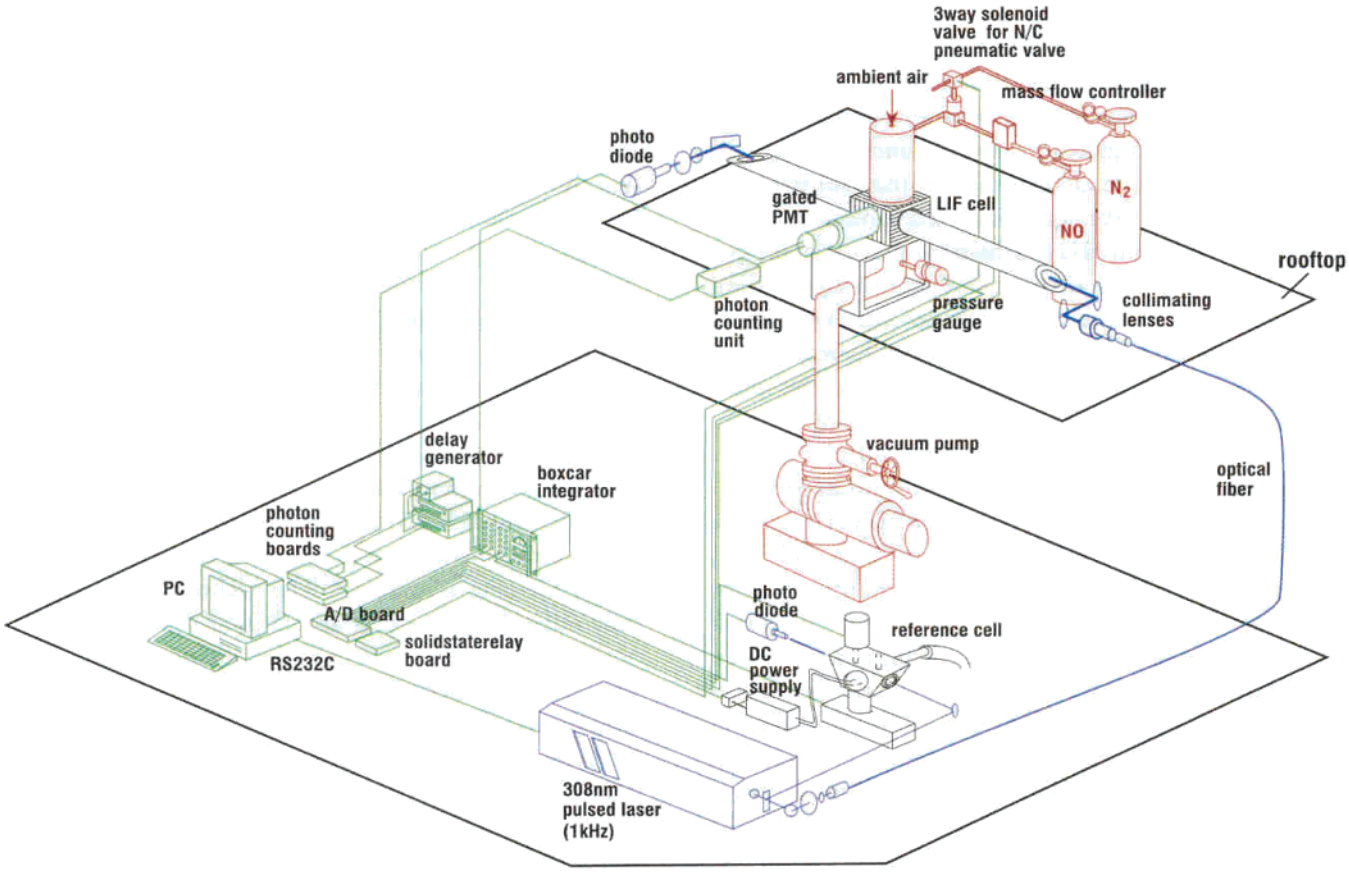

Figure 1. Schematic diagram of the FAGE apparatus operated by the University of Tokyo (researchers now located at the Frontier Research System for Global Change in Yokohama) for the detection of OH and HO_2 radicals in the atmosphere. (Reprinted with permission from ref 31. Copyright 2002 John Wiley & Sons Inc.) In this configuration there is only one ambient sampling cell, and hence OH and HO_2 measurements are made sequentially. Other instruments have either two cells or two optical axes within a single cell to allow simultaneous OH and HO_2 measurements. Common to all FAGE instruments are a high pulse repetition frequency laser and optical delivery system (blue), vacuum pump and gas flow system (red), fluorescence detection and data acquisition system (green), and reference cell (black). The 308-nm laser shown is a frequency-doubled dye laser that is pumped by the second harmonic (532 nm) of a pulsed YAG laser.

backed by a large vacuum pump. The levels of O_3 interference using FAGE at 308 nm have been confirmed in several ways. A chemical modulator (for example, perfluoropropene, C_3F_6),[83] if added to the gas expansion below the sampling nozzle,[75] removes almost all of the ambient OH through addition to the C=C double bond, and any observed OH signal must then originate from a laser-generated source. Earlier methods used hydrogen-containing scrubbing species (for example, isobutane to remove ambient OH),[84] but there is still the potential to generate OH through abstraction of a H atom from isobutane by $O(^1D)$ generated from laser photolysis of O_3. Field measurements performed during the night in clean environments,[85] or during an almost total solar eclipse,[86] or in the lower stratosphere in darkness (O_3 > 200 ppbv) have reported OH levels below the detection limits (determined by calibration; see section 6, below). Laboratory experiments in which flows containing O_3 at known (and sometimes very high) concentration (but with no OH) impinge at the nozzle give an estimation of the level of interference.[75,87] Modeling has also provided an important indicator of the absence of significant interference. The model needs to be able to calculate the time-resolved production of OH in different quantum states during the laser pulse from the $O(^1D) + H_2O$ reaction, and to calculate the fraction of OH LIF signal (integrated over the entire laser pulse) from the quantum state used in field monitoring that originates from laser-generated OH compared to OH that is naturally present. Energy-transfer processes for both the ground and electronically states of OH must be explicitly included. Several approaches have been used,[44,88] such as the use of a master equation.[89]

A detailed comparison of the various FAGE instruments is beyond the scope of this review, and the reader is referred to the references in Table 1 for further details. Figure 1 shows the experimental setup for a FAGE system. Common to all instruments are a gas expansion, a high-prf laser system, a very efficient fluorescence collection system, an electronically gated detector that is operated in photon-counting mode, and a calibration system. The need for a calibration system is a major disadvantage of FAGE, and is considered in section 6 below. Although in principle the sensitivity of the instrument per OH molecule detected can be calculated, it requires knowledge of a wide range of experimental parameters (for example, fluorescence collection efficiency or optical transmission) that are either difficult to calculate or change with time, and so calibration is necessary. All instruments repeatedly scan the laser wavelength from on-resonance with an OH transition

to off-resonance, well away from a transition. Either two discrete wavelengths are used, or the wavelength is scanned continually over an individual rotational transition. This spectral modulation enables the background signal due to laser-scattered light to be subtracted from the OH LIF signal, and improves the signal-to-random noise ratio. Chemical modulation of OH has been used by one group as the background subtraction method in all field measurements,[90] and occasionally by others,[75] to exclude systematic error due to unrecognized interferences, including nonphotolytic sources. Although reduced in magnitude considerably by the sampling nozzle, scattered sunlight at 308 nm will be transmitted efficiently by the collection optics and the narrow-band interference filter used to discriminate against other wavelengths, and forms a continuous background to the pulsed LIF signal that must be subtracted. The sunlight component is determined by counting photons between laser pulses (using a long integration gate to improve statistics) when there is neither LIF nor laser-scattered signal present. At night, when there is no sunlight, the detection limit is lower.

The instrument at Penn State uses a multipass White cell arrangement, designed carefully to avoid beam overlap, to generate a high number of photons from OH fluorescence per laser pulse.[75] The other FAGE instruments use a single laser pass, which, although generating fewer OH LIF photons (for a given laser power), enables superior imaging of the laser-focal volume onto the photocathode of the detector.[84,87,91,92] Both photomultipliers and microchannel plates have been used as detectors to count individual photons. The former have the advantage of higher gain, but can be bulky, and it is more difficult to rapidly switch the gain (requiring the switching of high voltages), although high-performance systems have been developed.[58,75,76] Microchannel plates are smaller and are easier to gate, but are much more expensive and have a lower gain. Recently a new small, compact channel multiplier that offers some advantages of each has been utilized.[80] A variety of sharp-edged pinholes with aperture diameters between 0.4 and 1.2 mm, mounted as part of either a conically shaped skimmer[75,84,87,92] or flatter nozzle assemblies,[75,91,92] have been used to sample the atmosphere from the ground, and the use of different materials suggests that losses on the surfaces of the nozzle are small.[75] The signal levels are extremely small. For [OH] = 1×10^6 molecule cm^{-3}, and using a typical laser prf of 5 kHz, the LIF signal generated for single-pass excitation is only ca. 10 counts s^{-1} (i.e., from 5000 laser pulses). Most laser pulses do not lead to any detected photons from OH LIF! For comparison, the combined background signal from laser scatter and solar scatter at noon is $\sim$50−100 counts s^{-1} (with approximately equal contributions). Without gating of the detector, the laser scatter background signal is very large (thousands of counts s^{-1}), and in some cases may lead to saturation of or even damage to the detector.

The sensitivity of a FAGE instrument depends on a large number of factors, the discussion of which is beyond the scope of this review. Further details concerning these factors for individual instruments can be found in refs 73, 75, 84, 85, 87, and 91−96, which discuss experimental parameters. There are two different subsonic flow regions in the FAGE expansion that have been used for OH excitation. The first is fairly close to the nozzle, directly downstream of the supersonic region, where the flow closely resembles that of a molecular beam. The second region is farther downstream, after the subsonic jet has contacted the cell walls. A considerable period of laboratory development has been necessary for all instruments, paying particular attention to optimization of the cell pressure, nozzle-to-laser axis distance, nozzle diameter, fluorescence collection efficiency (use of large, coated optics), overlap of laser and molecular beams, suppression of laser scatter through the use of baffles and an efficient gating system, and the choice of the rotational transition (the lowest rotational levels are normally excited via transitions in the Q_1 branch). Other factors include the quantum yield of the detector, the delay and width of the gate during which photons are counted (determining the fraction of the fluorescence lifetime that can be recorded), and the laser spectral line width and pulse energy. In some cases, the gas expansion has been carefully interrogated as a function of distance from the nozzle,[92,97] with measurement of rotational temperature and gas density. It is wise to avoid laser excitation close to a shock front with large gradients in density or temperature, and these experiments, when combined with computational fluid dynamics calculations,[84,97] have aided greatly in the design and optimization of FAGE instruments.

Advantages of the FAGE technique include direct excitation of OH following in situ sampling, and excellent sensitivity and selectivity, with no major reported interferences. Several groups have recorded a laser excitation scan of OH present in the atmosphere that agrees well with theoretical spectra, providing compelling evidence that OH is indeed being measured. The Penn State ground-based instrument (GTHOS) has been modified for aircraft operation (ATHOS).[98] Disadvantages of FAGE include the need for a calibration, cost, size and weight (although the lasers are now small, the pumps remain fairly large), and high electrical power usage.

Although not deployed in the field, an alternative laser-pumping scheme deserves mention. A two-photon LIF method that avoids the problem of O_3 interference and offers excellent discrimination from laser-scattered light (e.g., from aerosols) or fluorescence from other species was suggested at Georgia Tech in 1984.[99] OH is first excited to $v'' = 1$ in the ground $^2\Pi_i$ state using a pulsed IR laser at 2.8 μm, and a very short time later it is further excited via the $A^2\Sigma^+ - X^2\Pi_i$ (0,1) band to the $v' = 0$ state of the excited state with a second pulsed laser at 345 nm. Fluorescence is collected in the (0,0) band at 310 nm, as with the FAGE method above, but with three advantages. First, 345 nm is below the energy threshold for any significant $O(^1D)$ production from O_3 photolysis (although there is a small quantum yield due to a spin-forbidden channel,[100] the cross-section is extremely small). Second, the fluorescence

is blue-shifted from either laser pulse, and hence scattered light and nonresonant fluorescence from aerosols is eliminated. Third, measurements are possible at ambient pressure, so that a wall-less inlet may be used. However, despite further development,[47] the method has not been implemented for field work, due to the absence of a suitable pulsed laser source at 2.9 μm. Georgia Tech has developed a two-photon method for the detection of NO, and has flown an instrument on several field missions.[101,102] However, for OH, although the calculated sensitivity is excellent[99] and the method is direct and highly selective, it is difficult to generate IR radiation with sufficient pulse energy to excite a significant fraction of OH to $v'' = 1$, and the requirement for two tunable laser systems is a serious constraint. The advantages over modern FAGE instruments operating at 308 nm are much less than for the early 282-nm versions, but the absence of an expansion (and hence large pumps) is a significant advantage over FAGE. The two-photon method for OH detection has not undergone recent development.

The LIF method has also been used to measure the in situ chemical lifetime, τ, of OH, given by

$$\tau^{-1} = \sum_i [i] k_{\mathrm{OH}+i} \qquad (4)$$

where $[i]$ is the concentration of sink species i (for example, CO, CH_4, VOCs) and $k_{\mathrm{OH}+i}$ is the bimolecular rate coefficient for reaction of the sink with OH. OH is generated from 185-nm photolysis of H_2O vapor within a sliding injector, and is then mixed with ambient air in a flow tube, and its reactive decay is measured by changing the reaction time (moving the injector) before being sampled and detected by LIF. Brune and co-workers have developed a lifetime instrument and made measurements of τ in urban air,[103−105] and an instrument is under development at the University of Leeds.[106] The value of τ can be compared with a calculation that uses the co-located measurements of the concentrations of species i that react with OH, and provides a test of how completely the sinks of OH are accounted for in the model. Care must be exercised in the correct interpretation of the OH decay, as OH can be generated through reaction of HO_2 with NO.[106]

5.1.2. Differential Optical Absorption Spectroscopy (DOAS)

Development of the DOAS method for the measurement of tropospheric OH began in the 1970s in Germany,[107] with the first field measurements in 1975[107] and in the early 1980s.[108,109] The major advantage of an absorption technique is that it is self-calibrating via the Beer−Lambert law,

$$I = I_0 \exp(-\sigma_{\mathrm{OH},\lambda}[\mathrm{OH}]l) \quad \text{or} \quad [\mathrm{OH}] = \ln(I_0/I)/(\sigma_{\mathrm{OH},\lambda} l) \qquad (5)$$

where I_0 and I are the light intensity before and after transmission through the atmosphere, respectively, $\sigma_{\mathrm{OH},\lambda}$ is the absorption cross-section of OH at the wavelength and spectral resolution used, and l is the path length. [OH] is the concentration averaged over the light path. The absolute accuracy of the DOAS method is limited only by the accuracy of $\sigma_{\mathrm{OH},\lambda}$ and l. Although $\sigma_{\mathrm{OH},\lambda}$ is a function of pressure, temperature, and instrumental resolution, the value is known for OH to an accuracy of 7%,[110] and thus DOAS measurements provide a primary standard with which to compare other measurement techniques, as long as the same air mass can be sampled. There is also a general atmospheric absorption, but as this varies smoothly with wavelength, a measurement of I/I_0 from OH alone can be obtained if absorption across an OH rotational line is measured. At atmospheric pressure, the line width of an OH transition, controlled by pressure and Doppler broadening, is very narrow (2.6 pm), and so the light at the end of the optical path must be spectrally resolved at very high resolution (resolving power 500 000) in order to obtain a differential optical absorption. Conventional light sources (for example, Xe arc lamps) do not possess sufficient intensity over such a narrow wavelength range for sufficient return signal to be observed, and hence laser sources must be used. Experimentally, the best achievable I_0/I is ~1.00001−1.000001, but even for $I_0/I = 1.00001$, and using $\sigma_{308} \approx 10^{-16}$ cm^2 molecule^{-1} (the strongest absorption for OH is at 308 nm), a concentration of 10^6 molecules cm^{-3} corresponds to a long path length of 1 km.

Figure 2 shows the experimental setup for a DOAS instrument with a multipass configuration. In earlier designs,[109,111] the long path length was achieved using a well-collimated laser light source and a retroreflector (to reflect the laser beam to a receiving telescope and detector) that were separated by up to 10.6 km (often across a valley). A disadvantage of this approach is the considerable averaging of air masses, and recent designs (as shown in Figure 2) incorporate a multipass arrangement with mirrors separated by 10−40 m,[110,112] between which the laser light passes several hundred times. Alignment of such systems can be difficult, but multipass DOAS systems have proven sufficiently rugged for operation aboard ships.[113]

Measurement of the differential absorption across one or more rotational transitions of OH has been achieved in two ways. In the first, the spectral output of the laser pulse is sufficiently wide that it encompasses the required spectral bandwidth covering several lines. The central laser wavelength is thus kept fixed. The instrument at Fritz Peak[111] used a pulsed XeCl excimer laser at 308 nm, whereas the Jülich instruments used a mode-locked frequency-doubled picosecond pulsed dye laser system, with a Fourier transform limited bandwidth of 0.41 nm (fwhm) at 308 nm.[110,114] The return laser pulse is resolved with a high-resolution spectrograph and an optical multichannel detector, and a spectral range of 0.26 nm is recorded covering six OH absorption lines of the A−X (0,0) transition. This large spectral detection range facilitates the subtraction of interfering absorption signals of other atmospheric trace gases that absorb in the same region, such as SO_2, HCHO, and naphthalene. The short laser pulse and high pulse repetition frequency help to avoid scat-

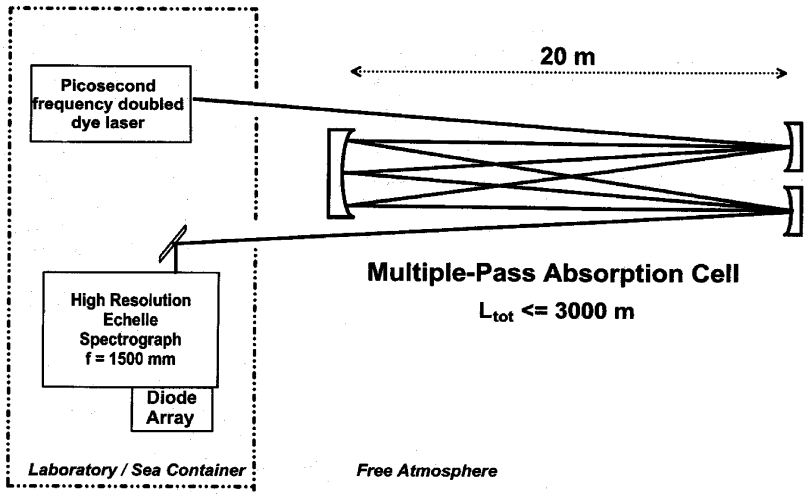

Figure 2. Experimental setup of the folded long-path DOAS system operated by Forschungszentrum Jülich. (Reprinted with permission from ref 110. Copyright 1995 American Meteorological Society.) The optical multiple-reflection cell has a 20-m base length, and the picosecond laser light source and the diode array spectrometer are located in a sea container during field use. Other DOAS systems are similar, utilizing either a multipass arrangement, as shown here, or a single long path with retroreflector.

tering of the return beam by atmospheric turbulence. The spectral profile of the laser must be measured accurately before transmission into the atmosphere, and the wavelength sensitivity of the spectrograph (the pixel-to-pixel variation can be considerable) must also be known, so that any structures from those sources that may overlap the OH lines can be taken into account. The Jülich group have developed a novel method involving Monte Carlo analysis to evaluate the pixel-to-pixel variation.[115] It is important that the laser spectral profiles are uniform from one pulse to another.

The second method to measure a differential absorption spectrum of OH was used by the Frankfurt group. The wavelength of an Ar^+-pumped continuous-wave tunable ring dye laser is rapidly scanned across three rotational transitions of OH. The rapid scanning is achieved using an angle-tuned intracavity etalon, with a wavelength scan of 0.12 nm completed in 100 μs (less than the time scale of atmospheric fluctuations) with a scan repetition frequency of 1.3 kHz.[112,116] It is important that the output intensity of the radiation is constant as the laser is scanned, and this is achieved by using a closed-loop electro-optical modulation system. However, the laser intensity is not completely constant with wavelength, and must be measured and taken into account in the analysis. An advantage of this version of DOAS is that the wavelength dependence of the sensitivity of a spectrograph does not need to be known.

Common to all DOAS methods, and a distinct disadvantage, is the complex and time-consuming numerical analysis of the absorption spectrum necessary to extract OH concentrations. Absorption features from all atmospheric constituents except OH that exhibit narrowband absorption at 308 nm must first be subtracted from the measured absorption spectrum. Atmospheric aerosols absorb the laser radiation, but the change in absorption with wavelength is continuous, and is first subtracted using a polynomial fit. The UV absorption spectra of a number of trace components absorbing at 308 nm must be known at the spectral resolution of the instrument, and are calculated for SO_2, CH_2O, and (under polluted conditions) naphthalene, using laboratory data. Although the absorption coefficients of these species are about 10^4 smaller than those for OH, their atmospheric concentrations can be 10^4–10^5 times higher, leading to absorption structures that mask the weak OH features. Fortunately, water vapor, NO_2, and O_3 do not show any rotational fine structure in this spectral region, and any absorption is taken care of in the polynomial fit. The known interfering absorption features of the other trace gases are subtracted from the measured absorption spectrum using a nonlinear least-squares fitting procedure that uses individual reference spectra and varies the concentrations of SO_2, CH_2O, and naphthalene until the remaining absorption spectrum is closest to a reference spectrum of OH at its atmospheric concentration. The spectral deconvolution procedure generates concentrations of all interfering trace species as well as that of OH itself. A typical root-mean-square noise after deconvolution is 1×10^{-5}.[110,112] Sometimes absorptions due to unknown species also have to be removed, leading to a larger uncertainty.

As can be seen from Table 1, the sensitivity of the DOAS technique is not as good as that for LIF or CIMS, partly because of the interferences from other absorbers that must be subtracted. The averaging time for a given detection limit will depend on the concentration of the interfering absorbers present, as well as the path length. However, the detection limit (2σ) is $\sim 1 \times 10^6$ molecules cm^{-3} with 5 min averaging for a path length of $\sim$3 km,[110,113] enabling full diurnal profiles to be recorded, and with a much higher accuracy than other methods. A concern with the multipass methods is self-generation of OH that causes absorption in subsequent passes of the laser beam. Again, photolysis of ozone followed by reaction 2 poses the greatest threat, but at the low laser powers and beam diameters used, modeling[110] and measurements of OH at night or when the folded long

path is covered have shown interference to be at a level well below detection limits.[112] Although differential absorption methods have been used aboard aircraft for in situ measurements of other species (for example, N_2O, CH_4, and CH_2O), as yet no OH measurements have been attempted, because the distance between the multipass mirrors must be less than 10−40 m, resulting in a very large number of passes. Maintaining alignment of the laser beam in flight through mirror stabilization would be too difficult, and the losses on the mirrors would be higher.

The major advantages of DOAS are the absence of a calibration and the absence of a sampling nozzle/vacuum system (and hence wall losses). The major disadvantages are expensive laser systems, lower sensitivity, complex data reduction procedure, poor spatial resolution (but improved using multipass absorption paths), and not being able to make airborne measurements.

5.1.3. Chemical Ionization Mass Spectrometry (CIMS)

Although methods based on LIF and DOAS are the only two direct OH measurement techniques, nonspectrometric methods are highly desirable, as they will be subject to different interferences and errors. The ion-assisted OH measurement technique uses chemical, rather than optical, properties of OH, and takes advantage of the higher collection efficiency of ions compared to photons, through confinement in electric fields. The method lacks the spectral fingerprint of OH but is more sensitive than either the DOAS or LIF methods. In this real-time method, first developed at Georgia Tech in 1989 (subsequently moved to the National Center for Atmospheric Research, Boulder),[117] but now also used by the German Weather Service[118] and another group at Georgia Tech,[119] OH is converted on a one-to-one basis (titration), and on a time scale (10−20 ms) that is short compared to its chemical lifetime (0.1−1 s), into a molecule that can be readily ionized and detected by selected-ion chemical ionization mass spectrometry. Figure 3 shows the experimental setup for a CIMS instrument. Ambient air is drawn into an atmospheric pressure flow tube reactor, where OH is titrated into isotopically labeled $H_2{}^{34}SO_4$ via the reactions

$$OH + {}^{34}SO_2 + M \rightarrow H^{34}SO_3 + M \quad (6)$$

$$H^{34}SO_3 + O_2 \rightarrow {}^{34}SO_3 + HO_2 \quad (7)$$

$${}^{34}SO_3 + H_2O + M \rightarrow H_2{}^{34}SO_4 + M \quad (8)$$

Reaction 6 is the slowest step, and sufficient $^{34}SO_2$ is added to convert virtually all of the OH in ∼10 ms. The $H_2{}^{34}SO_4$ is ionized at atmospheric pressure by charge-transfer reactions with NO_3^- core ions. The NO_3^- ions are produced in a separate sheath gas containing HNO_3 (rather than ionizing the sampled air directly, which was found to generate a high background signal), and are guided by electric fields into the titrated air sample. The NO_3^- ions are mainly in the form of the cluster $NO_3^-{\cdot}HNO_3$, and

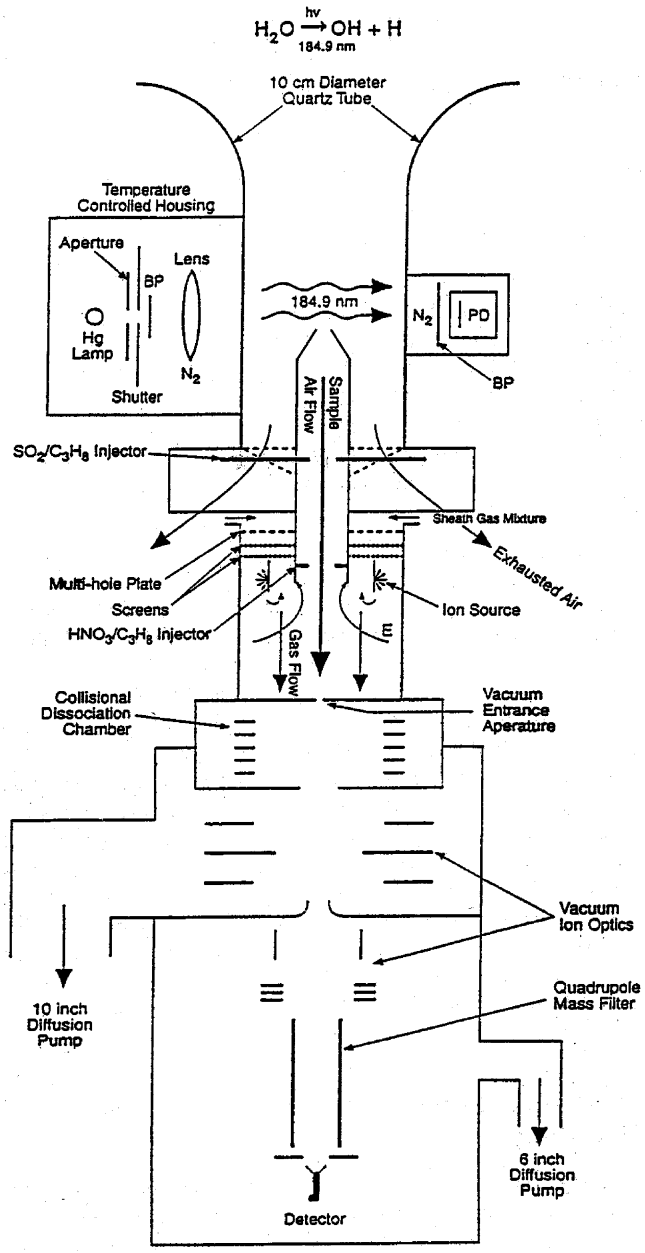

Figure 3. Schematic of the chemical ionization mass spectrometry (or ion-assisted) technique, as deployed by NCAR during the 1993 tropospheric OH Photochemistry experiment. (Reprinted with permission from ref 123. Copyright 1997 American Geophysical Union.) Also shown is the calibration source utilizing 184.9-nm photolysis of ambient water vapor.

react with $H_2{}^{34}SO_4$ to produce $H^{34}SO_4^-$ ions via the reaction[120]

$$NO_3^-{\cdot}HNO_3 + H_2{}^{34}SO_4 \rightarrow H^{34}SO_4^-{\cdot}HNO_3 + HNO_3 \quad (9)$$

The $H^{34}SO_4^-{\cdot}HNO_3$ cluster is fragmented into HNO_3 and $H^{34}SO_4^-$ in a collisional dissociation chamber, and after the flow is skimmed, the $H^{34}SO_4^-/NO_3^-$ ion ratio is measured using a differentially pumped quadrupole mass spectrometer and provides a measure of $[H_2{}^{34}SO_4]$, and hence of [OH].[117,121] The background $H^{34}SO_4^-$ signal resulting from reaction of ambient $H_2{}^{34}SO_4$ is very low due to the small

natural abundance of ^{34}S. Care is taken to ensure adequate mixing (perpendicular injection of the $^{34}SO_2/N_2$ mixture) and that only the central portion of the gas flow away from the walls enters the ionization region. The determination of $[H_2{}^{34}SO_4]$ (and hence [OH]) requires knowledge of the above ion ratio, the reaction time (fixed), and the rate coefficient of reaction 9, and so a calibration is not strictly necessary if these quantities are known. However, the rate coefficient is not accurately known, and so a more accurate calibration of the instrument is performed using a known concentration of OH generated from the 185-nm photolysis of water vapor (see section 6.1 below), a procedure that is also used in the field. The CIMS method is the most sensitive of all OH field instruments, with a detection limit of better than 10^5 molecules cm^{-3} for an averaging time of 5 min.[121,122] As the measurement is not instantaneous, care must be taken that HO_2 present in the atmosphere is not converted to OH (by reaction with NO or O_3) on the time scale of the conversion of OH into $H_2{}^{34}SO_4$, but as the titration is achieved in 10−20 ms, this interference is very small. High-purity propane is added at 100 times the concentration of $^{34}SO_2$, ∼5 cm downstream of the $^{34}SO_2$ injection point. The propane removes any additional OH that may be generated after the initial titration of OH into $H_2{}^{34}SO_4$, for example by recycling from HO_2 and RO_2 by reaction with NO or O_3, or in the ionization region. However, at high NO_x concentrations some regeneration does occur and must be corrected.[123] Propane is also added periodically along with $^{34}SO_2$ at the sample inlet (at about 10 times the $^{34}SO_2$ concentration) in order to remove >98% of OH from the airstream, to enable the background $H^{34}SO_4^-$ ion signal, which has not come from OH titration, to be determined. Interferences from reactions that compete with the relatively slow SO_3/H_2O reaction, the effect of H_2O on the $NO_3^-{\cdot}HNO_3 + H_2SO_4^-$ reaction, and wall losses have all been thoroughly investigated.[121,122] The early instrument required large diffusion pumps, making it unwieldy for aircraft operation, but these have now been replaced by turbomolecular pumps, and the method has been successfully flown on the NASA P-3B[124−126] and C-130[127] aircraft in a variety of missions that sample the boundary layer (see Table 3, below).

5.2. Measurement of Tropospheric HO_2

Although tropospheric abundances of HO_2 are about 100 times higher than those for OH, there have been far fewer determinations of HO_2. Consequently, the quality of HO_2 field measurements is not as well established as for OH. The paucity of HO_2 data is largely because, until very recently, no in situ spectroscopic method with sufficient sensitivity *and* short time response existed. Cavity ring-down spectroscopy, although not sufficiently sensitive for OH detection in the atmosphere, has recently been applied to HO_2 detection in the laboratory, using the A−X band in the near-IR,[128] and perhaps offers promise in the future. Three methods have been demonstrated in the field for detection of HO_2, namely chemical conversion to OH followed by detection of the OH generated using laser-induced fluorescence at low pressure, matrix isolation ESR, and a sulfur-chemistry peroxy-radical amplifier combined with detection via CIMS, which is able to discriminate HO_2 from total peroxy radicals. Table 2 summarizes the detection sensitivity, accuracy, and field deployment of instruments used to measure HO_2. Each is now considered in turn.

5.2.1. Reaction with NO Followed by FAGE Detection of OH

The only method to have been widely used to measure HO_2 is chemical conversion to OH by reaction with added NO, followed by detection of the generated OH using the FAGE technique. As long as a significant fraction of HO_2 can be converted to OH, the signal-to-noise using instruments capable of measuring OH ought to be excellent, as ambient HO_2 concentrations are much higher than for OH, typically ∼100 during the daytime in clean air. If a single fluorescence cell is used, then only sequential measurements of OH and HO_2 are possible, with alternate switching of the NO flow to measure either OH or the sum of OH and HO_2. Both the fraction of HO_2 converted to OH and the sensitivity of the instrument toward OH must be calibrated. As both OH and HO_2 measurements rely on the detection of LIF from OH in the same cell, the ratio $[HO_2[/[OH]$ can be determined with higher accuracy than for OH or HO_2 separately, as the sensitivity of the cell toward OH need not be known (although the effect of NO quenching of the OH LIF signal should be taken into account). However, as OH and HO_2 are short-lived species, measurement of the instantaneous HO_2/OH ratio is desirable, and has been achieved with some instruments through simultaneous measurement of both species, using two detection axes, either in the same cell[129−131] or in two separate cells.[58,59,80,84,93,96,132,133]

A disadvantage of this method is the indirect nature of the measurement, as HO_2 must first be converted to OH prior to spectroscopic detection through the reaction

$$HO_2 + NO \rightarrow OH + NO_2 \qquad (10)$$

and sufficient NO must be added to ensure rapid conversion in the short reaction time between NO addition and the OH excitation region (typically ∼1 ms in the fast flows employed). There is a competing termolecular reaction,

$$OH + NO + M \rightarrow HONO + M \qquad (11)$$

and hence it is not possible to convert all of the HO_2 into OH, and high concentrations of NO must be avoided. The design of the NO injector and its position within the expansion, the NO flow rate, and the operating pressure all affect the fraction of HO_2 converted and must be chosen carefully. Up to 95% conversion of HO_2 into OH has been reported.[75] The bimolecular complex H_2O-HO_2 has been observed experimentally with a dissociation enthalpy of 36 ± 16 kJ mol^{-1},[134,135] and if the temperature is cold enough in the region of the expansion immediately below the sampling nozzle, significant HO_2 radicals

Table 2. Measurement Techniques and Research Groups for Boundary-Layer Detection of Tropospheric HO_2

method	group	limit of detection/ molecules cm^{-3}[a]	time response[b]	1σ uncertainty[c]	field campaigns where instrument deployed[d]	comments	references
$HO_2 \rightarrow OH$ conversion, followed by detection of OH by LIF at low pressure (FAGE)	University of Leeds, UK	5.4×10^5, SNR = 1, 2.5 min	30 s	31%	EASE96, EASE97, AEROBIC, SOAPEX-2, PUMA-1, PUMA-2, PRIME, NAMBLEX	two cells for simultaneous OH and HO_2 measurement	80,91,94,136,184, 185,192,221
	Forschungszentrum Jülich, Germany	9×10^5, SNR = 2, 80 s	40 s	10%	ALBATROSS, BERLIOZ	also deployed on ship, two fluorescence cells, simultaneous OH, HO_2	133,182
	Pennsylvania State University, USA	1.4×10^5, SNR = 2, 30 s[e]	30 s	16%	TOHPE, PROPHET-1, PROPHET-2, SOS-Nashville, TEXAQS, PMTACS-NY (ground); SUCCESS, SONEX, PEM Tropics B, TRACE-P (aircraft)	multipass White cell, also deployed on aircraft, single cell, two optical axes, simultaneous OH, HO_2	75,82,95,98,105, 130,186,222−226
	Portland State University, USA	1×10^6, 6 min	6 min	$\pm 10^6$ molecules cm^{-3}	LAFRS, Pullman	four fluorescence cells, simultaneous OH, HO_2	59,84,90
	University of Tokyo (now Frontier Research, Yokohama), Japan	3.6×10^6, SNR = 2, 1 min (2.1×10^6 without solar scatter)	1 min	24%	ORION, Oki Island, Rishiri Island	single cell, sequential OH and HO_2 data	31,92,227−230, 255−257
matrix isolation electron spin resonance (MIESR)	Forschungszentrum Jülich, Germany	2.5×10^7, 30 min	30 min	2.5×10^7 molecules cm^{-3}	BERLIOZ, Schauinsland		60,61,138,258− 260
RO_x chemical conversion/chemical ionization mass spectrometry (ROXMAS)	Max Planck Institute for Nuclear Physics, Heidelberg, Germany	0.5 pptv	1 min	18%	MINATROC		143
	NCAR	0.5−1 pptv	1 min		TOPSE		144

[a] Defined using eq 34 where possible, giving the SNR (signal-to-noise ratio) if reported, and signal integration period. The detection limit varies from campaign to campaign, and an attempt has been made to quote the best published detection limit for a given instrument while deployed in the field. Detection limits for operation in the laboratory are not given (unless there are no published field deployments). For FAGE instruments, no attempt has been attempted to standardize the detection limit for a given level of solar scattered radiation. [b] Typical time period for which data are reported in the literature. However, the time response of the instrument may be much better than this, e.g., 1 s. [c] 1σ combined precision and accuracy, unless otherwise stated. [d] See Glossary of Field Campaign Acronyms at end of review and Table 3 for details. [e] Detection limit quoted for ground-based instrument. [f] NCAR, National Center for Atmospheric Research. A blank entry denotes unknown performance (in the open literature).

may be scavenged within condensing clusters of water vapor, and may not be available for conversion to OH. In the Leeds instrument, operating at a cell pressure of 0.7−1 Torr, and with a nozzle diameter of 1 mm, rotational temperatures as low as 25 K have been measured for distances of <25 mm from the nozzle. If the NO is added close to this region, the fraction of HO_2 converted to OH is observed to have a strong dependence on the water vapor mole fraction (x_{H_2O}) between $0 < x_{H_2O} < 0.5\%$, but across the ambient range ($x_{H_2O} = 0.5-2\%$) the fraction of HO_2 converted is relatively constant.[91] If the NO is added farther downstream, or if the cell pressure is higher, then the fraction converted becomes larger.[136] Other groups report no such water vapor dependence of the fraction of HO_2 that is converted into OH, probably as a result of operating at higher cell pressures (up to 4 Torr) or by the use of smaller nozzle diameters, which reduces the strong cooling in the region probed by the laser.[92,133]

Care must be taken to ensure that the extra OH signal observed upon the addition of NO originates solely from conversion of HO_2. Organic peroxy radicals, RO_2, also react rapidly with NO via the reaction

$$RO_2 + NO \rightarrow RO + NO_2 \quad (12)$$

but in order to constitute an interference for the measurement of HO_2, RO must be converted to HO_2 via the reaction

$$RO + O_2 \rightarrow HO_2 + R'CHO \quad (13)$$

The rate coefficient for this reaction is small (for R = CH_3, $k = 1.9 \times 10^{-15}$ cm^3 molecule^{-1} s^{-1}), and at the low pressures in the FAGE cell, only a very small fraction of RO is converted into HO_2, which must then react with another molecule of NO to form OH. The insensitivity of FAGE toward RO_2 has been demonstrated by generating a high concentration of an RO_2 species outside the sampling nozzle and observing if there is any measurable OH signal upon the addition of NO,[92,95,133] and also by modeling of the relevant RO_2/HO_2 conversion chemistry.[75,85,95] For CH_3O_2[133] and $C_2H_5O_2$,[92] the detection sensitivity was measured to be only ~5% of the HO_2 value. However, for more complex peroxy radicals (for example, β-hydroxyalkyl peroxy radicals), the corresponding alkoxy (RO) radical is known to decompose rapidly, with some products reacting quickly with O_2 to form HO_2.[137] Further investigation of the possible interference for HO_2 measurements from this class of RO_2 is needed.

A significant HO_2 interference generated in the fluorescence cell in the presence of ozone and water vapor has been observed by one group,[133] and must be subtracted from ambient measurements. The origin of the interfering "dark" source of HO_2 is not understood, but may be the product of a surface reaction.

5.2.2. Matrix Isolation Electron Spin Resonance (MIESR)

First demonstrated in 1978,[60,138] the method of matrix isolation with detection of HO_2 by electron spin resonance spectroscopy is the only direct method for HO_2, and is highly selective. Air is expanded through a supersonic nozzle into a low-pressure region, where it impinges on a coldfinger containing a solid matrix (D_2O ice) at −196 °C. After sufficient material has been deposited, the sample is kept frozen at cryogenic temperatures, and is transferred to the laboratory for analysis. Although the method is direct, the sampling times are long (30 min), and the number of measurements is limited by the number of coldfingers available. Other species can also be analyzed simultaneously from the ESR spectrum: for example, other RO_2 radicals, NO_3 radicals, and NO_2. The method is calibrated with a known concentration of HO_2 radicals generated from the photolysis of water vapor in air (see section 6.1, below). The uncertainty of the MIESR method is given as $\pm 2.5 \times 10^7$ cm^{-3}.[139]

5.2.3. RO_x Chemical Conversion/Chemical Ionization Mass Spectrometry (ROXMAS)

A relatively new method uses a modified chemical amplifier that converts peroxy radicals to gaseous sulfuric acid via a chain reaction with NO and SO_2, with detection of the sulfuric acid by CIMS.[140−143] The method was first developed by the Max Planck Institute in Heidelberg, but has now also been adopted by NCAR.[144] The reaction sequence used is

$$RO_2 + NO \rightarrow NO_2 + RO \quad (14)$$

$$RO + O_2 \rightarrow HO_2 + R'CHO \quad (15)$$

$$HO_2 + NO \rightarrow OH + NO_2 \quad (16)$$

$$OH + SO_2 + M \rightarrow HOSO_2 + M \quad (17)$$

$$HOSO_2 + O_2 \rightarrow HO_2 + SO_3 \quad (18)$$

$$SO_3 + H_2O \rightarrow H_2SO_4 \quad (19)$$

The high sensitivity of CIMS and the low atmospheric background of gaseous H_2SO_4 means that only short chain lengths of 10−15 are required, compared to a chain length of ~200 in a conventional NO/CO PERCA with detection of NO_2 using luminol fluorescence,[145] for which there is a considerable background. The H_2SO_4 is detected by CIMS in the same manner as for OH detection described above.[120] Isotopically labeled $^{34}SO_2$ is not required, as [HO_2] and [RO_2] are much higher than [OH], and so the background H_2SO_4 concentration is much smaller than that generated via the amplifier chemistry via reactions 14−19. The conversion efficiency of RO_2 to HO_2 depends on [O_2], [NO], and [SO_2], and by diluting the atmospherically sampled air with either [O_2] or [N_2] buffer gas, speciated measurements of either RO_2 or HO_2 have been made.[143] If N_2 is added as a buffer, the conversion of RO to HO_2 is suppressed, and the H_2SO_4 mainly stems from ambient HO_2. If O_2 is added as a buffer, the RO-to-HO_2 conversion is favored, and both HO_2 and RO_2 are measured. In HO_2 mode, the RO_2-to-HO_2 conversion is ~25−30%, whereas in RO_2 mode it is ~90%. The method gives good speciation only if CH_3O_2 makes a major contribution to total RO_2. Under other conditions, the

method gives only an upper limit for $[HO_2]$ and a lower limit for $[\sum RO_2]$. Interference from RO_2, generated from thermal decomposition of PAN or HO_2NO_2, was found to be negligible. The method has been demonstrated during the MINATROC[143] and TOPSE[144] field campaigns, although only total peroxy radical concentrations were reported in the latter.[144]

6. Calibration of Instruments

With the exception of methods based on optical absorption that are self-calibrating according to the Beer−Lambert law (eq 5 above), all methods for the detection of OH and HO_2 require calibration to determine the signal observed while sampling a known free radical concentration. Although it is possible, in principle, to calculate the sensitivity of a given field instrument, the result is unreliable, as many assumptions need to be made about instrumental parameters, some of which may vary with time. A very large amount of effort has gone into the calibration of OH field instruments, perhaps the most difficult of all tasks associated with this measurement. The signal, S, generated by the instrument is related to [OH] by

$$S = C_{OH}[OH] \tag{20}$$

where C_{OH} is the calibration constant. Good agreement between C_{OH} obtained in a calibration and one calculated from a knowledge of instrumental parameters implies that the sensitivity of the instrument is well understood. Concentrations of radicals similar to those observed in the field must be generated and made to impinge upon the sampling nozzles of instruments under the same operating conditions of pressure, temperature, and absolute humidity as in the field. Care must be taken to ensure that any loss of radicals between the point of generation and the sampling nozzle is fully understood. It is important that regular calibrations are performed in the field. The accuracy of a field measurement is only as good as the accuracy of the calibration, and much effort has gone into the development of robust methodologies that can easily be set up.

6.1. Photolysis of Water Vapor at 184.9 nm

Only one method is used widely by the HO_x measurement community to calibrate instruments in the field, having been applied to a number of measurement techniques.[92,93,95,123,142,146−149] The vacuum−ultraviolet photolysis of water vapor using a pen-ray mercury lamp is a convenient source of OH radicals at atmospheric pressure:

$$H_2O \xrightarrow{184.9\ nm} OH + H \tag{21}$$

and if photolysis is performed in air (or in N_2 with a small flow of added O_2), HO_2 is rapidly produced:

$$H + O_2 + M \rightarrow HO_2 + M \tag{22}$$

It is highly desirable to perform this calibration in moist air to ensure that the conditions are very similar to those encountered during ambient sampling. In the photolysis region, equal concentrations of OH and HO_2 are generated, and if the degree of loss of OH and HO_2 between generation and sampling is identical (this loss must be known), then equal concentrations impinge on the sampling nozzle, this being particularly convenient for methods that detect both OH and HO_2. The photolysis normally takes place in a flow tube in which the gas flow rate is sufficiently high that chemical or wall losses do not change the radical concentration in the center of the flow tube between production and sampling. If a small flow of CO is added to the calibration gas mix, the OH generated by photolysis is converted to HO_2, and only HO_2 impinges on the sampling nozzle. If a suitable hydrocarbon is added instead, the method can be used to generate a particular RO_2 species.[147] Generation of OH without HO_2 under ambient conditions is possible, but only in the absence of O_2 (e.g., using N_2 as the buffer), but the environment is then not as representative of ambient sampling.

The rate of OH production in the photolysis region is given by

$$d[OH]/dt = [H_2O]\sigma_{H_2O,184.9\ nm}\phi_{OH}F_{184.9\ nm} \tag{23}$$

where σ is the water vapor absorption cross-section, ϕ is the photodissociation quantum yield of OH, and F is the photon flux of the lamp, all at 184.9 nm. $d[OH]/dt$ is equivalent to $d[HO_2]/dt$, as the $H + O_2 + M$ reaction is very fast at atmospheric pressure. Integrating eq 23 yields

$$[OH] = [HO_2] = [H_2O]\sigma_{H_2O,184.9\ nm}\phi_{OH}F_{184.9\ nm}t \tag{24}$$

where t is the photolysis exposure time. The absorption spectrum of H_2O exhibits no structure at 184.9 nm, and the value of $\phi_{OH} = 1$ is well established. There is now agreement across several groups[136,148,150] on a value of $\sigma_{H_2O,184.9\ nm} = (7.2 \pm 0.2) \times 10^{-20}$ cm^2, some 30% higher than earlier recommended values.[151,152] The absolute water vapor concentration is determined with good accuracy using commercial instrumentation, either by a chilled mirror dew point hygrometer, or by IR absorption spectroscopy. The largest error in [OH] comes from F and t, which are difficult quantities to determine accurately. Two approaches have been used. In the first, F is determined absolutely at the center of the flow tube using a phototube that has been calibrated against a known standard, traceable to a National Standard.[95,123] t is calculated from the flow velocity at the center of the flow tube (i.e., that part of the flow sampled by the instrument), requiring knowledge of the volumetric flow rate, the flow tube diameter, and the radial variation in the velocity. In the second method, neither F nor t is measured directly; rather, the product Ft is determined using an O_2 chemical actinometer.[92,93,142,146−149] In air, photolysis of O_2 by the Hg pen lamp leads to

$$O_2 \xrightarrow{184.9\ nm} O + O \tag{25}$$

$$2(O + O_2 + M \rightarrow O_3 + M) \tag{26}$$

where M = O_2, N_2, and the ozone concentration is given by

$$[O_3] = [O_2]\sigma_{O_2,184.9\ nm}\phi_{O_3}F_{184.9\ nm}t \qquad (27)$$

A commercial O_3 analyzer (based on UV absorption) is used to determine [O_3], and if $\sigma_{O_2,184.9\ nm}$ and ϕ_{O_3} are known, Ft can be calculated and substituted into eq 24 to give [OH] or [HO_2]. The ratio of eqs 24 and 27 yields

$$[OH] = [HO_2] = \frac{[O_3][H_2O]\sigma_{H_2O}\phi_{OH}}{[O_2]\sigma_{O_2}\phi_{O_3}} = \frac{[O_3][H_2O]\sigma_{H_2O}}{2[O_2]\sigma_{O_2}} \qquad (28)$$

as $\phi_{OH} = 1$ and $\phi_{O_3} = 2$. Care must be taken when using eq 28 to calculate [OH]. The O_2 absorption spectrum in the Schumann−Runge bands around 185 nm is highly structured, and because of self-absorption by O_2, the value of $\sigma_{O_2,184.9\ nm}$ is dependent on the absorption path length used.[153] $\sigma_{O_2,184.9\ nm}$ also depends on the operating characteristics of the pen lamp itself, as the spectral output is a function of lamp age and operating current, and the spectral profile of the emission is modified as it propagates along the absorption path. The conclusion from several studies[92,93,143,148,149,154] is that the effective cross-section $\sigma_{O_2,184.9\ nm}$ must be measured for the lamp used in the field calibration, and under conditions (e.g., O_2 absorption column) identical to those used in the field. A wide range of [OH] can be generated by varying [H_2O] or [O_3], but as the sensitivity of the instrument may be a function of [H_2O], it is desirable to calibrate as closely as possible to ambient [H_2O]. In the boundary layer, the H_2O mole fraction is usually somewhere in the range 1−3%, but in order to generate [OH] ≈ 10^6−10^7 molecules cm^{-3}, this means that the value of Ft in eq 24 must be very small, and the amount of O_3 generated is well below the detection limits of commercial O_3 analyzers. This problem has been circumvented by establishing a linear relationship between [O_3] and relative lamp flux (measured using a phototube) at high fluxes where O_3 can be easily measured.[133,136] The lamp flux is then attenuated, with either an optical filter or a gas filter of N_2O (while keeping other the operating conditions the same), to generate OH in the range 10^6−10^7 cm^{-3}. The measured relative lamp flux is used to calculate [O_3], from which [OH] can be found. The accuracy of the method is determined largely by the accuracy of the O_3 concentration, and not by the accuracy of $\sigma_{O_2,184.9\ nm}$ (±4%) or $\sigma_{H_2O,184.9\ nm}$ (±3%). Once the linearity of instruments has been established across a wide range of [OH], calibration is normally carried out for a single [OH] concentration at ∼10^8 molecules cm^{-3}.

As both OH and O_3 are generated by photolysis, they exhibit a radial concentration profile across the calibration flow tube. OH is sampled by the field instrument from the center of the flow tube, where the axial velocity is highest, whereas the O_3 concentration is measured in the excess flow that is not sampled by the field instrument, and hence is an average concentration across a range of smaller axial velocities. It is therefore necessary to know the ratio

$$P = [O_3]_{excess}/[O_3]_{center} \qquad (29)$$

For a perfectly laminar profile and uniform lamp flux across the tube, $P = 2$, but as neither of these conditions is necessarily satisfied, the value of P should be measured through measurement of the O_3 radial profile, and has been found to be close to 2 by several groups.[94,133] The P factor is a function of flow tube length and the fraction of the gas flow that is sampled by the fluorescence cell. Other groups have deliberately increased the flow velocity to increase the Reynolds number and generate turbulent flow, resulting in a more uniform velocity flow profile that was verified using pitot tube measurements.[75,95] However, OH wall losses are increased.

As [H_2O] is quite variable in the atmosphere, the H_2O dependence of the instrument sensitivity must be known. Water vapor is known to quench electronically excited OH($A^2\Sigma^+$) at the gas-kinetic rate,[155] and for LIF methods the sensitivity is reduced by ∼10−15% for each 1% mole fraction of water vapor, the precise value being dependent on the cell pressure. However, in some cases, the reduction in OH sensitivity is much greater than this, being a factor of 1.7−2.2 lower at ambient levels of water vapor compared to that found under very dry conditions (<100 ppm).[87,91,132] The explanation may be the scavenging of OH via the formation of weakly bound complexes of OH with water vapor clusters that nucleate in the supersaturated conditions of the cold supersonic expansion. The dissociation enthalpy for the bimolecular complex OH−H_2O has been calculated to be 23.5 kJ mol^{-1}.[135] Very cold rotational temperatures as low as 25 K have been measured close to the sampling nozzle of FAGE expansions,[97] and several complexes of the type OH−M have been characterized spectroscopically.[156,157] The drop in sensitivity for some instruments appears to have been ameliorated by reducing the degree of cooling in the expansion, through the use of higher cell operating pressures or smaller nozzle diameters,[133] or probing away from the very cold region where thermalization to background temperatures has occurred.[92,95]

The systematic error in the calibration varies between groups, but for the Jülich LIF instrument is quoted as ±16% for OH,[133] and is caused by the measurement accuracy of H_2O and O_3, the measurement errors of the absorption cross-sections of H_2O and O_2, and the correction of the water vapor dependence of the LIF detection sensitivity. For aircraft OH measurements, the sensitivity of the instrument as a function of inlet pressure (altitude) must also be calibrated, ideally in flight, and the 184.9-nm photolysis of ambient water vapor (outside the aircraft) is used to generate a known concentration of OH.[158−161] At higher altitudes, where the atmosphere becomes very dry, it becomes difficult to generate sufficient OH above instrumental detection limits.[159,161]

A concern for the HO_x measurement community is the reliance upon a single calibration method, namely the photolysis of water vapor. Some groups have used other calibration methods that are applicable only in the laboratory, and often for OH concentrations many orders of magnitude higher than ambient levels. However, these calibrations are extremely valuable. Two groups have utilized DOAS, with a long-path atmospheric pressure multipass cell equipped with UV lamps to generate OH positioned directly above a FAGE expansion nozzle, to measure the OH concentration that is sampled using laser absorption at 308 nm.[75,92] The absorption path length was ~10−100 m, and so very high [OH], ~10^{11}−10^{12} molecules cm^{-3}, was used, causing problems of signal overload in the LIF cell. Care must be taken to ensure that the OH concentration is uniform across the cell (FAGE can only sample at one point). Although the uncertainty in this calibration method is high (±20−50%), the signal levels were found to be linear with those determined at much lower [OH] using H_2O photolysis.

For FAGE, the internal absolute sensitivity of the instrument (not including inlet losses) can be determined through generation of OH at the pressure of the measurement using the titration reaction,

$$H + NO_2 \rightarrow OH + NO \qquad (30)$$

with H atoms generated in a discharge of H_2. The method was developed for stratospheric OH instruments during the 1970s (using resonance fluorescence[162]) and 1980s (using LIF[50]), and has been applied to FAGE.[75] The method has limited use, however, as the flow regime is different than that during ambient sampling, OH can easily be generated from impurities in the discharge, and the inlet losses, under ambient conditions, which may be significant, are not determined.

6.2. Decay Rate of Hydrocarbons through Reaction with OH

The OH concentration used for calibration can be calculated via the measured loss rate of a hydrocarbon for which the rate coefficient for reaction with OH is known. The method has been used in the field by Portland State University to calibrate a FAGE instrument.[79,84,163] The hydrocarbon, NO, and water vapor are admitted into a continuously stirred tank reactor (CSTR) made of Teflon film that is irradiated by a bank of UV lamps, and which is sampled by the FAGE instrument (away from the walls of the reactor). The mechanism for OH generation is not clearly understood (and is unimportant as long as there are no OH spatial gradients), and the hydrocarbon (1,3,5-trimethylbenzene, TMB) concentration is measured in the chamber in-flow and out-flow by gas chromatography while OH is measured simultaneously by FAGE. The OH concentration is given by

$$[OH] = \left(\frac{[HC]_i}{[HC]_o} - 1\right)/(\tau k) \qquad (31)$$

where k is the rate coefficient for the reaction of OH with TMB (6×10^{-11} cm^3 $molecule^{-1}$ s^{-1}), τ is the chamber residence time (measured by the decay of an unreactive species), and $[HC]_i$ and $[HC]_o$ are the concentrations of TMB in the in-flow and out-flow, respectively. OH concentrations of ~4×10^6 molecule cm^{-3} were generated during illumination, inferred using eq 31. The calibration is time-consuming (>1 h) and the apparatus is quite bulky, and there are a number of questionable assumptions, such as the absence of spatial OH gradients within the CSTR.

6.3. Reaction of O_3 with Alkenes as a Source of OH

The reaction of O_3 with alkenes is recognized as an important source of OH, particularly in forested and urban environments,[164] and the yield of OH, α, from many of these reactions has been measured in the laboratory.[165−171] These reactions offer a convenient source of OH for the calibration of field instruments, as first suggested by Hard et al. in 1995.[84] The OH concentration is governed by competition between production from the O_3/alkene reaction, taking place via several steps, and removal by reactions of OH with the alkene and with O_3 and by OH loss on the walls of the flow tube that is interfaced to the field instrument. The steady-state OH concentration is given by[172]

$$[OH] = \frac{k_{O_3+A}\alpha[O_3][A]}{k_{OH+A}[A] + k_{OH+O_3}[O_3] + k_w} \qquad (32)$$

where A is the alkene species, α is the yield of OH, and k_w is the first-order rate coefficient for wall loss. Measurements of the OH signal at various [A] and $[O_3]$ enables calibration of the instrument's OH response and a measurement of k_w. As [A] becomes large, eq 32 above simplifies to

$$[OH] = \frac{k_{O_3+A}\alpha[O_3]}{k_{OH+A}} \qquad (33)$$

The advantage of this method is that there is no need to measure photon fluxes, effective absorption cross-sections that may be lamp or path length dependent, or flow velocities. Also, the chemical generation and removal of OH gives a more uniform radial profile compared with photolysis. The accuracy of the method (±43%)[172] is dependent on uncertainties in kinetic data and $[O_3]$, measured using a commercial analyzer. The precision is given as ±8%.[172] Two groups have developed this method for the calibration of OH field instruments that use the FAGE technique,[172,173] and in one case have shown good agreement with the H_2O photolysis method.[173]

6.4. Other Methods

A continuous O_3/H_2O calibration, requiring simultaneous measurement of ambient O_3 and H_2O, was developed by Georgia Tech for the calibration of the aircraft two-photon LIF technique.[47] A second laser system is required to photolyze O_3 to generate $O(^1D)$, which subsequently reacts with H_2O to generate OH.

As mentioned in section 6.1, this method has not been widely adopted. The generation of OH via the $H + NO_2 \rightarrow OH + NO$ reaction, with H atoms generated in a discharge of H_2, is commonly used a source of OH at low pressure, but is not suitable for the calibration of field instruments that sample atmospheric pressure.

7. Sensitivity of Instruments and Lower Detection Limits

It is difficult to accurately compare the sensitivity of different instruments. The sensitivity of an instrument is the signal generated, be it absorbance, photon counts, or ion counts, per molecule of the species that is being detected. The sensitivity is the value of C, as defined in eq 20. The lowest concentration of a particular species that can be measured, often called the limit of detection (LOD), or minimum detectable concentration, $[X]_{min}$, is a balance between the sensitivity and the magnitude/variability of the background signal.

For DOAS instruments, the sensitivity depends on the OH transition chosen and the optical path length, whereas the background depends largely on the detector noise. $[OH]_{min}$ depends on the ability to distinguish structured absorption due to OH at different wavelengths from detector noise. The diode array pixel-to-pixel variability can make the measurement of very weak absorptions difficult. For the LIF method, the sensitivity depends on many factors, a discussion of which is outside the scope of this review, including laser power, the fluorescence collection efficiency, and the detector sensitivity. The background signal is from laser-scattered light, scattered solar radiation, and detector noise (dark count), all of which must be suppressed as much as possible. The background-limited minimum detectable concentration, or LOD (using OH as an example), is given by[75,87]

$$[OH]_{min} = \frac{SNR}{C_{OH}}\sqrt{\frac{S_{back}}{t}\left(\frac{1}{m} + \frac{1}{n}\right)} \qquad (34)$$

where SNR is the required signal-to-noise ratio at the detection limit, C_{OH} is the sensitivity (signal counts per second observed per OH molecule), S_{back} is the total background signal counts per second, t is the measurement time (seconds), m is the number of OH measurements (of duration t), and n is the number of background measurements (also of time t). The square-root term is the standard deviation of the background signal, and can be lowered by increasing the measurement time t. A lower $[OH]_{min}$ can also be achieved by making repeated measurements of the OH signal *and* the background, each of duration t. The total measurement period to achieve a given $[OH]_{min}$ is $T = (m + n)t$.

Tables 1 and 2 list the lower detection limits for field instruments for the measurement of tropospheric OH and HO_2, respectively, using, where possible, the same integration period and SNR. The tables also show the uncertainty of the measurement. As can be seen, for OH detection, the lower detection limit for the DOAS method is inferior to other methods, but the uncertainty (accuracy) is superior.

8. Intercomparisons

Confidence in a measurement technique will be raised considerably if it can be demonstrated to give the same OH (or HO_2) concentration as measured by a second instrument based on a fundamentally different technique, while sampling at the same location. In this section, we give examples from the (rather limited) intercomparisons that have taken place thus far. Measurements of OH and HO_2 made at the same time and location using two or more completely different methods are extremely rare, yet such a comparison of the data in different environments is the *best* method to validate the methodology used, and to demonstrate to the atmospheric chemistry community the reliability of OH measurements. Accurate measurements of OH are essential to provide robust modeling of atmospheric chemistry. The NASA Chemical Instrumentation Test and Evaluation (CITE-1) intercomparisons in 1983 (ground-based) and 1984 (aircraft) established that two LIF instruments and a ^{14}CO instrument were, at that time, not able to measure OH reliably in the atmosphere.[174] More recent intercomparisons have been more successful, but none of these have been formally blind intercomparisons, when the groups involved are not aware of each other's findings prior to submission of datasets. Care must be taken to take into account any differences in spatial resolution of the instruments that may lead to sampling of different air masses, and also differing integration periods. In this section, we review ground and airborne intercomparisons.

8.1. Ground-Based OH Intercomparisons

There have been four intercomparisons during field deployments. In July−August 1991, an informal intercomparison took place in the Rocky Mountains at Fritz Peak, Colorado, between the NOAA long-path DOAS instrument and the Georgia Tech SICI-MS instrument.[175−177] There were six days of good overlap, although the intercomparison was complicated by the local in situ and long-path (10.3 km, average 120 m above a forested valley) nature of the two techniques. The in situ measurements were made at the retroreflector end of the long path. On clear days there was generally good agreement, becoming worse under cloudier conditions.

During the 1993 Tropospheric OH photochemistry experiment (TOHPE), an extensive intercomparison was carried out, again at Fritz Peak. Four instruments were deployed to measure OH during the campaign, but only two, the NOAA DOAS and Georgia Tech CIMS instruments, performed well enough to enable a meaningful comparison.[178] The derived OH concentrations agreed within error limits ($\pm$30%, 2σ) over half of the time, and a quarter of the time disagreement could be explained by differences in concentrations of trace gases (for example, NO_x) that control the OH abundance over the long path and at the in situ site. Overall, the long-path

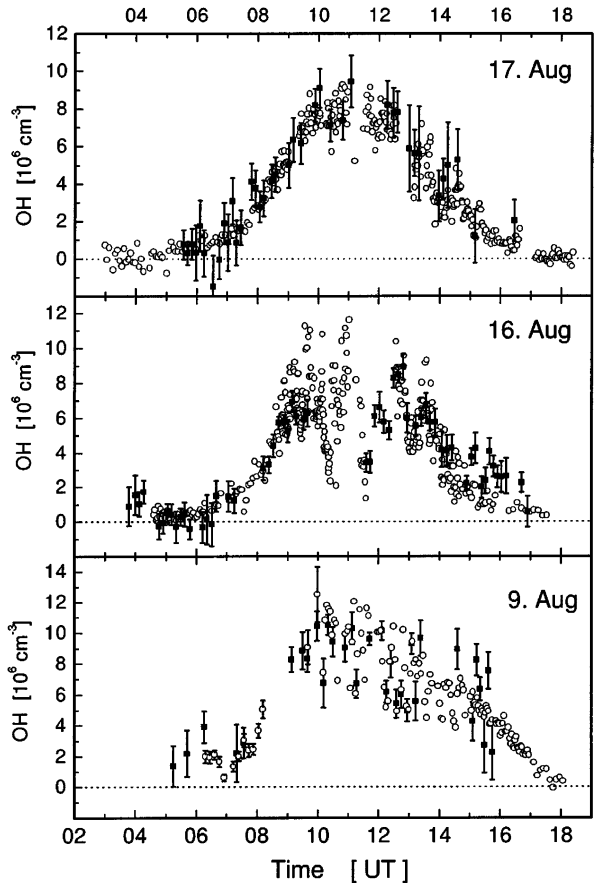

Figure 4. OH intercomparison during the 1994 POPCORN field campaign. Diurnal concentration profiles of OH measured by FAGE (○; scaled by a factor of 1.09) and DOAS (■) on August 9, 16, and 17, 1994. Local noon is 11:17 UT. (Reprinted with permission from ref 179. Copyright 1998 Kluwer Academic Publishers.)

instrument measured OH concentrations ~20% higher than the ion-assisted in situ instrument under clean and clear conditions, with an r^2 correlation value of 0.62. A subsequent change in the accepted value of $\sigma_{185\,nm}$ for water vapor, relevant for the calibration of the CIMS instrument, brought the two sets of data into even better agreement, reinforcing the importance of the need for accurate calibration methods. The intercomparison of the FAGE instrument with the CIMS instrument was not as good, mainly due to poor performance of the dye laser.[95] TOHPE showed that OH measurements in the troposphere could be performed with good accuracy.

In situ OH measurements by laser-induced fluorescence at low pressure (FAGE) and folded long-path absorption (DOAS) were carried out during the POPCORN campaign, held in a clearing in a cornfield in rural northeast Germany in August 1994.[148,179,180] Both instruments were developed and operated by Forschungszentrum Jülich, and the extensive OH dataset allowed an intercomparison of relative diurnal profiles and simultaneously measured absolute concentrations, as shown in Figure 4. The distance between the multipass mirrors of the DOAS instrument was 38.5 m, and most of the time both instruments sampled the same air and agreed well in the measured relative diurnal variations. Only for a few points did the measurements significantly disagree, and this was attributed to a perturbation of the DOAS measurements by a local OH source (possibly electrical sparking by the motor of a vacuum pump). Both instruments clearly demonstrated their specificity of OH detection by the measurement of ambient air spectra which unambiguously identified OH by its spectral signature. The mean detection limit for the LIF instrument was 5×10^5 molecules cm^{-3} (SNR = 2, 60 s measurement time), with a calibration accuracy of ~16%, compared to a mean DOAS detection limit of 1.5×10^6 molecules cm^{-3} (SNR = 2, 200 s integration time), with an uncertainty of only 7%. There was a reasonably large dataset (195 overlapping data pairs, each with specified measurement errors), and a detailed statistical analysis (neglecting 58 points for data from the rogue wind sector) yielded a correlation coefficient of $r^2 = 0.81$ and a weighted linear fit with a gradient of 1.09 ± 0.04, with LIF concentrations being lower on average by 9%. Thus, 80% (r^2) of the DOAS variance is explained by the LIF variance, and the scatter of the data points around the regression line (not shown) is explained by the imprecisions of the DOAS and LIF instruments. The systematic errors in the OH instruments are time-invariant, such as the uncertainties in the absorption cross-sections used in DOAS and in the LIF calibration. The systematic errors produce no variance but influence the slope of the regression line (not shown). The OH detection sensitivity of the LIF instrument changed several times during the campaign, due to modifications of instrumental operating parameters, but had no influence on the level of agreement with the DOAS measurements.

The apparent excellent agreement between the instruments during POPCORN, as initially reported,[180] was brought into question by a change in the value of the recommended absorption cross-section for O_2 at 185 nm, which changed the calibration constant of the LIF instrument.[154] However, upon further analysis, the absorption cross-section for H_2O at 184.9 nm that had previously been used was also found to be incorrect,[148] and fortuitously, this brought the value of $\sigma_{H_2O}/\sigma_{O_2}$ to 5.8, close to its originally used value of 6.25.[180] Of the intercomparisons undertaken thus far, the POPCORN study is the clearest demonstration that both DOAS and LIF have reliably detected OH in the atmosphere. The good accuracy of the DOAS method recommends it as a primary standard for intercomparisons.

An informal intercomparison took place at a clean-air site near Pullman, in eastern Washington state, USA, in Oct−Nov 1992, and involved a FAGE instrument operated by Portland State University (PSU) and a ^{14}CO radiocarbon instrument operated by Washington State University (WSU).[181] OH concentrations were close to the detection limits for both instruments, but very long signal integration periods were necessary (30−60 min in the case of FAGE), and there was only overlap of 22 data points on two days. The correlation coefficient for the two measurements was high ($r^2 = 0.74$); however, the slope of the regression line (WSU/PSU) was 2.9, showing either that the two instruments are not measuring the same

OH or there is a serious discrepancy in the calibration.

OH was measured by DOAS and LIF during the ALBATROSS campaign that took place aboard the R/V Polarstern, which sailed from the north to the south Atlantic during Oct−Nov 1996. The DOAS measurements were compared to the calculations of a simple chemical model and published by Brauers et al.,[113] but the comparison between the methods has not yet been published in the open literature,[182] and so is not discussed further here. During the PARFORCE-2 1999 campaign at Mace Head, on the west coast of Ireland, OH was measured by a CIMS instrument operated by the German Weather Service,[118] and a joint attempt was also made to measure OH using the salicylic acid method (see section 5.1, above) by York University (Ontario) and the MPI for Chemistry at Mainz.[67] Unfortunately, the latter method did not produce any reliable data, and hence no intercomparison was possible.

8.2. Aircraft-Based OH Intercomparisons

A very exciting experiment took place over the tropical Pacific Ocean during the 1999 Pacific Exploratory Mission (PEM) Tropics B campaign. Measurements of OH were made by a CIMS instrument, operated by NCAR aboard a P-3B aircraft,[124] and also by a FAGE instrument operated by Penn State aboard a DC-8 aircraft.[160] The two techniques and inlet geometries are very different, and so the chances of common interferences or calibration errors are minimized. The experiment was not a direct intercomparison, as the aircraft did not fly wing-tip to wing-tip; rather, the two aircraft sampled the same location at the same altitude, but at different times (but only ~1 h different in some cases). In the marine boundary layer, there was exceptionally good agreement between the two aircraft's OH measurements, while for a comparison at 5.5 km (FAGE/CIMS OH ratio of ~1.5), the concentration difference was, on average, similar to the uncertainty in the OH measurement for each instrument.[125]

In March and April 2001, the NASA DC-8 and P-3B aircrafts flew within ~1 km of each other on three occasions during the TRACE-P campaign in order to intercompare similar measurements on the two aircraft in clean air in the western Pacific.[183] OH was measured on the DC-8 and P-3B using the FAGE and CIMS techniques, respectively. There are significant discrepancies, but the error bars are quite large. Although both OH instruments tracked changes in OH production associated with changes in NO_x and $J(O^1D)$, a plot of the CIMS versus FAGE OH data gave a constrained fit of slope 1.5 (within combined uncertainties). A calibration problem associated with these measurements was suggested—not surprisingly, given the difficulty of calibrating these instruments in flight. A direct HO_2 comparison was not possible, although the sum of HO_2 and RO_2 was measured on the P-3B using CIMS, and so with some assumptions about the HO_2/RO_2 ratio, an indirect HO_2 comparison was made.[183]

8.3. HO_2 Intercomparisons

There has only been one intercomparison of HO_2 measurements made in the atmosphere, performed during the 1998 BERLIOZ campaign near Berlin. HO_2 was measured at a common sampling height of 8−10 m using the MIESR technique and by conversion to OH with detection by LIF.[139] There was excellent agreement between the two methods: a plot of $[HO_2]$(LIF) versus $[HO_2]$(MIESR) yielded a slope of 1.03 ± 0.08 and an intercept of 0.15 ± 0.47 ppt (errors are 1σ). For the 15 data points, the correlation coefficient was $r^2 = 0.88$.

HO_2 (measured either by chemical conversion with NO/FAGE or by MIESR) and RO_2 (measured by the PERCA method or by MIESR) have been measured simultaneously at several field sites under a variety of conditions.[139,184−186] The RO_2/HO_2 ratio provides a probe of the different HO_x production mechanisms, and is an important target parameter for models, but as comparison is not made of the same species, these results are not discussed in this review. During the aircraft TRACE-P campaign, HO_2 was measured using chemical conversion with NO/FAGE, and RO_2 by chemical conversion/CIMS (with some capability for discrimination of HO_2 from total peroxy radicals), and hence some comparison was possible.[183] Despite the higher atmospheric concentration relative to OH, there have been far fewer measurements of HO_2, largely because HO_2 cannot be detected directly using a sensitive optical method, and further intercomparisons of this species in the field are badly needed. For detection by LIF after conversion with NO, HO_2 is easier to measure compared with OH as the signal-to-noise is higher, but there is a greater relative difficulty in the accurate calibration of HO_2 concentrations. With the advent of large daylight simulation chambers (for example, the EUPHORE chamber at Valencia and the SAPHIR chamber at Jülich), there is an opportunity for the intercomparison of OH and HO_2 instruments while observing the same, but artificial, atmosphere. As long as sampling conditions are similar to the real atmosphere, these chambers will allow intercomparisons over extended periods, and they are beginning to be used for this purpose.

[**Note Added in Proof.** Ren et al. (*J. Geophys. Res.* **2003**, *108*, 4605) report a recent intercomparison of HO_2 at a rural site using FAGE/NO conversion and chemical conversion/CIMS (in HO_2 mode). Diurnal variations of HO_2 agreed to within about 40%.]

9. Field Measurements of OH and HO_2 Radicals

Table 3 lists the major field campaigns since 1991 in which measurements of OH and/or HO_2 were made, and includes information on the dates, location (with altitude and terrain type), and types of instruments deployed. Only ground-based field campaigns and aircraft campaigns with significant periods spent in the boundary layer are included. The chemistry of HO_x radicals in the upper troposphere was recently reviewed by Jaegle et al.,[187] and contained a synthesis of measurements from the STRAT (ER-2), SUCCESS (DC-8), and SONEX (DC-8) missions (see Glossary for acronyms). In this review, space does not permit

Table 3. Major Campaigns since 1991 in Which Field Measurements of OH and/or HO_2 Were Made in the Troposphere[a]

campaign or acronym[b]	year	dates	location			type of environment	platform	OH	HO_2	comments	references
			place	lat.	long.						
Fritz Peak	1991	July−Aug	Fritz Peak Colorado, USA	40°N	105°W	forested	ground	CIMS, DOAS		2687-m altitude, intercomparison	175,176
Schauinsland	1991	late summer	Schauinsland/Black Forest, Germany	48°N	8°E	continental	ground	DOAS	MIESR	548-m altitude	112,260
MLOPEX-2	1992	April−May	Mauna Loa, Hawaii, USA	20°N	156°W	free-troposphere	ground	CIMS		3400-m altitude	121,245,261
Taunus	1992	Sept	Taunus mountains, Germany	50°N	8°E	continental, rural	ground	DOAS		825-m altitude	112,116
Pullman	1992	Oct	Pullman, Washington, USA	47°N	117°W	continental, rural	ground	LIF, ^{14}CO		intercomparison	84,181
SCATE	1993	Feb	Palmer Station, Antarctica	65°S	64°W	coastal MBL[c] (on rock)	ground	CIMS			262
TOHPE	1993	Aug−Oct	Fritz Peak and Idaho Hill, Colorado, USA	40°N	105°W	forested	ground	CIMS, DOAS, LIF, scrubbing	LIF	2687−3070-m altitude, inter-comparison	66,70,95,123, 178,186,201, 242,244,263
LAFRS	1993	Sept	Claremont California, USA	33°N	117°W	polluted urban	ground	LIF	LIF		90
Izana	1993 1994	Aug−Sept May	Izana Station, Tenerife	28°N	16°W	free troposphere	ground	DOAS		2368-m altitude	112,234,240
POPCORN	1994	Aug	Pennewit, Germany	54°N	12°E	continental, rural	ground	LIF, DOAS		intercomparison	93,132,148, 154,179,232, 233,264
WAOSE95	1995	June	Weybourne, UK	53°N	1°E	coastal MBL	ground	DOAS			236,241
ACE-1	1995	Oct−Dec	out of Hobart, Tasmania	various	various	MBL and free/ upper troposphere	aircraft P-3B	CIMS		measurements in clouds	158,159,265
SUCCESS	1996	April−May	western continental USA	various	various	BL and upper troposphere	aircraft DC-8	LIF	LIF	in and around clouds and contrails	82,223
EASE96	1996	July−Aug	Mace Head, Ireland	53°N	10°W	coastal MBL	ground	LIF	LIF		91,184,266
ALBATROSS	1996	Oct−Nov	North and South Atlantic	68°N−50°S	various	open ocean MBL	ship	LIF, DOAS	LIF	aboard ship R/V Polarstern	113,182
PEM Tropics A	1996	Aug−Oct	Christmas Island, Kiribati	various, Central Pacific	various	MBL and free/ upper troposphere	aircraft P-3B	CIMS			126,203,267
EASE97	1997	Apr−May	Mace Head, Ireland	53°N	10°W	coastal MBL	ground	LIF	LIF		185,221
AEROBIC	1997	July−Aug	Pertouli, Greece	40°N	21°E	forested	ground	LIF	LIF	1180-m altitude	94,192
PROPHET-1	1998	August	Pellston, Michigan, USA	46°N	85°W	forested	ground	LIF	LIF		130,210,225
BERLIOZ	1998	July−Aug	Pabstthum, Germany	53°N	13°E	rural and urban plume	ground	LIF	LIF, MIESR	intercomparison	133,139,212, 258,268
Oki Island	1998	July/Aug	Oki Island, Japan	36°N	133°E	coastal MBL	ground		LIF		227−230,255
PARFORCE-1	1998	Sept	Mace Head, Ireland	53°N	10°W	coastal MBL	ground	scrubbing			67
ISCAT-1	1998−1999	Nov−Jan	South Pole, Antarctica	90°S	102°W	ice sheet	ground	CIMS		2837-m altitude	248,269
SOAPEX-2	1999	Jan−Feb	Cape Grim, Tasmania	41°S	142°E	coastal MBL	ground	LIF	LIF		136
PEM-Tropics B	1999	March−Apr	tropical Pacific	various	various	MBL and free/ upper troposphere	aircraft P-3B and DC-8	LIF, CIMS	LIF	intercomparison	124,125,224, 267,270

Table 3. (Continued)

campaign or acronym[b]	year	dates	location			type of environment	platform	OH	HO_2	comments	references
			place	lat.	long.						
PUMA-1	1999	June	Birmingham, UK	53°N	2°W	polluted urban	ground	LIF	LIF		
PARFORCE-2	1999	June	Mace Head, Ireland	53°N	10°W	coastal MBL	ground	CIMS			118
SOS-Nashville	1999	June−July	Cornelia Fort, Nashville, Tennessee, USA	36°N	88°W	polluted urban	ground	LIF	LIF		104,131
PRIME	1999	July−Aug	Ascot, UK	51°N	1°W	polluted urban	ground	LIF	LIF	OH measurement during solar eclipse	86
BAYSOFI	1999	August	Hohenpeissenberg, Germany	48°N	11°E	continental, rural	ground	CIMS		980-m altitude, OH measurement during solar eclipse	252,253
ORION	1999	Aug	Okinawa Island, Japan	27°N	128°E	coastal MBL	ground	LIF	LIF		31,227,228, 255
PUMA-2	2000	Jan−Feb	Birmingham, UK	53°N	2°W	polluted urban	ground	LIF	LIF	winter campaign	
Rishiri Island	2000	June	Rishiri Island, Japan	45°N	141°E	coastal MBL	ground	LIF	LIF		31,256
MINATROC	2000	June−July	Monte Cimone, Italy	44°N	11°E	continental, rural, free troposphere	ground		CIMS	2165-m altitude	143
SONTAS	2000	June−July	Simcoe, Southern Ontario, Canada	50°N	94°W	rural continental	ground	scrubbing			67
PROPHET-2	2000	July−Aug	Pellston, Michigan, USA	46°N	85°W	forested	ground	LIF	LIF		
ISCAT-2	2000−2001	Nov−Jan	South Pole, Antarctica	90°S	102°W	ice sheet	ground	CIMS	CIMS		
TOPSE	2000	Feb−May	USA, Canada, Arctic	various	various	above remote continental and ice sheet	aircraft	CIMS	CIMS		144 127
HOPE	2000	June−July	Hohenpeissenberg, Germany	48°N	11°E	continental	ground	CIMS		980-m altitude	250
HAFEX	1998−2000	Apr98−Aug00	Hohenpeissenberg, Germany	48°N	11°E	continental	ground	CIMS		long-term study, 980-m altitude	251
TEXAQS	2000	Aug−Sept	Houston, Texas, USA	29°N	95°W	polluted urban	ground	LIF	LIF		
TRACE-P/ACE-Asia	2001	Mar−April	Western Pacific	various	various	mainly above Pacific ocean	aircraft P-3B and DC-8	LIF, CIMS	LIF, CIMS		183
PMTACS-NY	2001	June−Aug	New York City, USA	41°N	74°W	polluted urban	ground	LIF	LIF		105,226
PROPHET-3	2001	Jul−Aug	Pellston, Michigan, USA	46°N	85°W	forested	ground	CIMS			119
MINOS	2001	August	Finokalia Station, Crete, Greece	35°N	26°E	coastal MBL	ground	CIMS			249
NAMBLEX	2002	July−Sept	Mace Head, Ireland	53°N	10°W	coastal MBL	ground	LIF	LIF		80

[a] Table includes all ground- and sea-based measurements, together with aircraft measurements that sampled the boundary layer, but does not include aircraft campaigns that primarily sample the upper troposphere or stratosphere. For a review of OH and HO_2 measurements in the upper troposphere, see Jaegle et al.[24] For a review of stratospheric field campaigns in which OH and HO_2 were measured, see Heard.[33] As a general rule, campaigns are listed only where a full suite of supporting measurements were made, enabling a modeling comparison to be undertaken. [b] See the Glossary of Field Campaign Acronyms given at end of the review. [c] MBL, marine boundary layer. A blank entry indicates that measurements of this species were not made.

a detailed discussion of all the field campaigns included in Table 3, nor a comparison of OH and HO_2 measured in different environments. Instead, representative campaigns are chosen to illustrate the behavior of OH and HO_2 radicals in three types of chemical environments, and how well observed concentrations agree with the calculations of numerical models. The choice of campaigns is purely personal, and we regret that it has not been possible to discuss many interesting and important findings from other field campaigns. The three boundary layer environments we discuss are classified as (1) unpolluted marine, (2) forested continental, and (3) polluted urban.

9.1. Comparison of Modeled and Measured Concentrations of OH and HO_2

Modeling is generally conducted in parallel with field measurements. The models provide a means of understanding the key processes governing radical production and loss and, for example, ozone and PAN formation. A wide range of chemical mechanisms has been used, ranging from the explicit master chemical mechanism[188,189] to condensed (reduced or lumped) mechanisms, such as the regional atmospheric chemistry model (RACM).[190] The main assumption made in the intercomparison of modeled and measured OH and HO_2 is that the radicals are sufficiently short-lived that they are transported over negligible distances during their lifetimes. Thus, provided all longer-lived species that affect the concentrations of these radicals are measured in the same location as the radical measurements, a zero-dimensional box model can be used, with the concentrations of the longer-lived species constrained to their measured values. There are a number of issues. The radical lifetimes are ~1 s for OH and ~100 s for HO_2, and transport distances can be significant, especially for HO_2, even in moderate winds. Any local concentration inhomogeneities can, therefore, lead to difficulties. Care is also needed to ensure collocation of all relevant measurements. It is also increasingly recognized that meteorological measurements must also be made to characterize the dynamical state of the boundary layer in the measurement region. For most of the campaigns discussed here, this issue was addressed, at best, in a limited way. Other issues involve the need to measure all relevant species concentrations, photolysis rates, etc. This requirement can generally be met in clean environments, but is much more difficult in polluted locations; for example, it is not generally possible to measure all VOCs, or even hydrocarbons.[191] Another significant problem associated with VOC measurements is poor time resolution, compared with the good time resolution usually achieved for free radicals, NO_x, ozone, and $J(O^1D)$. This problem is especially important for oxygenated hydrocarbons. These compounds either can be transported to the measurement site or are generated photochemically in situ, leading to rapid temporal variation in their concentrations, and can act either as sources of OH and other free radicals through photolysis or as a sink through reaction with OH. Finally, heterogeneous effects can be significant and often represent a substantial source of uncertainty in radical loss processes, because of inadequate knowledge of uptake coefficients or of the nature of the aerosol surface or of the aerosol size distribution.

9.1.1. OH and HO_2 Observations in the Unpolluted Marine Boundary Layer, and Comparison with Models

The marine boundary layer has been the subject of a large number of field campaigns, largely as it is a location where pristinely clean air can be sampled that has had little or no perturbation due to anthropogenic activity, and the chemistry of the "natural" atmosphere can be interrogated. The majority of observations have been made at the coast (SCATE, WAOSE95, EASE96, EASE 97, PARFORCE, Oki Dogo, Okinawa, Rishiri, SOAPEX-2, NAMBLEX, MINOS). Only the shipborne ALBATROSS and selected airborne campaigns (ACE-1, PEM Tropics A, B, TRACE-P) have sampled in the boundary layer from above the open ocean in remote areas. In this section, we review OH measurements from the SOAPEX-2 campaign, held at Cape Grim, Tasmania, in January−February 1999.[136] We compare these briefly to those taken during the ALBATROSS campaign, held aboard the R/V Polarstern in the tropical Atlantic Ocean in 1996, and the PEM-Tropics A and B campaigns, held above the remote Pacific Ocean in 1996 and 1999. For all three campaigns, a comparison with model calculations has been performed, and the insights obtained are reviewed, together with a discussion of the major processes that control the rates of production and destruction of OH and HO_2.

Their short lifetimes ensure that OH and HO_2 are essentially in steady state and so can be linked to the time-dependent measured concentrations of the longer-lived species via algebraic equations. Unfortunately, because of the nonlinearities introduced by peroxy−peroxy reactions, the steady-state equations can rarely be solved analytically, except by approximation, and numerical methods are necessary. Under these conditions, it is often just as easy to solve the full time-dependent differential equations.

Comparisons were made of the measured [OH] and [HO_2] from the SOAPEX-2 campaign with results from a zero-dimensional box model, in which the concentrations of longer-lived species were constrained to measured values. The model was constructed using a procedure developed by Carslaw et al.[184,185,192] and was based on the master chemical mechanism (MCM). The MCM contains mechanisms for the oxidation of 125 primary emitted species and contains a good deal of redundancy unless it is tailored for a particular campaign, especially in a clean environment such as that at Cape Grim. The measured concentrations of non-methane hydrocarbons (NMHCs), CO, and CH_4 were used to define a reactivity index (RI) with OH, based solely on loss of OH by reaction with NMHCs, CH_4, and CO. The RI is the fractional loss of OH with a specific species, averaged over a day. It was found that the whole campaign could be accurately represented by including reaction schemes from the MCM for only the following NMHCs: ethane, propane, ethene, propene, *trans*- and *cis*-2-butene, 1-butene, *trans*- and *cis*-

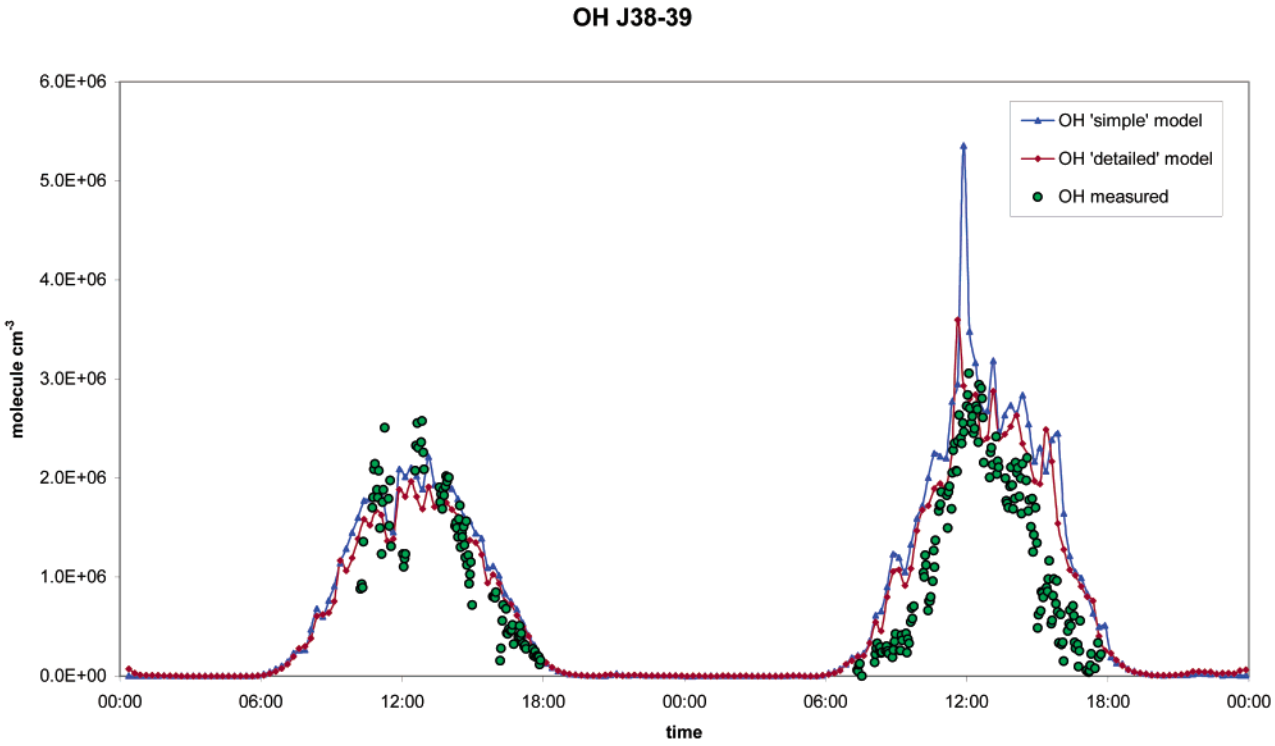

Figure 5. OH measurements recorded using a FAGE instrument on February 7−8, 1999, at Cape Grim, Tasmania, during the SOAPEX-2 campaign, together with box model calculations using a simple (inorganic, CO, CH_4 chemistry only, 95 reactions) and a more detailed (inorganic, CO, CH_4, 23 non-methane hydrocarbons, 5107 reactions) chemical scheme from the master chemical mechanism (version 3).

pentene, ethyne, isoprene, 1,3-butadiene, dimethyl sulfide, benzene, and toluene. Together with CO and CH_4, these species accounted for over 99% of the OH loss, even on the most polluted days. Since OH reacts also with NO_2 and secondary species such as HCHO, it is clear that this procedure provides a chemical mechanism that sufficiently accounts for OH chemistry. Under baseline conditions, which are of concern here, air masses arriving at Cape Grim contained very low concentrations of VOCs, and CO and CH_4 accounted for most of the OH loss (>92%), with the highest 16 NMHC species in the RI contributing only 5% to the OH loss.

On these baseline days, [NO] and [NO_2] were low (~2 and 10 ppt, respectively), while daily averages of other species were as follows: [O_3] ≈ 15−20 ppb, [CH_4] ≈ 1690 ppb, [CO] ≈ 40 ppb, and HCHO ≈ 200 ppt. Figure 5 shows a comparison between modeled and measured [OH] for February 7 and 8, 1999 (days of year 38 and 39). Slightly less good agreement was obtained on days 46 and 47, with the model overestimating the mid-day concentrations by 20−30%. A correlation plot (measured vs modeled [OH]) for all four baseline days gave $r^2 = 0.84-0.87$. Model/measurement agreement was less good for HO_2 than for OH. No measurements of HO_2 were made on days 38 and 39, but in comparisons made on days 46 and 47, the model returned mid-day concentrations roughly 70% greater than the measurements. Since no aerosol surface area measurements were made in the SOAPEX-2 campaign, the effect of incorporating uptake on aerosols was investigated using a value of the reactive aerosol surface area of 1.0×10^{-7} cm^{-1}, representative of the clean marine boundary layer.[193] It was found that good agreement could be obtained between measurements and model if the accommodation coefficient for HO_2 was equated to unity. This remains simply an observation and in no way rationalizes the model/measurement comparison, although it is worth noting that the accommodation coefficient for HO_2 varies substantially with aerosol type.[194] Aerosol uptake has little effect on [OH], either directly, because of the short atmospheric lifetime of OH, or indirectly through HO_2, because of the limited regeneration of OH from HO_2 (see below).

Two methods of global sensitivity analysis were employed to assess the model, the Morris one-at-a-time (MOAT) analysis and a Monte Carlo analysis with Latin hypercube sampling.[195] The MOAT analysis is an efficient screening method that provides a means of ranking the significance of both observables (e.g., constrained concentrations) and parameters (e.g., rate coefficients) in the calculation of a model output [OH] and [HO_2]. Since it is a global method, it allows for and provides a measure of the importance of interactions between model parameters, but does not provide specific information on which interactions are important. It has clear advantages over local methods, because of the inherent nonlinearity of the chemical kinetics involved in atmospheric oxidation. The MOAT analysis demonstrated the importance for OH of the $J(O^1D)$ measurements and of the rate parameters for O^1D with H_2O and N_2, and for HO_2 of the measurements of [HCHO] and of $J(HCHO \rightarrow 2H + CO)$. Carslaw et al.[184] had previously commented on the sensitivity of OH to the rate coefficient for $O^1D + N_2$ and its associated large uncertainty in an analysis of the 1996 EASE campaign at Mace Head, Ireland. Recent measurements at Georgia Tech, NOAA, and the University of Leeds

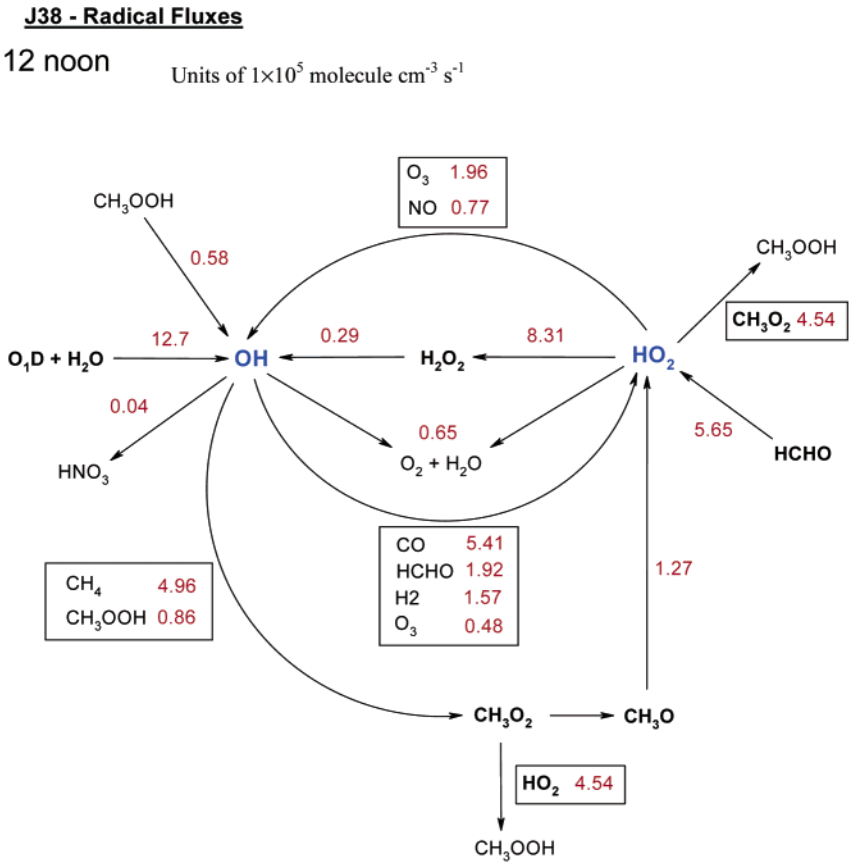

Figure 6. Rates of reaction (in units of 10^5 molecules cm^{-3} s^{-1}) in the SOAPEX-2 campaign at Cape Grim, Tasmania, on February 7, 1999, at 12:00 noon.

have slightly revised the rate coefficient and significantly reduced its uncertainty.[196] The new values were used in the SOAPEX-2 model, and the MOAT analysis emphasizes the dependence of [OH] on this parameter. The HO_2 results reflect the importance of HCHO photolysis as a radical source. Our poor understanding of the mechanism of formation of HCHO (see below) emphasizes the importance of the HCHO measurements but also stresses a significant deficiency in the chemical model.

The Monte Carlo analysis was used to determine the overall model uncertainty and gave 2σ values of 30−40% for OH and 25−30% for HO_2. The measurement uncertainties were 40% for OH and 50% for HO_2.[136] These results emphasize the quality of the agreement between model and measurement for OH: there is overlap of model and measurement for HO_2 when the uncertainties are included; however, the consistency of the model overestimate suggests a significant discrepancy. A statistical measure of the quality of the model/measurement comparison over a whole campaign is needed.

Figure 6 shows a reaction flux diagram for noon on day 38, which guides understanding of the chemical mechanism under very clean conditions. Reactions of OH with NMHC are not included, and the rates of each of the main reactions are shown on the diagram in units of 1×10^5 molecules cm^{-3} s^{-1}. Photolysis is the major initiation mechanism, with photolysis of both ozone and formaldehyde providing the main routes to radical formation. Termination occurs almost exclusively via $HO_2 + HO_2$ and $HO_2 + CH_3O_2$. Propagation reactions of OH are dominated by reaction with CH_4 and CO, with minor contributions from HCHO, H_2, O_3, and CH_3OOH. The low concentration of NO results in only limited formation of NO_2 in the propagation cycle, and regeneration of OH from HO_2 occurs primarily via reaction with O_3 rather than NO. Because significant initiation occurs via both OH and HO_2, the analysis of the chain characteristics are complex,[197] but a rough measure of the chain length can be obtained from the ratio of the rate of formation of OH via propagation (from HO_2) to the rate of initiation (or termination). The value obtained is 0.14, demonstrating the inefficiency of the chain cycle. The chain cycle itself leads to a net loss of O_3 at mid-day, but this is overshadowed by its loss by photolysis. For the reactions shown, the total rate of OH production (16.3×10^5 molecules cm^{-3} s^{-1}) is slightly higher than its rate of destruction (15.89×10^5 molecules cm^{-3} s^{-1}) because several minor reactions that remove OH (for example, OH + H_2O_2 and HONO) are not included in the analysis.

The HCHO concentration is surprisingly high and cannot be accounted for by methane chemistry under the conditions pertaining at Cape Grim. Ayers et al.[198] suggested that isoprene might act as a source, but this cannot explain [HCHO] on day 38, because the measured isoprene concentrations were so low (≤2ppt). The source of HCHO on day 38 is not evident, but it clearly plays an important role, especially in radical initiation.

The approach used in the interpretation of the SOAPEX-2 campaign, and also in the EASE 96 and

97 campaigns at Mace Head in western Ireland, is similar in principle to earlier investigations, although it employed a more detailed chemical mechanism. Poppe et al.[199] examined the results of the Dueselbach (1983), Schauinsland (1984), and Jülich (1987, 1988) campaigns using the regional acid deposition model (RADM2)[200] mechanism, finding generally good agreement between measured and modeled [OH] (within 20%, with the model overestimating). McKeen et al.[201] used the mechanism of Lurmann et al.[202] for a comparison with [OH] measurements in the TOHPE campaign in Colorado. The model overestimated the measurements by 50%, and the authors suggested that an unmeasured biogenic hydrocarbon was present that acted as a sink for OH. The concentrations of NO were much higher than those found at Cape Grim, so that feedback to HO_2 and hence to OH was much more efficient because of the faster peroxy + NO reactions. As a result, [OH] shows a much weaker dependence on the total VOC concentration than reciprocal first power, because of the contribution to OH formation from HO_2 + NO. McKeen et al.[201] were consequently forced to require that reaction of the unkown biogenic hydrocarbon with OH generated HO_2 as a product through the normal propagation cycle, but instead of conversion back to OH, there was significant loss of HO_2 radicals via, for example, scavenging by aerosol. Even so, concentrations of ~2 ppbv of the unknown biogenic were required.[201]

The model/measurement comparison of [OH] in the tropical Pacific boundary layer during PEM Tropics A[203] provides an interesting comparison with the SOAPEX-2 results. The campaign took place near Christmas Island, Kiribati, and the comparison relates to OH and other measurements made on the NASA P-3B aircraft.[126] The model used was that developed by Crawford et al. in 1999.[204] Excellent agreement was found for OH, with the model lying only 15−20% below the measured values and well within the combined uncertainties. [HO_2] was not measured. There are very close parallels between the reaction rates calculated for this campaign and those shown in Figure 6. The percentage contributions of the main OH formation reactions were $O^1D + H_2O$ = 81% (78%), $HO_2 + O_3$ = 5% (12%), $HO_2 + NO$ = 4% (5%), and $CH_3OOH + h\nu$ = 2% (4%), with the SOAPEX-2 results shown in parentheses. The major difference was the importance of H_2O_2 photolysis, which contributed 8% of the total (vs 2% in SOAPEX-2). The dominant OH sinks were CO = 34% (34%), CH_4 = 27% (31%), and CH_3OOH = 11% (5%). The major difference in the two sets of results relates to the significance of HCHO as a radical source. HCHO was not measured in the P-3B flight in PEM Tropics A and is not quoted as a significant HO_x source, while it contributes 30% of the total HO_x sources in SOAPEX-2. This discrepancy emphasizes the importance of a better understanding of the HCHO budget. HCHO was measured during the PEM Tropics B campaign, and included in a photochemical box model for comparison with OH and HO_2 measurements made aboard the DC-8 using FAGE.[160] HCHO photolysis was a significant HO_x source at higher altitudes, but for z < 1 km accounted for < 5%.[160] However, HCHO photolysis accounted for 10−20% of HO_2 production. Altitude profiles of the average $[OH]_{model}/[OH]_{meas}$ for different geographical regions in the tropical Pacific showed that, in the boundary layer (z < 1 km), the model overpredicted OH in all regions, with $[OH]_{model}/[OH]_{meas} \approx 1.3-2$.

During the ALBATROSS cruise in the southern Atlantic between 5°N and 40°S, with NO < 20 pptv and CO < 80 ppbv, a comparison was made between DOAS-measured OH (6% accuracy) and the predictions of a 27- reaction steady-state model based on $CO-CH_4$ chemistry only.[113] The model included peroxide and HCHO photolysis, together with their reaction with OH. On average, there was a model overprediction of ~17%,[205] within the combined measurement/model uncertainties. The mole fractions of HCHO were relatively high, but a change of ±30% in the HCHO concentration changed the modeled OH by only 3%.

9.1.2. OH and HO_2 Observations in Forested Continental Regions, and Comparison with Models

Some of the most unusual behavior of OH and HO_2 radicals has been observed in forested regions, remote from any major urban sources, but subject to elevated concentrations of biogenic hydrocarbons, such as isoprene and monoterpenes. These species, although they react with OH very rapidly (the rate coefficient for OH + isoprene is close to the gas kinetic limit), can also be a source of OH and HO_2 through their reaction with ozone, proceeding via the Criegee mechanism.[206,207] In this section, we review the behavior of OH and HO_2 observed during the PROPHET campaigns, held in a deciduous forest in Michigan, USA, and also the AEROBIC campaign, held in a fir forest in the Pindos mountains of northern Greece, together with model comparisons. The chemical composition and also the local meteorology within and above the forest canopy are complex.

The main biogenic hydrocarbons found in these campaigns were isoprene and the monoterpenes. Isoprene emissions increase with both solar flux and leaf temperature, while monoterpene emissions show little light dependence.[208] Atmospheric concentrations of isoprene consequently peak during the day, while the monoterpenes peak at night, when their main removal mechanism, reaction with OH, is slow. Isoprene reacts very quickly with OH, leading to formation of the carbonyl compounds methyl vinyl ketone and methacrolein. Isoprene chemistry leads to substantial radical production, both from the direct, rapid, primary chain and from photolysis of secondary aldehydes and especially HCHO.[209] Terpenes also react quickly with OH, but their high night-time concentrations mean that their slower reactions with O_3 become important. Ozone reacts with alkenes to form a Crieege biradical, which can generate OH on decomposition,[206,207] together with carbonyl compounds. Thus, ozone + monoterpene reactions provide a potential night-time source of OH. While the chemical mechanism for isoprene oxidation is quite well understood, the experimental base for monoterpene oxidation is much less secure.

A measurement campaign in a forested region in northwestern Greece provides an illustration of the impact of biogenic hydrocarbon emissions on the chemistry. Carslaw et al.[192] analyzed four days in detail, which had mid-day [NO] and [NO_2] in the range 60−100 ppt and 1−3 ppb, respectively, and [O_3] ≈ 80 ppb. A wide range of biogenic compounds were observed. Construction of the chemical mechanism from the MCM was based again on the reactivity index approach. For the whole campaign, OH loss by reaction with primary NMHCs, CO, and methane was dominated by isoprene, which accounted for ∼60%, while ∼20% of OH reaction occurred with monoterpenes. Limonene was the dominant monoterpene sink for OH, with contributions also from α- and *β*-pinene, camphene, sabinene, carene, *p*-cymene, 1,8-cineole, and terpinene. Ninety-seven percent of OH loss via primary species could be accounted for by adding CO, CH_4, C_2H_4, C_3H_6, and *i*-C_4H_8. At the time of the analysis, α-pinene was the only monoterpene included in the MCM. The other monoterpenes were incorporated in the mechanism by initial reaction with OH, O_3, and NO_3, scaled according to the rate of reaction with each individual monoterpene. The subsequent degradation was then modeled using the α-pinene mechanism. The detailed consequences of this substitution are hard to assess, although there are mechanistic similarities between limonene and α-pinene in their reactions with both OH and O_3. The high night-time concentrations of the monoterpenes results in their domination of night-time OH loss. While the model calculations show nonzero night-time concentrations, OH and HO_2 were not measured at night, because of experimental difficulties, although significant concentrations of both were measured in the late evening. The following discussion, in consequence, focuses on the daytime chemistry.

The measured mid-day [OH] (averaged over the period 11:00−15:00) was in the range (3−6) × 10^6 cm^{-3} over the four days with sufficient ancillary data for analysis. [HO_2] showed much more substantial variation over the range (0.4−6.1) × 10^8 cm^{-3}. Interestingly, the modeled [OH] values, which were in the range (1.0−1.7) × 10^6 cm^{-3}, were *lower* than the measured values, with mid-day ratios in the range 0.6−0.16, in contrast with most other analyses of boundary layer measurements. The measured and modeled HO_2 comparison was much more variable, with the model considerably overestimating [HO_2], by factors of 15 and 5, on the days when the measured [HO_2] values were lower. There was better agreement on the days when the measured [HO_2] values were higher, with modeled-to-measured ratios of 0.6 and 1.3. The origin of these discrepancies is not clear. A sensitivity analysis for both [OH] and [HO_2] showed that they are comparatively insensitive to changes in NMHC concentrations. Changes in NMHC concentrations in the model by a factor of 2 resulted in changes to the radical concentrations of only 2−14%, reflecting the considerable buffering of the radical concentrations by the chain mechanism, as was found in TOHPE.

The reaction mechanism provides an interesting contrast with that for Cape Grim. Initiation via OH occurred through both ozone photolysis (∼60%) and O_3 + isoprene and monoterpenes (∼40%), while HO_2 formation involved a wide range of carbonyl intermediates. Termination was dominated by peroxy−peroxy radical reactions, but [NO] was sufficiently high to ensure that the propagation cycle was maintained, with substantial regeneration of OH from HO_2 and a chain length of ∼0.7. Interestingly, over 50% of the OH loss occurred through reaction with secondary species generated in the degradation of isoprene and the monoterpenes (or strictly the α-pinene surrogate). The net ozone production rate over the four days peaked at 20 ppb h^{-1} and occurred primarily in the morning because of the diurnal variation in [NO].

Model measurement comparisons under conditions of high biogenic VOC concentrations have also been reported by Tan et al.[129] and by Sillman et al.[210] for OH and HO_2 at Pellston, Michigan, during the PROPHET 1998 campaign. The site is in a deciduous hardwood forest, with a FAGE fluorescence cell positioned atop a 31-m tower, 10 m above the forest canopy, and separated from the laser (housed on the ground) via an optical fiber. The Tan et al. analysis used a simple box model, while the Sillman et al. analysis used a 1-D model to examine the effects of vertical transport. The Tan et al. study[129] was based on the RACM chemical mechanism,[190] but with more detailed chemistry for isoprene, α-pinene, and limonene oxidation. Sillman et al.[210] used a mechanism adapted from that of Lurman et al.[202] A shortcoming during PROPHET was the absence of measured photolysis frequencies. $J(NO_2)$ was calculated from an Eppley radiometer positioned at the site, but other *J* values were calculated using the Madronich algorithm[211] and scaled to a UV-B instrument located 3 km distant. The uncertainty in the model is estimated to typically a factor of 2.6 for OH and a factor of 2.1 for HO_2. Figure 7 shows 24-h averaged OH and HO_2 concentrations, measured during the PROPHET-1 campaign (1998), together with model calculations.[210] The models both generate daytime [OH] a factor of ∼2.7 lower than the measured values, while the modeled [HO_2] was about 30% higher than measured. Both radicals were measured at night, when quite high concentrations were found ([OH] ≈ 0.04 ppt, [HO_2] ≈ 2−3 ppt).[130] The model was able to reproduce these concentrations if half of the night-time monoterpenes consisted of species that react rapidly with O_3, such as α-terpinene, in contrast to more slowly reacting species such as α-pinene; however, the calculated [HO_2] + [RO_2] was much higher than that observed.

Sillman et al.[210] investigated the atmospheric chemical significance of the high night-time [OH]. They found that the high concentrations were limited to a shallow surface layer (0−25 m) and that the rapid simulated decrease in isoprene concentration with altitude arose principally from vertical dilution. Measurement of concentrations of both radicals and VOCs as a function of altitude within the night-time boundary layer would be of greater value in testing

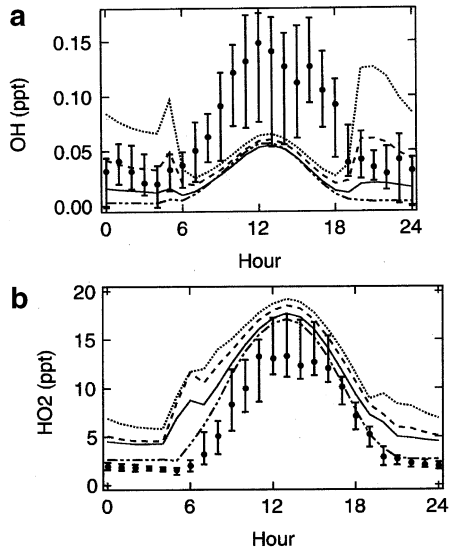

Figure 7. OH (a) and HO_2 (b) versus time of day measured at Pellston, Michigan, USA, during the PROPHET summer 1998 campaign, compared with model values. Measured values represent the hourly mean (●) and upper and lower 67th percentiles (vertical bars). Models are for standard scenario (solid line), scenario in which 50% of emitted terpenes are represented by fast-reacting species (dashed line), scenario for 100% of emitted terpenes represented by fast-reacting species (dotted line), and scenario with zero terpenes (dashed−dotted line). (Reprinted with permission from ref 210. Copyright 2002 American Geophysical Union.)

this result. Two further PROPHET field campaigns have taken place at the Pellston site. At the first, in summer 2000, OH and HO_2 radicals were again measured by LIF on top of the 30-m tower, with results similar to those obtained during the campaign in 1998. However, during the summer 2001 campaign, OH was measured at 30 m using a CIMS instrument from Georgia Tech.[119] Although similar daytime OH values were observed compared to the previous campaigns (being higher than model predictions), typical OH night-time values were below the instrument detection limit (3×10^5 molecules cm^{-3}),[119] inconsistent with the previous FAGE measurement.[130] These results may indicate a systematic difference between the two techniques that needs further investigation.

9.1.3. OH and HO_2 Observations in Polluted Urban Environments, and Comparison with Models

Despite 90% of the human population residing in large cities, there have been only a very small number of field campaigns in urban environments where OH and/or HO_2 concentrations have been measured. One reason for this is that, until recently, instrumentation was not sufficiently advanced to measure a large enough number of trace gas species to accurately define the budget of OH and HO_2 for the complex chemical environment typical of urban centers. With the advent of instruments to measure real-time oxygenated VOCs, as well as a larger number of hydrocarbons, and also the actinic flux spectrum, so that the photolysis frequency of any desired species can be measured (subject to laboratory spectroscopy information being available), the models are beginning to become sufficiently constrained for a meaningful comparison with OH and HO_2 measurements to be made. In this section, we review the PUMA campaigns, made in summer 1999 and winter 2000, close to the city center of Birmingham, UK, and also the BERLIOZ (Berliner Ozonexperiment) campaign, which under some conditions sampled the plume from Berlin in the summer of 1998.

The chemistry in an urban environment becomes complex because of the large numbers of emitted VOCs. Most of these are hydrocarbons, but oxidation leads to the production of significant concentrations of oxygenated compounds, which are important both in the propagation reactions, through reactions with OH, and in radical production chemistry through photolysis. The major difficulty lies in the measurement of time series for such a vast range of compounds. The problems arise for compounds above C_8; progress is being made in the use of comprehensive (2-D) chromatography,[191] although the technique has not been widely applied in field campaigns. For hydrocarbons, some progress can be made through the use of speciated emissions inventories, scaling concentrations using the measured species and assuming that local sources dominate. It is much more difficult for secondary species. Concentrations can be generated using chemical models, but the long lifetimes of the species demand models which incorporate atmospheric transport. One approach is to assume that the chemistry is invariant with location and to simulate the carbonyl chemistry using a box model, iterating each day or set of days until the concentrations converge. Such an approach assumes that the atmospheric composition at the monitoring site is the same as that in the advected air parcel for a time period which is long compared with the lifetime of the carbonyl compound. An alternative approach is to use a trajectory model. The difficulties here relate to the realistic representation of emissions and the initialization of the trajectory. One simplifying feature of urban chemistry is the dominance of linear termination, especially via $OH + NO_2$, but also through nitrate formation for the larger peroxy radicals. Under these conditions, peroxy−peroxy radical reactions are unimportant.

Model measurement comparisons in a polluted environment, with high concentrations of anthropogenic NMHC and NO_x, are exemplified by intriguing summer and winter experiments during PUMA in Birmingham, UK. The surprising result, as shown in Figure 8, which parallels the night-time measurements in Pellston, was the observation of high [OH] in winter, despite the low light intensity: the ratio of $J(O^1D)_{summer}/J(O^1D)_{winter}$ was ~15 at local solar noon, while the corresponding ratio $[OH]_{summer}/[OH]_{winter}$ at solar noon (where OH peaks in both cases) is only ~2. For HO_2, the corresponding value of $[HO_2]_{summer}/[HO_2]_{winter}$ was closer to unity. Clearly, non-photochemical initiation processes are important. Figure 9 shows comparisons between OH measurements and models. A reaction rate analysis led to the following main conclusions:

1. The reactions between ozone + alkenes provided the major winter source of OH, with a rate that was

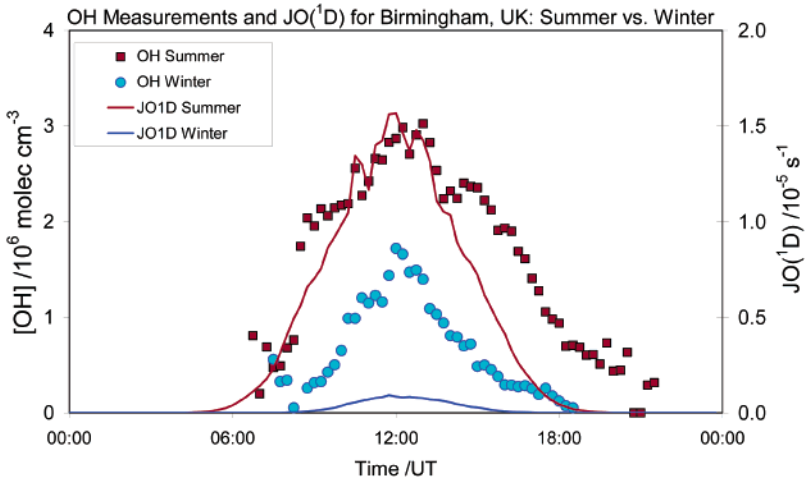

Figure 8. Diurnal variation of OH for the summer 1999 and winter 2000 PUMA campaigns, held at the University of Birmingham, UK, together with the corresponding variation of the rate of O_3 photolysis, $J(O^1D)$. Each point represents a 15-min time interval, and the concentration shown is the average of all values recorded for a given campaign during that time interval (summer 14 days, winter 11 days). The OH concentration in winter is much higher than expected from O_3 photolysis alone.

25 times larger than that of $O^1D + H_2O$. Note that the model gives a nonzero OH profile at night, although no measurements were made.

2. HO_2 and RO_2 formation from carbonyl photolysis was significant, even in winter, and carbonyls also acted as a significant co-reactant with OH in the propagation cycle.

3. The high $[NO_x]$ ensures that termination is dominated by HNO_3 and organic nitrate formation and that peroxy radicals react primarily with NO, thus sustaining the chain cycle. Thus, a chain length of ~3 was found, much longer than the values found in the SOAPEX-2 and AEROBIC campaigns.

This observation of the importance of secondary chemistry, as source of both radicals and OH co-reactants, is significant and reflects related calculations. It also points to a problem and a potential source of substantial uncertainty in the constrained box modeling approach. There were measurements of very few oxygenates in the PUMA campaign, and so the model has to rely on calculated concentrations; indeed, the model shows that, in addition to HCHO, a very wide range of species together contribute significantly to the secondary chemistry. The problems associated with such calculations have been noted above. There have recently been substantial improvements in experimental techniques for measuring oxygenates in the field, which will provide crucial information in future OH measurement model comparisons. The recent NAMBLEX campaign at Mace Head (see Table 3) on the west coast of Ireland used such techniques, and they are proving essential to the analysis, even under quite unpolluted conditions.

No attempt was made in these modeling studies to investigate the vertical distribution of [OH], or of the OH precursors, so that the significance of the high winter-time OH to processing of VOCs in the boundary layer has not been assessed.

Platt et al.[139] have reported model/measurement comparisons for the BERLIOZ campaign in 1998, which relates to experiments 50 km from Berlin. Most of the radical species (OH, HO_2, RO_2, NO_3) were measured using more than one technique. A box model based on the MCM was used both to make the comparisons and to examine the principal chemical processes. July 20 was examined in particular detail, when high NO_x conditions ($[NO_2] \approx 10-15$ ppb) gave way to lower NO_x conditions ($[NO_2] \approx 1-2$ ppb) at ~10.00 h. Figure 10 shows measured and modeled OH and HO_2 concentrations for this day. Good agreement was found under high NO_x conditions, noting in particular the importance of HONO photolysis near dawn (before 06:00 h). HONO photolysis was found to contribute up to 20% of the total OH formed in a 24-h period.[212] After 10:00 h, the agreement was less good, with the model overestimating [OH] by ~25%. Much better agreement was obtained for HO_2. Figure 10 also shows an HO_2 intercomparison for July 20 for measurements made by the FAGE and MIESR techniques.

As noted above, it is important that stable methods are developed for assessing the uncertainties in models and providing a statistical measure of the quality of agreement between model and measurement. Some progress has been made, using methods of global sensitivity analysis,[195] but there is still a long way to go. While the master chemical mechanism is based on explicit chemical kinetics, there are many areas of considerable uncertainty. Aromatics, which contribute substantially to urban chemistry, have particularly uncertain mechanisms. Some progress has been made toward resolving areas of uncertainty using the large European photoreactor (EUPHORE) at Valencia in Spain to test and develop the appropriate components of the MCM.[197] The experiments were conducted on single aromatics at high concentrations (~500 ppbv), and with $[NO_x]$ spanning the conditions needed for NMHC and NO_x control. One of the EUPHORE chambers has a wide range of measurement techniques for gas-phase species, including FAGE for both OH and HO_2. Measurements on toluene, for example, demonstrated that the MCM significantly underestimates

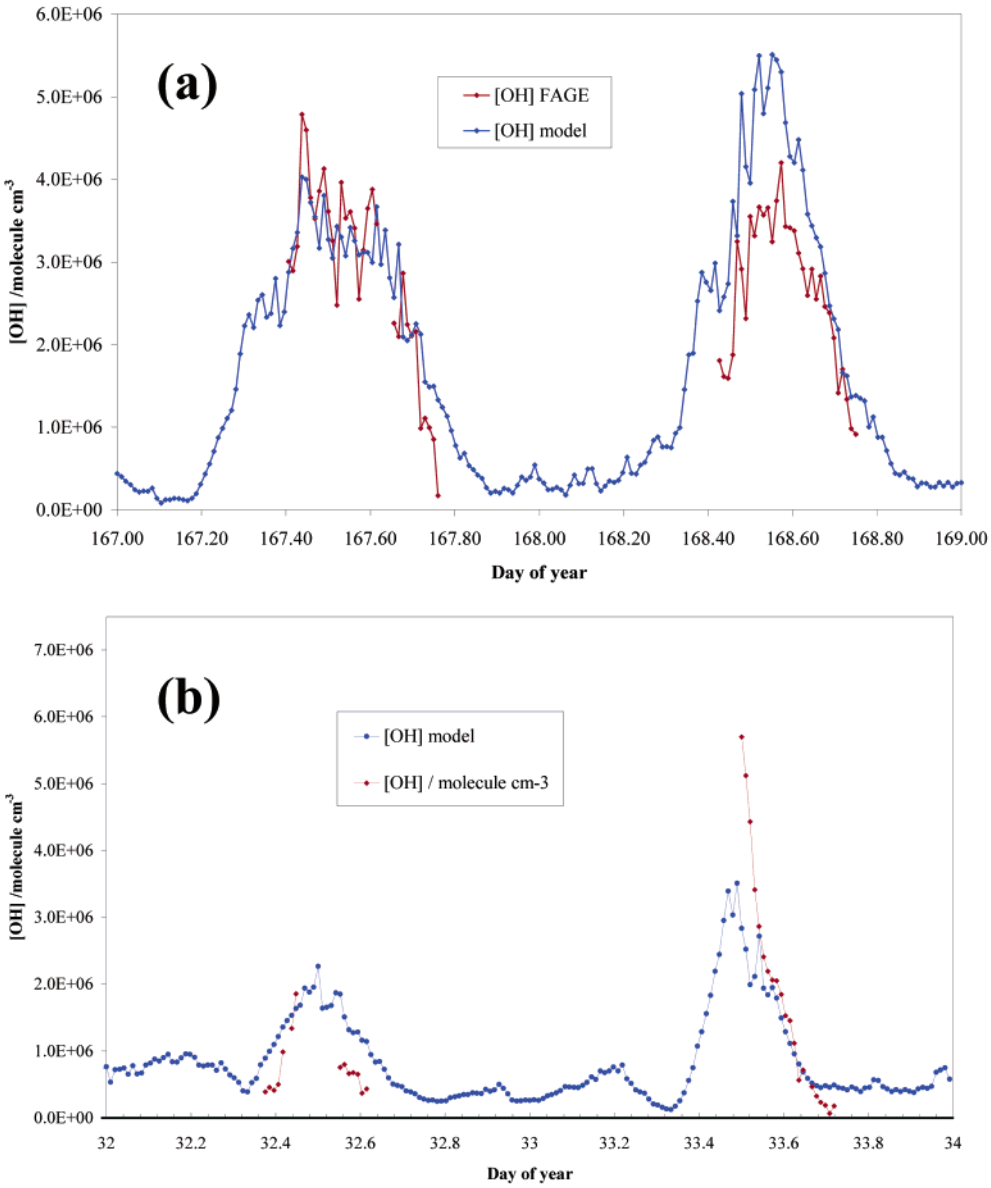

Figure 9. Measured (FAGE) and modeled OH concentrations (15-min average) during the PUMA campaigns held at the University of Birmingham, UK, for (a) summer 1999 (June 16−17) and (b) winter 2000 (February 1−2) periods. The model calculations used the master chemical mechanism, with 12 600 reactions and 4500 chemical species.

the measured [OH], while [O_3] is overestimated by 30%. These are substantial differences in these single-compound measurements. Their influence on model uncertainties for urban systems with large numbers of primary NMHC has not yet been assessed.

10. Summary and Prognosis

As a result of vigorous activity over the past 10 years or so, there have been numerous measurements of OH and HO_2 radicals by several groups, using a variety of techniques. As a result of stringent laboratory testing and field intercomparison exercises, confidence in OH measurements is now well-established. The situation is satisfactory for HO_2, but further instrument development is necessary. Differences between measurements and constrained model predictions are now being discussed in terms of an incomplete understanding of the underlying chemistry, or gaps in the photochemical and kinetics database, rather than dwelling on instrument inadequacies.

From studies in very clean air under conditions of low NO_x, a consistent picture is beginning to emerge of agreement within 25%, and certainly within model and measurement uncertainties. Collocated measurements of OH, HO_2, and oxygenated VOCs (particularly HCHO) are essential, even in clean environments, but especially in polluted environments, because of their impact on radical formation and also on OH removal in propagation steps. The NAMBLEX campaign, held in Ireland in 2002, included measurements of a range of oxygenated species, including acetaldehyde and alcohols. The total loading of oxygenated VOCs was greater than that of NMHCs and, even in clean air, reaction with oxygenated VOCs was responsible for ~20% of the OH loss, compared with ~7% for NMHCs. Model/measure-

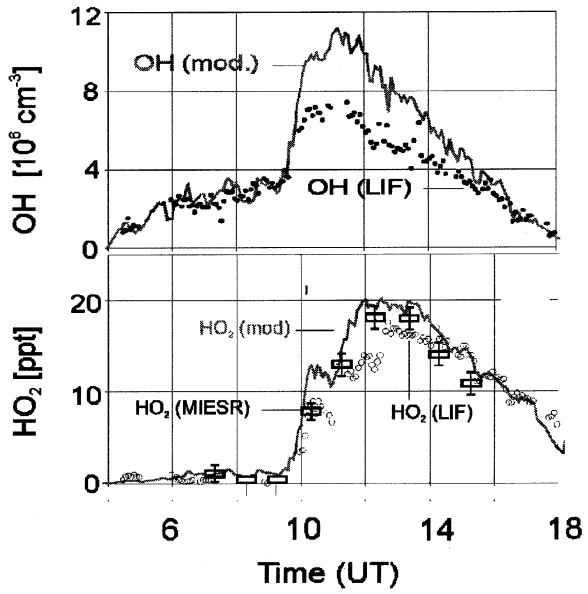

Figure 10. OH (FAGE) and HO_2 (FAGE, MIESR) measurements for July 20, 1998, during the BERLIOZ campaign, held 50 km northwest of the center of Berlin, together with model calculations using the master chemical mechanism. Adapted from ref 139, with kind permission of Kluwer Academic Publishers.

ment agreement for OH was improved considerably when oxygenated VOCs were included.

In more polluted air at higher NO_x, the situation is more variable: sometimes there is good agreement, and at other times there is not. Secondary chemistry becomes more important due to the very large number of VOCs that accompany air masses with higher NO_x.

Although several instrument intercomparisons have been performed, there is a need to intercompare the results of model calculations for the same set of constraining variables. Although the future predictions of a variety of climate models has been compared,[213,214] the same is not true for zero-dimensional box models with mechanisms designed to predict concentrations of OH and HO_2. One of the reasons is that, in some cases, field data taken during a campaign are embargoed until a particular modeling group, funded as part of the collaborative project and utilizing one particular mechanism only, has had time to simulate the conditions and calculate levels of free radicals for comparison. It is rare for other modeling groups to subsequently return to the dataset (once made public), utilizing a different model, after initial publication of model/measurement comparisons. Such re-examination should be encouraged.

Instruments for the measurement of OH and HO_2 are very expensive, both to construct and to maintain. A high level of expertise is required to operate instruments and, as a general rule, instruments cannot be left for long periods unattended. As a consequence, there are only a handful of groups worldwide, and each group typically participates in only one major field campaign per year. There is a need for much cheaper instruments that are easier to operate and that can be left unattended for longer periods of time. Ideally these should be lightweight and compact and use small amounts of electrical power, so that a wide range of platforms, including small aircraft, can be used. However, if chemical mechanisms are to be tested through HO_x measurements and comparison with models, it is important that OH measurements are accompanied by ancillary measurements of source and sink species. Trends in global or regional [OH], and hence any changes in the oxidizing capacity of the atmosphere, that will have an influence on future climate have been estimated from measurements of methyl chloroform, the emission rates of which are well known, and which is removed only by reaction with OH.[2,3] Trends in stratospheric OH have been estimated from OH total column measurements made over 20 years over Fritz Peak, Coloardo,[215] and Lauder, New Zealand.[216] But the column is heavily weighted to high altitudes, and there is little information on trends in the troposphere. Continuous measurements of tropospheric OH from a geographically diverse range of ground-based instruments or from satellites would, for the first time, enable any long-term trends in global or regional OH levels to be monitored directly. This ideal is clearly some way off, although there are some very compact instruments undergoing development in the laboratory, such as cavity ring-down spectrometers[128] or locked cavity absorption techniques using small continuous diode lasers.[217] The idea of intracavity laser spectroscopy for ultrasensitive detection of atmospheric OH was first suggested in 1991,[218] but only recently have suitable continuous-wave laser sources become available.

Chemical mechanisms are reasonably secure for smaller alkanes and alkenes, although many rate constants are parametrized using structure−activity relations.[188] There has been a considerable activity in recent years in the investigation of the chemistry of oxygenated compounds, and much progress has been made. Major uncertainties remain in the chemistry of aromatics. There are several reaction routes following addition of OH to the aromatic ring, and there is a poor understanding, especially of the ring-opening routes that are photochemically active.[197] The reactions are difficult to study because the secondary compounds are much shorter-lived than the parent aromatic, so their concentrations are low. The chemistry of the monoterpenes is also poorly defined.

Many of the problems in chemical mechanisms relate to the secondary chemistry. Even for smaller carbonyl compounds, there are significant uncertainties in the wavelength dependence of the quantum yields. Much of the secondary chemistry for the larger species in the MCM is obtained by analogy. There is little direct information on the kinetics and photochemistry, especially of larger and/or multifunctional oxygenates. More detailed measurements of rate coefficients and product and quantum yields are needed. The task is huge and probably experimentally unachievable in the short or even medium term, and significant advances are needed using quantum mechanical (ab initio or density functional) techniques, linked to selected experimental verification and to the development of approximate generic methods, such those developed by Sumathi et al.[219]

This approach is more common in combustion, but there it is aided by the less stringent requirements placed on the calculation of maxima in the potential energy surface through the impact of high temperatures on the exponential in the Arrhenius expression.

Several approaches have been used to construct chemical mechanisms for models. Our own work has been based on the MCM. This has the advantage that explicit chemistry and a wide range of primary compounds are included. As noted above, though, some of this chemistry is very uncertain, especially for aromatics; the aromatic mechanisms have recently been updated and many improvements incorporated, although difficulties remain. Another difficulty with the MCM is the sheer size of the mechanisms that are generated, which can make interpretation difficult. An alternative approach is to use a reduced or partially lumped mechanism, such as RACM.[190] For more polluted conditions, it is then difficult to assess the quality of the secondary chemistry, which urban measurements have demonstrated to be so important. Some progress has been made in reducing the dimension of explicit mechanisms, using sensitivity analysis, and in the use of low-dimensional manifolds, based on a time scale analysis.[220]

While the gas-phase chemical mechanisms for clean environments are quite well defined, some disagreements between model and measurement remain, especially for HO_2. The most likely source of difficulty is heterogeneous chemistry, especially at sites such as Mace Head. For urban campaigns, the complexities of the mechanism and of the VOC mix are so considerable that model uncertainties are necessarily high and good model/mechanism agreement should not be anticipated, and the questions that can realistically be posed need careful planning and experiment. Perhaps a major aim of such campaigns should be to use them as scenarios to test the more qualitative features of the chemistry. The surprises generated by the PUMA campaign show that we still have much to learn about oxidation chemistry in polluted environments.

For longer-lived species, such as CO_2 and O_3, measurement of the flux, for example into/out of a forest canopy or leaf stomata, has proven extremely useful in understanding details of the carbon cycle or the harmful effects of O_3. Measurement of fluxes requires concentration measurements with very high time resolution (usually >10 Hz), accompanied by micrometeorological measurements of the 3-D components of the wind velocity. Alternatively, spatially resolved measurements, for example vertically throughout a forest canopy, combined with 3-D wind measurements, can yield fluxes and, although technically very difficult, are being performed. Eddy covariance measurements are used to combine concentrations/wind measurements to calculate fluxes. For short-lived free radicals, such as OH and HO_2, measurement of fluxes has not yet been performed, as measurement at repetitions of 10 Hz or higher, or spatially resolved measurements, are technically extremely challenging. However, such measurements should be attempted, as very little is known about the uptake of free radicals by plants, for example. Lightweight devices capable of being translated vertically within a forest canopy are being developed.

Field measurements of OH show considerable variability on time scales of 10−30 s (the shortest time interval typically reported), due to rapid changes in the parameters that control the rate of OH production and loss. The fluctuations in the OH concentration may be due to changes in light intensity, or to turbulent mixing in the vicinity of the inlet, resulting in fluctuations in the concentration of source and sink species (although there would need to be a spatial concentration gradient for this to occur). The effect of turbulent mixing upon OH concentrations, and the implications of this for comparison of measured OH concentrations with the predictions of a chemistry-only box model, warrant further study. However, to achieve this aim, OH measurements together with those of its controlling variables are required on shorter time scales, and the micrometeorology of the sampling region must also be established. A feature of recent field campaigns is the increasing collaboration between atmospheric chemists and physicists, the latter making detailed measurements of boundary layer structure, to understand any local mixing effects.

11. Acknowledgments

The authors wish to thank many people who have helped with the development of the Leeds FAGE instrument and the construction of the box model based on the master chemical mechanism: N. Bell, C. Bloss, W. Bloss, L. Carpenter, N. Carslaw, D. Creasey, J. Dixon, G. Evans, C. Floquet, T. Gravestock, P. Halford-Maw, T. Ingham, P. Jacobs, M. Jenkin, G. Johnson, J. Lee, C. Reyner, S. Saunders, R. Sommariva, J. Spence, and B. J. Whitaker.

12. Glossary of Field Campaign Acronyms

ACE	aerosols characterization experiment
ACE-Asia	aerosols characterization experiment, off the coast of Asia
AEROBIC	aerosols formation from biogenic organic carbon
ALBATROSS	air chemistry and lidar studies of tropospheric and stratospheric species on the Atlantic Ocean
BAYSOFI	Bayerische Sonnenfinsternis
BERLIOZ	Berliner ozone experiment
EASE96	eastern Atlantic summer experiment 1996
EASE 97	eastern Atlantic spring experiment 1997
HAFEX	Hohenpeissenberg aerosol formation experiment
HOPE	Hohenpeissenberg photochemical experiment
ISCAT	investigation of sulfur chemistry in the Antarctic troposphere
LAFRS	Los Angeles free radical study
MINATROC	mineral dust and tropospheric chemistry
MINOS	Mediterranean intensive oxidant study
MLOPEX	Mauna Loa Observatory photochemistry experiment
NAMBLEX	North Atlantic marine boundary experiment

ORION	observations at a remote island of Okinawa
PARFORCE	new particle formation and fate in the coastal environment
PEM	Pacific exploratory mission
PMTACS-NY	PM2.5 technology assessment and characterization study—New York
POPCORN	photochemistry of plant-emitted compounds and OH radicals in northeastern Germany
PRIME	peroxy radical intercomparison exercise
PROPHET	program for research on oxidants: photochemistry, emissions, and transport
PUMA	observation, modeling, and management of urban air pollution
SCATE	sulfur chemistry in the Antarctic troposphere experiment
SOAPEX	southern ocean atmospheric photochemistry experiment
SONEX	subsonic assessment, ozone and nitrogen oxide experiment
SONTAS	southern Ontario aerosol study
SOS	southern oxidants study
SUCCESS	subsonic aircraft: contrails and clouds effect special study
TEXAQS	Texas air quality study
STRAT	stratospheric tracers of atmospheric transport
TOHPE	tropospheric OH photochemistry experiment
TOPSE	tropospheric ozone production about the spring equinox
TRACE-P	transport and chemical evolution over the Pacific
WAOSE	Weybourne Atmospheric Observatory summer experiment

13. References

(1) Prinn, R. G. *Geophys. Res. Lett.* **1985**, *12*, 597.
(2) Prinn, R. G.; Weiss, R. F.; Miller, B. R.; Haung, J.; Alyea, F. N.; Cunnold, D. M.; Fraser, P. J.; Hartley, D. E.; Simmonds, P. G. *Science* **1995**, *269*, 187.
(3) Krol, M.; Lelieveld, J. *J. Geophys. Res.−Atmos.* **2003**, *108*, 4125.
(4) Derwent, R. G.; Carslaw, N.; Simmonds, P. G.; Bassford, M.; O'Doherty, S.; Ryall, D. B.; Pilling, M. J.; Lewis, A. C.; McQuaid, J. B. *J. Atmos. Chem.* **1999**, *34*, 185.
(5) McKeen, S. A.; Liu, S. C.; Hsie, E. Y.; Lin, X.; Bradshaw, J. D.; Smyth, S.; Gregory, G. L.; Blake, D. R. *J. Geophys. Res.−Atmos.* **1996**, *101*, 2087.
(6) McKeen, S. A.; Liu, S. C. *Geophys. Res. Lett.* **1993**, *20*, 2363.
(7) Roberts, J. M.; Fehsenfeld, F. C.; Liu, S. C.; Bollinger, M. J.; Hahn, C.; Albritton, D. L.; Sievers, R. E. *Atmos. Environ.* **1984**, *18*, 2421.
(8) Ehhalt, D. H.; Rohrer, F.; Wahner, A.; Prather, M. J.; Blake, D. R. *J. Geophys. Res.−Atmos.* **1998**, *103*, 18981.
(9) Volz-Thomas, A.; Kolahgar, B. *J. Geophys. Res.−Atmos.* **2000**, *105*, 1611.
(10) Hewitt, C. N.; Harrison, R. M. *Atmos. Environ.* **1985**, *19*, 545.
(11) Crosley, D. R.; Hoell, J. M. *Future directions for HxOy detection*; NASA Conference Publication No. 2448; SRI International: Menlo Park, CA, 1986.
(12) Crosley, D. R. *Local measurement of tropospheric HOx*; NASA Conference Publication No. 3245; SRI International: Menlo Park, CA, 1994.
(13) Crosley, D. R. *J. Atmos. Sci.* **1995**, *52*, 3299.
(14) Crosley, D. R. Conference on Atmospheric Chemistry, Nashville, TN, 1994.
(15) Thompson, A. M. *J. Atmos. Sci.* **1995**, *52*, 3315.
(16) O'Brien, R. J.; Hard, T. M. In *Measurement challenges in atmospheric chemistry*; Newman, L., Ed.; ACS Advances in Chemistry Series 232; American Chemical Society: Washington, DC, 1993, p 322.
(17) Eisele, F. L.; Bradshaw, J. D. *Anal. Chem.* **1993**, *65*, 5, 927A.
(18) Ehhalt, D. H.; Dorn, H.-P.; Hofzumahaus, A. In *The Chemistry of the Atmosphere: Its Impact on Global Change, IUPAC, Chemistry of the 21st Century*; Calvert, J. G., Ed.; Blackwell Scientific Publications: Oxford, 1994.
(19) Crosley, D. R. In *Current problems and progress in atmospheric chemistry*; Barker, J. R., Ed.; World Scientific Publishing: River Edge, NJ, 1995.
(20) Ehhalt, D. H. *Phys. Chem. Chem. Phys.* **1999**, *1*, 5401.
(21) Ehhalt, D. H. In *Global Aspects of Atmospheric Chemistry, Topics in Physical Chemistry*; Baumgartel, H., Grunbein, W., Hensel, F., Zellner, R., Eds.; Steinkopff-Verlag: Darmstadt, 1999; Vol. 6.
(22) Ehhalt, D. H.; Rohrer, F. *J. Geophys. Res.* **2000**, *105*.
(23) Clemitshaw, K. C. In *Encyclopedia of Atmospheric Sciences*; Holton, J. R., Pyle, J. A., Curry, J. A., Eds.; Elsevier: Amsterdam, 2003.
(24) Jaegle, L.; Jacob, D. J.; Brune, W. H.; Wennberg, P. O. *Atmos. Environ.* **2001**, *25*, 469.
(25) Penkett, S. A.; Law, K. S.; Cox, R. A.; Kasibhatla, P. In *The Changing Atmosphere. An integration and Synthesis of a Decade of Tropospheric Chemistry Research*; Brasseur, G. P., Prinn, R. G., Pszenny, A. A. P., Eds.; Springer: Heidelberg, 2002.
(26) Finlayson-Pitts, B. J.; Pitts, J. N. J. *Chemistry of the lower atmosphere. Theory, Experiments and Applications*; Academic Press: San Diego, 2000.
(27) Wayne, R. P. *Chemistry of Atmospheres*, 3rd ed.; Oxford Science Publications: Oxford, 2000.
(28) Brasseur, G.; Orlando, J. J.; Tyndall, G. *Atmospheric chemistry and global change*; Oxford University Press: Oxford, 1999.
(29) Heard, D. E. *Atmos. Environ.* **1998**, *32*, 801.
(30) Brune, W. H. *Science* **1992**, *256*, 1154.
(31) Kanaya, Y.; Akimoto, H. *Chem. Record* **2002**, *2*, 199.
(32) O'Brien, R. J.; Hard, T. M. In *Measurement challenges in atmospheric chemistry*; Newman, L., Ed.; ACS Advances in Chemistry Series; American Chemical Society: Washington, DC, 1993; p 323.
(33) Heard, D. E. In *Encyclopedia of Atmospheric Sciences*; Holton, J. R., Pyle, J. A., Curry, J. A., Eds.; Elsevier: Amsterdam, 2003.
(34) Levy, H. *Science* **1971**, *173*, 141.
(35) Atkinson, R.; Baulch, D. L.; Cox, R. A.; Crowley, J. N.; Hampson, R. F.; Kerr, J. A.; Rossi, M.; Troe, J. Summary of evaluated kinetic and photochemical data for atmospheric chemistry, IUPAC, see http://www.iupac-kinetic.ch.cam.ac.uk/, 2002.
(36) Weinstock, B.; Niki, H. *Science* **1972**, *176*, 290.
(37) Weinstock, B. *Science* **1969**, *168*, 224.
(38) McConnell, J. C.; McElroy, M. B.; Wofsy, S. C. *Nature* **1971**, *233*, 187.
(39) Baardsen, E. L.; Terhune, R. W. *Appl. Phys. Lett.* **1972**, *21*, 209.
(40) Wang, C. C.; Davis, L. I., Jr. *Phys. Rev. Lett.* **1974**, *32*, 349.
(41) Wang, C. C.; Davis, L. I., Jr.; Wu, C. H.; Japar, S.; Niki, H.; Weinstock, B. *Science* **1975**, *189*, 797.
(42) Davis, D. D.; Heaps, W.; McGee, T. *Geophys. Res. Lett.* **1976**, *3*, 331.
(43) Wang, C. C.; Davis, L. I., Jr.; Wu, C. H.; Japar, S. *Appl. Phys. Lett.* **1975**, *28*, 14.
(44) Smith, G. P.; Crosley, D. R. *J. Geophys. Res.* **1990**, *95*, 16427.
(45) Hanabusa, M.; Wang, C. C.; Japar, S.; Killinger, D. K.; Fisher, K. *J. Chem. Phys.* **1977**, *66*, 2118.
(46) Davis, D. D.; Rodgers, M. O.; Fischer, S. D.; Asai, K. *Geophys. Res. Lett.* **1981**, *8*, 69.
(47) Rodgers, M. O.; Bradshaw, J.; Sandholm, S.; KeSheng, S.; Davis, D. D. *J. Geophys. Res.* **1985**, *90*, 12819.
(48) Davis, L. I., Jr.; Guo, C.; James, J. V.; Morris, P. T.; Postiff, R.; Wang, C. C. *J. Geophys. Res.* **1985**, *90*, 12835.
(49) Beck, S. M. et al. *J. Geophys. Res.* **1987**, *92*, 1977.
(50) Stimpfle, R. M.; Anderson, J. G. *Geophys. Res. Lett.* **1988**, *15*, 1503.
(51) Heard, D. E. In *Encyclopedia of Atmospheric Sciences*; Holton, J. R., Curry, J. A., Pyle, J. A., Eds.; Elsevier: Amsterdam, 2003.
(52) Wennberg, P. O.; Cohen, R. C.; Hazen, N. L.; Lapson, L. B.; Allen, N. T.; Hanisco, T. F.; Oliver, J. F.; Lanham, N. W.; Demusz, J. N.; Anderson, J. G. *Rev. Sci. Instrum.* **1994**, *65*, 1858.
(53) Campbell, M. C.; Sheppard, J. C.; Au, B. F. *Geophys. Res. Lett.* **1979**, *6*, 175.
(54) Felton, C. C.; Sheppard, J. C.; Campbell, M. J. *Nature* **1988**, *335*, 53.
(55) Felton, C. C.; Sheppard, J. C.; Campbell, M. J. *Environ. Sci. Technol.* **1990**, *24*, 1841.
(56) Anderson, J. G.; Grassl, H. J.; Shetter, R. E.; Margitan, J. J. *Geophys. Res. Lett.* **1981**, *8*, 289.
(57) Stimpfle, R. M.; Wennberg, P. O.; Lapson, L. B.; Anderson, J. G. *Geophys. Res. Lett.* **1990**, *17*, 1905.
(58) Hard, T. M.; O'Brien, R. J.; Chan, C. Y.; Mehrabzadeh, A. A. *Environ. Sci. Technol.* **1984**, *18*, 768.
(59) Hard, T. M.; Chan, C. Y.; Mehrabzadeh, A. A.; O'Brien, R. J. *J. Geophys. Res.−Atmos.* **1992**, *97*, 9785.
(60) Mihelcic, D.; Ehhalt, D. H.; Klomfass, J.; Kulessa, G. F.; Schmidt, U.; Trainer, M. *Ber. Bunsen-Ges. Phys. Chem., Chem. Phys.* **1978**, *82*, 16.
(61) Mihelcic, D.; Volzthomas, A.; Patz, H. W.; Kley, D. *J. Atmos. Chem.* **1990**, *11*, 271.
(62) Cantrell, C. A.; Stedman, D. H. *Geophys. Res. Lett.* **1982**, *9*, 846.

(63) Cantrell, C. A.; Stedman, D. H.; Wendel, G. J. *Anal. Chem.* **1984**, *56*, 1496.
(64) Lightfoot, P. D.; Cox, R. A.; Crowley, J. N.; Destriau, M.; Hayman, G. D.; Jenkin, M. E.; Moortgat, G. K.; Zabel, F. *Atmos. Environ. A-Gen. Top.* **1992**, *26*, 1805.
(65) Cantrell, C. A.; Shetter, R. E.; McDaniel, A. H.; Calvert, J. G. In *Measurement challenges in atmospheric chemistry*; Newman, L., Ed.; ACS Advances in Chemistry Series; American Chemical Society: Washington, DC, 1993.
(66) Chen, X.; Mopper, K. *J. Atmos. Chem.* **2000**, *36*, 81.
(67) Salmon, R.; Schiller, C. L.; Harris, G. W. *J. Atmos. Chem.* **2003**, in preparation.
(68) Ren, X.; Shao, K.; Miao, G.; Tang, X. *China Environ. Sci.* **2000**, *21*, 115.
(69) Ren, X.; Shao, K.; Shao, G.; Tang, X. *Huanjung Huaxue* **2001**, *20*, 81.
(70) Crosley, D. R. *J. Geophys. Res.* **1997**, *102*, 6495.
(71) Watanbe, T.; Yoshida, M.; Fujiwara, S.; Abe, K.; Onoe, A.; Hirota, M.; Igarashi, S. *Anal. Chem.* **1982**, *54*, 2470.
(72) Wennberg, P. O.; Stimpfle, R. M.; Weinstock, E. M.; Dessler, A. E.; Lloyd, S. A.; Lapson, L. B.; Schwab, J. J.; Anderson, J. G. *Geophys. Res. Lett.* **1990**, *17*, 1909.
(73) Matsumi, Y.; Kono, M.; Ichikawa, T.; Takahashi, K.; Kondo, Y. *Bull. Chem. Soc. Jpn.* **2002**, *75*, 711.
(74) Hard, T. M.; O'Brien, R. J.; Cook, T. B.; Tsongas, G. A. *Appl. Opt.* **1979**, *18*, 3216.
(75) Stevens, P. S.; Mather, J. H.; Brune, W. H. *J. Geophys. Res.−Atmos.* **1994**, *99*, 3543.
(76) Creasey, D. J.; Halford-Maw, P. A.; Heard, D. E.; Spence, J. E.; Whitaker, B. J. *Rev. Sci. Instrum.* **1998**, *69*, 4068.
(77) Hofzumahaus, A.; Holland, F. In *Optical Methods in Atmospheric Chemistry*; Schiff, H. I., Platt, U., Eds.; Proceedings of SPIE—the International Society for Optical Engineering, 1715; SPIE: Bellingham, WA, 1993.
(78) Dorn, H. P.; Neuroth, R.; Hofzumahaus, A. *J. Geophys. Res.−Atmos.* **1995**, *100*, 7397.
(79) Chan, C. Y.; Hard, T. M.; Mehrabzadeh, A. A.; George, L. A.; O'Brien, R. J. *J. Geophys. Res.−Atmos.* **1990**, *95*, 18569.
(80) Bloss, W. J.; Gravestock, T. J.; Heard, D. E.; Ingham, T.; Johnson, G. P.; Lee, J. D. *J. Environ. Monit.* **2003**, *5*.
(81) Wennberg, P. O.; Cohen, R. C.; Hazen, N. L.; Lapson, L. B.; Allen, N. T.; Hanisco, T. F.; Oliver, J. F.; Lanham, N. W.; Demusz, J. N.; Anderson, J. G. *Rev. Sci. Instrum.* **1994**, *65*, 1858.
(82) Tan, D.; Faloona, I.; Brune, W. H.; Weinheimer, A.; Campos, T.; Ridley, B.; Vay, S.; Collins, J.; Sachse, G. *Geophys. Res. Lett.* **1998**, *25*, 1721.
(83) Dubey, M. K.; Hanisco, T. F.; Wennberg, P. O.; Anderson, J. G. *Geophys. Res. Lett.* **1996**, *23*, 3215.
(84) Hard, T. M.; George, L. A.; O'Brien, R. J. *J. Atmos. Sci.* **1995**, *52*, 3354.
(85) Creasey, D. J.; Heard, D. E.; Lee, J. D. *J. Geophys. Res.* **2002**, *107*, 4091.
(86) Abram, J. P.; Creasey, D. J.; Heard, D. E.; Lee, J. D.; Pilling, M. J. *Geophys. Res. Lett.* **2000**, *27*, 3437.
(87) Holland, F.; Hessling, M.; Hofzumahaus, A. *J. Atmos. Sci.* **1995**, *52*, 3393.
(88) Hard, T. M.; Mehrabzadeh, A. A.; Chan, C. Y.; O'Brien, R. J. *J. Geophys. Res.−Atmos.* **1992**, *97*, 9795.
(89) Zeng, G.; Heard, D. E.; Pilling, M. J.; Robertson, S. H. *Geophys. Res. Lett.* **1998**, *25*, 4497.
(90) George, L. A.; Hard, T. M.; O'Brien, R. J. *J. Geophys. Res.−Atmos.* **1999**, *104*, 11643.
(91) Creasey, D. J.; Halford-Maw, P. A.; Heard, D. E.; Pilling, M. J.; Whitaker, B. J. *J. Chem. Soc., Faraday Trans.* **1997**, *93*, 2907.
(92) Kanaya, Y.; Sadanaga, Y.; Hirokawa, J.; Kajii, Y.; Akimoto, H. *J. Atmos. Chem.* **2001**, *38*, 73.
(93) Holland, F.; Aschmutat, U.; Hessling, M.; Hofzumahaus, A.; Ehhalt, D. H. *J. Atmos. Chem.* **1998**, *31*, 205.
(94) Creasey, D. J.; Heard, D. E.; Lee, J. D. *Atmos. Environ.* **2001**, *35*, 4713.
(95) Mather, J. H.; Stevens, P. S.; Brune, W. H. *J. Geophys. Res.−Atmos.* **1997**, *102*, 6427.
(96) Hard, T. M.; Chan, C. Y.; Mehrabzadeh, A. A.; George, L. A.; O'Brien, R. J. *J. Geophys. Res.* **1990**, *95*, 18.
(97) Creasey, D. J.; Heard, D. E.; Pilling, M. J.; Whitaker, B. J.; Berzins, M.; Fairlie, R. *Appl. Phys. B−Lasers Opt.* **1997**, *65*, 375.
(98) Faloona, I.; Tan, D.; Brune, W. H.; Jaegle, L.; Jacob, D. J.; Kondo, Y.; Koike, M.; Chatfield, R.; Pueschel, R.; Ferry, G.; Sachse, G.; Vay, S.; Anderson, B.; Hannon, J.; Fuelberg, H. *J. Geophys. Res.−Atmos.* **2000**, *105*, 3771.
(99) Bradshaw, J. D.; Rodgers, M. O.; Davis., D. D. *Appl. Opt.* **1984**, *23*, 2134.
(100) Ravishankara, A. R.; Hancock, G.; Kawasaki, M.; Matsumi, Y. *Science* **1998**, *280*, 60.
(101) Bradshaw, J. D.; Rodgers, M. O.; Sandholm, S. T.; KeSheng, S.; Davis, D. D. *J. Geophys. Res.* **1985**, *90*, 12861.
(102) Sandholm, S.; Smyth, S.; Bai, R.; Bradshaw, J. *J. Geophys. Res.* **1997**, *102*, 28651.
(103) Kovacs, T. A.; Brune, W. H. *J. Atmos. Chem.* **2001**, *39*, 105.
(104) Kovacs, T. A.; Brune, W. H.; Harder, H.; Martinez, M.; Simpas, J. B.; Frost, G. J.; Williams, E.; Jobson, T.; Stroud, C.; Young, V.; Fried, A.; Wert, B. *J. Environ. Monit.* **2003**, *5*, 68.
(105) Ren, X.; Harder, H.; Martinez, M.; Lesher, R. L.; Oliger, A.; Shirley, T.; Adams, J.; Simpas, J. B.; Brune, W. H. *Atmos. Environ.* **2003**, *37*, 3627.
(106) Bell, N.; Heard, D. E.; Pilling, M. J.; Tomlin, A. S. *Atmos. Environ.* **2003**, *37*, 2193.
(107) Perner, D.; Ehhalt, D. H.; Peatz, H. W.; Platt, U.; Roeth, E. P.; Volz, A. *Geophys. Res. Lett.* **1976**, *3*, 466.
(108) Hubler, G.; Perner, D.; Platt, U.; Tonnissen, A.; Ehhalt, D. H. *J. Geophys. Res.−Atmos.* **1984**, *89*, 1309.
(109) Platt, U.; Rateike, M.; Junkermann, W.; Rudolph, J.; Ehhalt, D. H. *J. Geophys. Res.−Atmos.* **1988**, *93*, 5159.
(110) Dorn, H. P.; Brandenburger, U.; Brauers, T.; Hausmann, H. *J. Atmos. Sci.* **1995**, *52*, 3373.
(111) Mount, G. H. *J. Geophys. Res.−Atmos.* **1992**, *97*, 2427.
(112) Armerding, W.; Spiekermann, M.; Walter, J.; Comes, F. J. *J. Atmos. Sci.* **1995**, *52*, 3381.
(113) Brauers, T.; Hausmann, M.; Bister, A.; Kraus, A.; Dorn, H. P. *J. Geophys. Res.−Atmos.* **2001**, *106*, 7399.
(114) Hausmann, M.; Brandenburger, U.; Brauers, T.; Dorn, H. P. *J. Geophys. Res.−Atmos.* **1997**, *102*, 16011.
(115) Hausmann, M.; Brandenburger, U.; Brauers, T.; Dorn, H. P. *Appl. Opt.* **1999**, *38*, 462.
(116) Armerding, W.; Spiekermann, M.; Comes, F. J. *J. Geophys. Res.−Atmos.* **1994**, *99*, 1225.
(117) Eisele, F. L.; Tanner, D. J. *J. Geophys. Res.−Atmos.* **1991**, *96*, 9295.
(118) Berresheim, H.; Elste, T.; Tremmel, H. G.; Allen, A. G.; Hansson, H. C.; Rosman, K.; Dal Maso, M.; Makela, J. M.; Kulmala, M.; O'Dowd, C. D. *J. Geophys. Res.−Atmos.* **2002**, *107*, 8100.
(119) Tanner, D.; Sjostedt, S.; Huey, G.; Slusher, D.; Chen, G.; Lefer, B.; Shetter, R.; Carroll, M.; Hengel, S.; Fortner, E.; Young, V. *Measurement and model results for gas phase OH and H_2SO_4 during PROPHET 2001*; AGU Fall Meeting, San Francisco, 2002; American Geophysical Union: Washington, DC, 2002; p A51A.
(120) Arnold, F.; Fabian, P. *Nature* **1980**, *282*, 55.
(121) Tanner, D. J.; Eisele, F. L. *J. Geophys. Res.* **1995**, *100*, 2883.
(122) Eisele, F. L. *J. Atmos. Sci.* **1995**, *52*, 3337.
(123) Tanner, D. J.; Jefferson, A.; Eisele, F. L. *J. Geophys. Res.−Atmos.* **1997**, *102*, 6415.
(124) Mauldin, R. L.; Eisele, F. L.; Cantrell, C. A.; Kosciuch, E.; Ridley, B. A.; Lefer, B.; Tanner, D. J.; Nowak, J. B.; Chen, G.; Wang, L.; Davis, D. *J. Geophys. Res.−Atmos.* **2001**, *106*, 32657.
(125) Eisele, F. L.; Mauldin, R. L.; Tanner, D. J.; Cantrell, C.; Kosciuch, E.; Nowak, J. B.; Brune, B.; Faloona, I.; Tan, D.; Davis, D. D.; Wang, L.; Chen, G. *J. Geophys. Res.−Atmos.* **2001**, *106*, 32683.
(126) Mauldin, R. L.; Tanner, D. J.; Eisele, F. L. *J. Geophys. Res.* **1999**, *104*, 5817.
(127) Mauldin, R. L.; Cantrell, C. A.; Zondlo, M. A.; Kosciuch, E.; Ridley, B. A. *J. Geophys. Res.* **2003**, *108*, 8366.
(128) Pushkarsky, M. B.; Zalyubovsky, S. J.; Miller, T. A. *J. Chem. Phys.* **2000**, *112*, 10695.
(129) Tan, D.; Faloona, I.; Simpas, J. B.; Brune, W.; Shepson, P. B.; Couch, T. L.; Sumner, A. L.; Carroll, M. A.; Thornberry, T.; Apel, E.; Riemer, D.; Stockwell, W. *J. Geophys. Res.−Atmos.* **2001**, *106*, 24407.
(130) Faloona, I.; Tan, D.; Brune, W.; Hurst, J.; Barket, D.; Couch, T. L.; Shepson, P.; Apel, E.; Riemer, D.; Thornberry, T.; Carroll, M. A.; Sillman, S.; Keeler, G. J.; Sagady, J.; Hooper, D.; Paterson, K. *J. Geophys. Res.−Atmos.* **2001**, *106*, 24315.
(131) Martinez, M.; et al. *J. Geophys. Res.* **2003**, *108*, 4617.
(132) Hofzumahaus, A.; Aschmutat, U.; Hessling, M.; Holland, F.; Ehhalt, D. H. *Geophys. Res. Lett.* **1996**, *23*, 2541.
(133) Holland, F.; Hofzumahaus, A.; Schafer, R.; Kraus, A.; Patz, H. W. *J. Geophys. Res.* **2003**, *108*, 8246.
(134) Aloisio, S.; Francisco, J. S.; Friedl, R. R. *J. Phys. Chem. A* **2000**, *104*, 6597.
(135) Aloisio, S.; Francisco, J. S. *Acc. Chem. Res.* **2000**, *33*, 825.
(136) Creasey, D. J.; Evans, G. E.; Heard, D. E.; Lee, J. D. *J. Geophys. Res.* **2003**, *108*, 4475.
(137) Jenkin, M. E., private communication, 2003.
(138) Mihelcic, D.; Musgen, P.; Ehhalt, D. H. *J. Atmos. Chem.* **1985**, *3*, 341.
(139) Platt, U.; Alicke, B.; Dubois, R.; Geyer, A.; Hofzumahaus, A.; Holland, F.; Martinez, M.; Mihelcic, D.; Klupfel, T.; Lohrmann, B.; Patz, W.; Perner, D.; Rohrer, F.; Schafer, J.; Stutz, J. *J. Atmos. Chem.* **2002**, *42*, 359.
(140) Reiner, T.; Hanke, M.; Arnold, F. *Geophys. Res. Lett.* **1998**, *25*, 47.
(141) Reiner, T.; Hanke, M.; Arnold, F.; H., Z.; Schlager, H. *J. Geophys. Res.* **1999**, *104*, 18647.
(142) Reiner, T.; Hanke, M.; Arnold, F. *J. Geophys. Res.−Atmos.* **1997**, *102*, 1311.
(143) Hanke, M.; Uecker, J.; Reiner, T.; Arnold, F. *Int. J. Mass Spectrom.* **2002**, *213*, 91.

(144) Cantrell, C. A.; Edwards, G. D.; Stephens, S.; Mauldin, L.; Kosciuch, E.; Zondlo, M. *J. Geophys. Res.* **2003**, *108*, 8371.
(145) Clemitshaw, K. C.; Carpenter, L. J.; Penkett, S. A.; Jenkin, M. E. *J. Geophys. Res.−Atmos.* **1997**, *102*, 25405.
(146) Aschmutat, U.; Hessling, M.; Holland, F.; Hofzumahaus, A. In *Physico-Chemical Behaviour of Atmospheric Pollutants*; Restelli, G., Angeletti, A., Eds.; European Commission: Brussels, 1994.
(147) Schultz, M.; Heitlinger, M.; Mihelcic, D.; Volz-Thomas, A. *J. Geophys. Res.−Atmos.* **1995**, *100*, 18811.
(148) Hofzumahaus, A.; Brauers, T.; Aschmutat, U.; Brandenburger, U.; Dorn, H. P.; Hausmann, M.; Hessling, M.; Holland, F.; PlassDulmer, C.; Sedlacek, M.; Weber, M.; Ehhalt, D. H. *Geophys. Res. Lett.* **1997**, *24*, 3039.
(149) Creasey, D. J.; Heard, D. E.; Lee, J. D. *Geophys. Res. Lett.* **2000**, *27*, 1651.
(150) Cantrell, C. A.; Tyndall, G.; Zimmer, A. *Geophys. Res. Lett.* **1997**, *24*, 2195.
(151) DeMore, W. B.; Sander, S. P.; Golden, D. M.; Hampson, R. F.; Kurylo, M. J.; Howard, C. J.; Ravishankara, A. R.; Kolb, C. E.; Molina, M. J. *Chemical kinetics and photochemical data for use in stratospheric modeling*; JPL Publication No. 97-4; California Institute of Technology: Pasadena, CA, 1997.
(152) Atkinson, R.; et al. *J. Phys. Chem. Ref. Data* **1997**, *26*, 1329.
(153) Jaegle, L.; Jacob, D. J.; Wennberg, P. O.; Spivakovsky, C. M.; Hanisco, T. F.; Lanzendorf, E. J.; Hintsa, E. J.; Fahey, D. W.; Keim, E. R.; Proffitt, M. H.; Atlas, E. L.; Flocke, F.; Schauffler, S.; McElroy, C. T.; Midwinter, C.; Pfister, L.; Wilson, J. C. *Geophys. Res. Lett.* **1997**, *24*, 3181.
(154) Lanzendorf, E. J.; Hanisco, T. F.; Donahue, N. M.; Wennberg, P. O. *Geophys. Res. Lett.* **1997**, *24*, 3037.
(155) Bailey, A. E.; Heard, D. E.; Henderson, D. A.; Paul, P. H. *Chem. Phys. Lett.* **1999**, *302*, 132.
(156) Lester, M. I.; Loomis, R. A.; Schwartz, B. L.; Walch, S. P. *J. Phys. Chem. A* **1997**, *101*, 9595.
(157) Anderson, D. T.; Todd, M. W.; Lester, M. I. *J. Chem. Phys.* **1999**, *110*, 11117.
(158) Mauldin, R. L.; Madronich, S.; Flocke, S. J.; Eisele, F. L.; Frost, G. J.; Prevot, A. S. H. *Geophys. Res. Lett.* **1997**, *24*, 3033.
(159) Mauldin, R. L.; Frost, G. J.; Chen, G.; Tanner, D. J.; Prevot, A. S. H.; Davis, D. D.; Eisele, F. L. *J. Geophys. Res.−Atmos.* **1998**, *103*, 16713.
(160) Tan, D.; Faloona, I.; Simpas, J. B.; Brune, W.; Olson, J.; Crawford, J.; Avery, M.; Sachse, G.; Vay, S.; Sandholm, S.; Guan, H. W.; Vaughn, T.; Mastromarino, J.; Heikes, B.; Snow, J.; Podolske, J.; Singh, H. *J. Geophys. Res.−Atmos.* **2001**, *106*, 32667.
(161) Eisele, F. L.; Mauldin, R. L.; Tanner, D. J.; Fox, J. R.; Mouch, T.; Scully, T. *J. Geophys. Res.−Atmos.* **1997**, *102*, 27993.
(162) Anderson, J. G. *Geophys. Res. Lett.* **1976**, *3*, 165.
(163) Hard, T. M.; Mehrabzadeh, A. A.; Pan, W. H.; O'Brien, R. J. *Nature* **1986**, *322*, 617.
(164) Paulson, S. E.; Orlando, J. J. *Geophys. Res. Lett.* **1996**, *23*, 3727.
(165) Paulson, S. E.; Sen, A. D.; Liu, P.; Fenske, J. D.; Fox, M. J. *Geophys. Res. Lett.* **1997**, *24*, 3193.
(166) Marston, G.; McGill, C. D.; Rickard, A. R. *Geophys. Res. Lett.* **1998**, *25*, 2177.
(167) Fenske, J. D.; Hasson, A. S.; Paulson, S. E.; Kuwata, K. T.; Ho, A.; Houk, K. N. *J. Phys. Chem. A* **2000**, *104*, 7821.
(168) Donahue, N. M.; Kroll, J. H.; Anderson, J. G.; Demerjian., K. L. *Geophys. Res. Lett.* **1998**, *25*, 59.
(169) Pfeiffer, T.; Forberich, O.; Comes, F. J. *Chem. Phys. Lett.* **1998**, *298*, 351.
(170) Kroll, J. H.; Clarke, J. S.; Donahue, N. M.; Anderson, J. G.; Demerjian, K. L. *J. Phys. Chem. A* **2001**, *105*, 1554.
(171) Siese, M.; Becker, K. H.; Brockmann, K. J.; Geiger, H.; Hofzumahaus, A.; Holland, F.; Mihelcic, D.; Wirtz, K. *Environ. Sci. Technol.* **2001**, *35*, 4660.
(172) Hard, T. M.; George, L. A.; O'Brien, R. J. *Environ. Sci. Technol.* **2002**, *36*, 1783.
(173) Taylor, S. M.Chem. Thesis, University of Leeds, 2003.
(174) Beck, S. M.; Bendura, R. J.; McDougal, D. S.; Hoell, J. M.; Gregory, G. L.; Curfman, H. J.; Davis, D. D.; Bradshaw, J.; Rodgers, M. O.; Wang, C. C.; Davis, L. I.; Campbell, M. J.; Torres, A. L.; Carroll, M. A.; Ridley, B. A.; Sachse, G. W.; Hill, G. F.; Condon, E. P.; Rasmussen, R. A. *J. Geophys. Res.−Atmos.* **1987**, *92*, 1977.
(175) Mount, G. H.; Eisele, F. L. *Science* **1992**, *256*, 1187.
(176) Eisele, F. L.; Mount, G. H.; Fehsenfeld, F. C.; Harder, J.; Marovich, E.; Parrish, D. D.; Roberts, J.; Trainer, M. *J. Geophys. Res.−Atmos.* **1994**, *99*, 18605.
(177) Mount, G. H.; Harder, J. W. *J. Atmos. Sci.* **1995**, *52*, 3342.
(178) Mount, G. H.; Eisele, F. L.; Tanner, D. J.; Brault, J. W.; Johnston, P. V.; Harder, J. W.; Williams, E. J.; Fried, A.; Shetter, R. *J. Geophys. Res.−Atmos.* **1997**, *102*, 6437.
(179) Hofzumahaus, A.; Aschmutat, U.; Brandenburger, U.; Brauers, T.; Dorn, H. P.; Hausmann, M.; Hessling, M.; Holland, F.; PlassDulmer, C.; Ehhalt, D. H. *J. Atmos. Chem.* **1998**, *31*, 227.
(180) Brauers, T.; Aschmutat, U.; Brandenburger, U.; Dorn, H. P.; Hausmann, M.; Hessling, M.; Hofzumahaus, A.; Holland, F.; PlassDulmer, C.; Ehhalt, D. H. *Geophys. Res. Lett.* **1996**, *23*, 2545.
(181) Campbell, M. J.; Hall, B. D.; Sheppard, J. C.; Utley, P. L.; O'Brien, R. J.; Hard, T. M.; George, L. A. *J. Atmos. Sci.* **1995**, *52*, 3421.
(182) Holland, F.; Hofzumahaus, A.; Sedlacek, M.; Weber, M. *Measurements of OH and HO_2 radicals in clean marine air during the ALBATROSS field campaign*; AGU fall meeting, San Francisco, 1999; American Geophysical Union: Washington, DC, 1999.
(183) Eisele, F.; Mauldin, L.; Cantrell, C.; Zondlo, M. A.; Apel, E.; Fried, A.; Walega, J.; Shetter, R.; Lefer, B.; Flocke, F.; Weinheimer, A.; Avery, M.; Vay, S.; G., S.; Singh, H.; Brune, W. H.; Harder, H.; Martinez-Harder, M.; Bandy, A.; Thornton, D.; Heikes, B.; Kondo, Y.; Riemer, D.; Sandholm, S.; Tan, D.; Dibb, J.; Talbot, R. *J. Geophys. Res.−Atmos.* **2003**, *108*, 8791.
(184) Carslaw, N.; Creasey, D. J.; Heard, D. E.; Lewis, A. C.; McQuaid, J. B.; Pilling, M. J.; Monks, P. S.; Bandy, B. J.; Penkett, S. A. *J. Geophys. Res.−Atmos.* **1999**, *104*, 30241.
(185) Carslaw, N.; Creasey, D. J.; Heard, D. E.; Jacobs, P. J.; Lee, J. D.; Lewis, A. C.; McQuaid, J. B.; Pilling, M. J.; Bauguitte, S.; Penkett, S. A.; Monks, P. S.; Salisbury, G. *J. Geophys. Res.−Atmos.* **2002**, *107*, art. no. 4190.
(186) Stevens, P. S.; Mather, J. H.; Brune, W. H.; Eisele, F.; Tanner, D.; Jefferson, A.; Cantrell, C.; Shetter, R.; Sewall, S.; Fried, A.; Henry, B.; Williams, E.; Baumann, K.; Goldan, P.; Kuster, W. *J. Geophys. Res.* **1997**, *102*, 6379.
(187) Jaegle, L.; Jacob, D. J.; Brune, W. H.; Faloona, I.; Tan, D.; Heikes, B. G.; Kondo, Y.; Sachse, G. W.; Anderson, B.; Gregory, G. L.; Singh, H. B.; Pueschel, R.; Ferry, G.; Blake, D. R.; Shetter, R. E. *J. Geophys. Res.−Atmos.* **2000**, *105*, 3877.
(188) Saunders, S. M.; Jenkin, M. E.; Derwent, R. G.; Pilling, M. J. *Atmos. Chem. Phys.* **2003**, *3*, 161.
(189) Jenkin, M. E.; Saunders, S. M.; Wagner, V.; Pilling, M. J. *Atmos. Chem. Phys.* **2003**, *3*, 181.
(190) Stockwell, W. R.; Kirchner, F.; Kuhn, M.; Seefeld, S. *J. Geophys. Res.−Atmos.* **1997**, *102*, 25847.
(191) Lewis, A. C.; Carslaw, N.; Marriott, P. J.; Kinghorn, R. M.; Morrison, P.; Lee, A. L.; Bartle, K. D.; Pilling, M. J. *Nature* **2000**, *405*, 778.
(192) Carslaw, N.; Creasey, D. J.; Harrison, D.; Heard, D. E.; Hunter, M. C.; Jacobs, P. J.; Jenkin, M. E.; Lee, J. D.; Lewis, A. C.; Pilling, M. J.; Saunders, S. M.; Seakins, P. W. *Atmos. Environ.* **2001**, *35*, 4725.
(193) Whitby, K. T.; Sverdup, G. M. *Environ. Sci. Technol.* **1980**, *9*, 477.
(194) Jacob, D. J. *Atmos. Environ.* **2000**, *34*, 2131.
(195) Saltelli, A.; Chan, K. R.; Scott, E. M. *Sensitivity Analysis*; Wiley and Sons Ltd.: Chichester, 2000.
(196) Ravishankara, A. R.; Dunlea, E. J.; Blitz, M. A.; Dillon, T. J.; Heard, D. E.; Pilling, M. J.; Strekowski, R. S.; Nicovich, J. M.; Wine, P. H. *Geophys. Res. Lett.* **2002**, *29*, art. no. 1745.
(197) Wagner, V.; Jenkin, M. E.; Saunders, S. M.; Stanton, J.; Wirtz, K.; Pilling, M. J. *Atmos. Chem. Phys.* **2003**, *3*, 89.
(198) Ayers, G. P.; Gillett, R. W.; Granek, H.; deServes, C.; Cox, R. A. *Geophys. Res. Lett.* **1997**, *24*, 401.
(199) Poppe, D.; Zimmermann, J.; Dorn, H. P. *J. Atmos. Sci.* **1995**, *52*, 3402.
(200) Stockwell, W. R.; Middleton, P.; Chang, J. S.; Tang, X. *J. Geophys. Res.−Atmos.* **2000**, *95*, 16343.
(201) McKeen, S. A.; Mount, G.; Eisele, F. L.; Williams, E. J.; Harder, J.; Goldan, P.; Kuster, W.; Liu, S. C.; Baumann, K.; Tanner, D. J.; Fried, A.; Sewell, S.; Cantrell, C. A.; Shetter, R. *J. Geophys. Res.* **1997**, *102*, 6467.
(202) Lurmann, F. W.; Lloyd, A. C.; Atkinson, R. *J. Geophys. Res.* **1986**, *91*, 10905.
(203) Chen, G.; Davis, D.; Crawford, J.; Heikes, B.; O'Sullivan, D.; Lee, M.; Eisele, F.; Mauldin, L.; Tanner, D.; Collins, J.; Barrick, J.; Anderson, B.; Blake, D.; Bradshaw, J.; Sandholm, S.; Carroll, M.; Albercook, G.; Clarke, A. *J. Atmos. Chem.* **2001**, *38*, 317.
(204) Crawford, J.; Davis, D.; Olson, J.; Chen, G.; Liu, S.; Gregory, G.; Barrick, J.; Sachse, G.; Sandholm, S.; Heikes, B.; Singh, H.; Blake, D. *J. Geophys. Res.−Atmos.* **1999**, *104*, 16255.
(205) Brauers, T.; Hausmann, M.; Bister, A.; Kraus, A. *J. Geophys. Res.* **2001**, *106*, 7399.
(206) Paulson, S. E.; Chung, M.; Sen, A. D.; Orzechowska, G. *J. Geophys. Res.−Atmos.* **1998**, *103*, 25533.
(207) Rickard, A. R.; Johnson, D.; McGill, C. D.; Marston, G. *J. Phys. Chem.* **1999**, *103*, 7656.
(208) Guenther, A. B.; Zimmerman, P. R.; Harley, P. C.; Monson, R. K.; Fall, R. *J. Geophys. Res.−Atmos.* **1993**, *98*, 12609.
(209) Carslaw, N.; Bell, N.; Lewis, A. C.; McQuaid, J. B.; Pilling, M. J. *Atmos. Environ.* **2000**, *34*, 2827.
(210) Sillman, S.; Carroll, M. A.; Thornberry, T.; Lamb, B. K.; Westberg, H.; Brune, W. H.; Faloona, I.; Tan, D.; Shepson, P. B.; Sumner, A. L.; Hastie, D. R.; Mihele, C. M.; Apel, E. C.; Riemer, D. D.; Zika, R. G. *J. Geophys. Res.* **2002**, *107*, 4043.
(211) Madronich, S. *J. Geophys. Res.−Atmos.* **1987**, *92*, 9740.

(212) Alicke, B.; Geyer, A.; Hofzumahaus, A.; Holland, F.; Konrad, S.; Patz, H. W.; Schafer, J.; Stutz, J.; Volz-Thomas, A.; Platt, U. *J. Geophys. Res.* **2003**, *108*, 8247.
(213) Zeng, G.; Pyle, J. A. *Geophys. Res. Lett.* **2003**, *30*, art. no. 1392.
(214) Prather, M.; Gauss, M.; et al. *Geophys. Res. Lett.* **2003**, *30*, 1100.
(215) Burnett, C. R.; Burnett, E. B. *Geophys. Res. Lett.* **1996**, *23*, 1925.
(216) Wood, S. W.; Keep, D. J.; Burnett, C. R.; Burnett, E. B. *Geophys. Res. Lett.* **1994**, *21*, 1607.
(217) Bakowski, B.; Corner, L.; Hancock, G.; Kotchie, R.; Peverall, R.; Ritchie, G. A. D. *Appl. Phys. B−Lasers Opt.* **2002**, *75*, 745.
(218) McManus, J. B.; Kolb, C. E. *Proc. SPIE−Int. Soc. Opt. Eng.* **1991**, *1433*, 340.
(219) Sumathi, R.; Carstensen, H. H.; Green, W. H. *J. Phys. Chem. A* **2001**, *105*, 8969.
(220) Tomlin, A. S.; Whitehouse, L.; Lowe, R.; Pilling, M. J. *Faraday Discuss.* **2001**, *120*, 125.
(221) Creasey, D. J.; Heard, D. E.; Lee, J. D. *J. Geophys. Res.−Atmos.* **2002**, *107*, 4091.
(222) Brune, W. H.; Stevens, P. S.; Mather, J. H. *J. Atmos. Sci.* **1995**, *52*, 3328.
(223) Brune, W. H.; Faloona, I. C.; Tan, D.; Weinheimer, A. J.; Campos, T.; Ridley, B. A.; Vay, S. A.; Collins, J. E.; Sachse, G. W.; Jaegle, L.; Jacob, D. J. *Geophys. Res. Lett.* **1998**, *25*, 1701.
(224) Tan, D.; Faloona, I.; Simpas, J. B.; Brune, W.; Olson, J.; Crawford, J.; Avery, M.; Sachse, G.; Vay, S.; Sandholm, S.; Guan, H.-W.; Vaughn, T.; Mastromarino, J.; Heikes, B. G.; Snow, J.; Podolske, J. R.; Singh, H. *J. Geophys. Res.* **2001**, *106*, 32667.
(225) Tan, D.; Faloona, I.; Simpas, J. B.; Brune, W.; Shepson, P. B.; Couch, T. L.; Sumner, A. L.; Carroll, M. A.; Thornberry, T.; Apel, E. C.; Riemer, D.; Stockwell, W. R. *J. Geophys. Res.* **2001**, *106*, 24407.
(226) Ren, X.; Harder, H.; Martinez, M.; Lesher, R.; Oliger, A.; Simpas, J. B.; Brune, W. H.; Schwab, J. J.; Demerjian, K. L.; He, Y.; Zhou, X.; Gao, H. *Atmos. Environ.* **2003**, *37*, 3639.
(227) Kanaya, Y.; Sadanaga, Y.; Nakamura, K.; Akimoto, H. *J. Geophys. Res.−Atmos.* **2001**, *106*, 24197.
(228) Kanaya, Y.; Matsumoto, J.; Kato, S.; Akimoto, H. *J. Geophys. Res.−Atmos.* **2001**, *106*, 24209.
(229) Kanaya, Y.; Sadanaga, Y.; Matsumoto, J.; Sharma, U. K.; Hirokawa, J.; Kajii, Y.; Akimoto, H. *Geophys. Res. Lett.* **1999**, *26*, 2179.
(230) Kanaya, Y.; Sadanaga, Y.; Matsumoto, J.; Sharma, U. K.; Hirokawa, J.; Kajii, Y.; Akimoto, H. *J. Geophys. Res.−Atmos.* **2000**, *105*, 24205.
(231) Brauers, T.; Hausmann, M.; Brandenburger, U.; Dorn, H. P. *Appl. Opt.* **1995**, *34*, 4472.
(232) Dorn, H. P.; Brandenburger, U.; Brauers, T.; Hausmann, M.; Ehhalt, D. H. *Geophys. Res. Lett.* **1996**, *23*, 2537.
(233) Hausmann, M.; Holland, F.; Kohlmann, J.-P.; Rohrer, F.; Ehhalt, D. H. Presented at the 23rd EGS Conference, Nice, 1998.
(234) Comes, F. J.; Armerding, W.; Spiekermann, M.; Walter, J.; Ruger, C. *Atmos. Environ.* **1995**, *29*, 169.
(235) Forberich, O.; Walter, J.; Comes, F. J. *Chem. Phys. Lett.* **1996**, *259*, 408.
(236) Forberich, O.; Pfeiffer, T.; Spiekermann, M.; Walter, J.; Comes, F. J.; Grigonis, R.; Clemitshaw, K. C.; Burgess, R. A. *J. Atmos. Chem.* **1999**, *33*, 155.
(237) Forberich, O.; Comes, F. J. *J. Chem. Soc., Faraday Trans.* **1997**, *93*, 2899.
(238) Comes, F. J.; Armerding, W.; Spiekermann, M.; Walter, J.; Ruger, C. *Ber. Bunsen-Ges. Phys. Chem., Chem. Phys.* **1993**, *97*, 1156.
(239) Comes, F. J.; Forberich, O.; Walter, J. *J. Atmos. Sci.* **1997**, *54*, 1886.
(240) Armerding, W.; Comes, F. J.; Crawack, H. J.; Forberich, O.; Gold, G.; Ruger, C.; Spiekermann, M.; Walter, J.; Cuevas, E.; Redondas, A.; Schmitt, R.; Matuska, P. *J. Geophys. Res.−Atmos.* **1997**, *102*, 10603.
(241) Grenfell, J. L.; Savage, N. H.; Harrison, R. M.; Penkett, S. A.; Forberich, O.; Comes, F. J.; Clemitshaw, K. C.; Burgess, R. A.; Cardenas, L. M.; Davison, B.; McFadyen, G. G. *J. Atmos. Chem.* **1999**, *33*, 183.
(242) Mount, G. H.; Brault, J. W.; Johnston, P. V.; Marovich, E.; Jakoubek, R. O.; Volpe, C. J.; Harder, J.; Olson, J. *J. Geophys. Res.−Atmos.* **1997**, *102*, 6393.
(243) Perner, D.; Platt, U.; Trainer, M.; Hubler, G.; Drummond, J.; Junkermann, W.; Rudolph, J.; Schubert, B.; Volz, A.; Ehhalt, D. H.; Rumpel, K. J.; Helas, G. *J. Atmos. Chem.* **1987**, *5*, 185.
(244) Eisele, F. L.; Mount, G. H.; Tanner, D.; Jefferson, A.; Shetter, R.; Harder, J. W.; Williams, E. J. *J. Geophys. Res.−Atmos.* **1997**, *102*, 6457.
(245) Eisele, F. L.; Tanner, D. J.; Cantrell, C. A.; Calvert, J. G. *J. Geophys. Res.* **1996**, *101*, 14.
(246) Eisele, F. L.; Mount, G. H.; Fehsenfeld, F. C.; Harder, J.; E, M.; Parrish, D. D.; Roberts, J.; Trainer, M. *J. Geophys. Res.* **1994**, *99*, 18605.
(247) Eisele, F. L. *Abstracts of Papers*, 205th National Meeting of the American Chemical Society, San Francisco, CA, Spring 1993; American Chemical Socitey: Washington, DC, 1993; p 69.
(248) Mauldin, R. L.; Eisele, F. L.; Tanner, D. J.; Kosciuch, E.; Shetter, R.; Lefer, B.; Hall, S. R.; Nowak, J. B.; Buhr, M.; Chen, G.; Wang, P.; Davis, D. *Geophys. Res. Lett.* **2001**, *28*, 3629.
(249) Berresheim, H.; Plass-Dulmer, C.; Elste, T.; Mihalopoulos, N.; Rohrer, F. *Atmos. Chem. Phys. Discuss.* **2003**, *3*, 1183.
(250) Handisides, C.; Plass-Dulmer, C.; Gilge, S.; Bingemer, H.; Berresheim, H. *Atmos. Chem. Phys. Discuss.* **2002**, *2*, 2507.
(251) Birmili, W.; Berresheim, H.; Plass-Dulmer, C.; Elste, T.; Gilge, S.; Wiedensohler, A.; Uhrner, U. *Atmos. Chem. Phys.* **2003**, *3*, 361.
(252) Fabian, P.; Winterhalter, M.; Rappengluck, B.; Reitmayer, H.; Stohl, A.; Koepke, P.; Schlager, H.; Berresheim, H.; Foken, T.; Wichura, B.; Haberle, K. H.; Matyssek, R.; Kartschall, T. *Meteorol. Z.* **2001**, *10*, 165.
(253) Fabian, P.; Rappengluck, B.; Stohl, A.; Werner, H.; Winterhalter, M.; Schlager, H.; Stock, P.; Berresheim, H.; Kaminski, U.; Koepke, P.; Reuder, J.; Birmili, W. *Meteorol. Z.* **2001**, *10*, 187.
(254) Watanabe, T.; Yoshida, M.; Fujiwara, S.; Abe, K.; Onoe, A.; Hirota, M.; Igarashi, S. *Anal. Chem.* **1982**, *54*, 2470.
(255) Kanaya, Y.; Matsumoto, J.; Akimoto, H. *J. Geophys. Res.−Atmos.* **2002**, *107*, 4368.
(256) Kanaya, Y.; Yokouchi, Y.; Matsumoto, J.; Nakamura, K.; Kato, S.; Tanimoto, H.; Furutani, H.; Toyota, K.; Akimoto, H. *Geophys. Res. Lett.* **2002**, *29*, art. no. 1212.
(257) Kanaya, Y.; Nakamura, K.; Kato, S.; Matsumoto, J.; Tanimoto, H.; Akimoto, H. *Atmos. Environ.* **2002**, *36*, 4929.
(258) Mihelcic, D.; Holland, F.; Hofzumahaus, A.; Hoppe, L.; Konrad, S.; Musgen, P.; Patz, H. W.; Schafer, H. J.; Schmitz, T.; Volz-Thomas, A.; Bachmann, K.; Schlomski, S.; Platt, U.; Geyer, A.; Alicke, B.; Moortgat, G. K. *J. Geophys. Res.−Atmos.* **2003**, *108*, 8254.
(259) Mihelcic, D.; Heitlinger, M.; Kley, D.; Musgen, P.; Volz-Thomas, A. *Chem. Phys. Lett.* **1999**, *301*, 559.
(260) Mihelcic, D.; Klemp, D.; Musgen, P.; Patz, H. W.; Volzthomas, A. *J. Atmos. Chem.* **1993**, *16*, 313.
(261) Eisele, F. L.; Tanner, D. J. *J. Geophys. Res.−Atmos.* **1993**, *98*, 9001.
(262) Jefferson, A.; Tanner, D. J.; Eisele, F. L.; Davis, D. D.; Chen, G.; Crawford, J.; Huey, J. W.; Torres, A. L.; Berresheim, H. *J. Geophys. Res.−Atmos.* **1998**, *103*, 1647.
(263) Crosley, D. R. *J. Geophys. Res.* **1997**, *102*, 6169.
(264) Brandenburger, U.; Brauers, T.; Dorn, H. P.; Hausmann, M.; Ehhalt, D. H. *J. Atmos. Chem.* **1998**, *31*, 181.
(265) Frost, G. J.; Trainer, M.; Mauldin, R. L.; Eisele, F. L.; Prevot, A. S. H.; Flocke, S. J.; Madronich, S.; Kok, G.; Schillawski, R. D.; Baumgardner, D.; Bradshaw, J. *J. Geophys. Res.−Atmos.* **1999**, *104*, 16041.
(266) Carslaw, N.; Jacobs, P. J.; Pilling, M. J. *J. Geophys. Res.* **1999**, *104*, 30257.
(267) Olson, J. R.; Crawford, J. H.; Davis, D. D.; Chen, G.; Avery, M. A.; Barrick, J. D. W.; Sachse, G. W.; Vay, S. A.; Sandholm, S. T.; Tan, D.; Brune, W. H.; Faloona, I. C.; Heikes, B. G.; Shetter, R. E.; Lefer, B. L.; Singh, H. B.; Talbot, R. W.; Blake, D. R. *J. Geophys. Res.−Atmos.* **2001**, *106*, 32749.
(268) Geyer, A.; Bachmann, K.; Hofzumahaus, A.; Holland, F.; Konrad, S.; Klupfel, T.; Patz, H. W.; Perner, D.; Mihelcic, D.; Schafer, H. J.; Volz-Thomas, A.; Platt, U. *J. Geophys. Res.−Atmos.* **2003**, *108*, 8249.
(269) Chen, G.; Davis, D.; Crawford, J.; Nowak, J. B.; Eisele, F.; Mauldin, R. L.; Tanner, D.; Buhr, M.; Shetter, R.; Lefer, B.; Arimoto, R.; Hogan, A.; Blake, D. *Geophys. Res. Lett.* **2001**, *28*, 3633.
(270) Wang, Y. H.; Liu, S. C.; Wine, P. H.; Davis, D. D.; Sandholm, S. T.; Atlas, E. L.; Avery, M. A.; Blake, D. R.; Blake, N. J.; Brune, W. H.; Heikes, B. G.; Sachse, G. W.; Shetter, R. E.; Singh, H. B.; Talbot, R. W.; Tan, D. *J. Geophys. Res.−Atmos.* **2001**, *106*, 32733.

CR020522S